5-1-2020

Application of soft robotic sensors to predict foot and ankle kinematic measurements

David Saucier

Application of soft robotic sensors to predict foot and ankle kinematic measurements

By

David Saucier

A Thesis
Submitted to the Faculty of
Mississippi State University
in Partial Fulfillment of the Requirements
for the Degree of Master of Science
in Electrical and Computer Engineering
in the Department of Electrical and Computer Engineering

Mississippi State, Mississippi

May 2020

Application of soft robotic sensors to predict

foot and ankle kinematic measurements

By

David Saucier

Approved:

John E. Ball
(Major Professor)

Cindy Bethel
(Committee Member)

Reuben F. Burch, V
(Committee Member)

Qian Du
(Graduate Coordinator)

Jason M. Keith
Dean
Bagley College of Engineering

Name: David Saucier

Date of Degree: May 1, 2020

Institution: Mississippi State University

Major Field: Electrical and Computer Engineering

Major Professor: John E. Ball

Title of Study: Application of soft robotic sensors to predict foot and ankle kinematic measurements

Pages of Study: 137

Candidate for Degree of Master of Science

The ankle joint complex is a common source of injury for various demographics and is often observed during gait analysis. I investigate using soft robotic sensors as a means for collecting kinematic data at the ankle joint complex. I validate the linearity of these sensors by measuring stretch against extension and against stretch from frontal and sagittal planar foot movements using a wooden ankle mockup. I then conduct a study involving ten participants who perform repetitive trials of four foot movements (plantarflexion, dorsiflexion, inversion and eversion) using ten different locations. Four optimal locations were identified for these movements based on linearity, accuracy, robustness, and consistency. Lastly, I validated soft robotic sensors against the human gait cycle. Twenty participants were recruited and performed twelve trials, walking across a flat surface and a cross-sloped surface while motion capture data and soft robotic sensor data was collected.

Key words: soft robotic sensors, sensor placement, wearables, ankle joint complex, motion capture, kinematics, gait analysis, multivariable linear modeling, data coupling

DEDICATION

I dedicate this thesis to my wife, Sydney.

ACKNOWLEDGEMENTS

I would like to thank the Athlete Engineering Research group for the tremendous effort put into this project. I was fortunate to work with many great students from other departments that made this interdisciplinary effort possible. I thank Alana Turner, Preston Robertson, Ethan Stewart, Tashfin Iftekar, and Pan Wei for their help with data collection. I thank Samaneh Davarzani and Phoebe Nguyen for their help with data curation and analysis. I thank Will Caroll and Preston Peranich for their help with developing a data collection module for the SRS.

I would especially like to thank Dr. Tony Luczak, who went through thick and thin with me for the many trials that were done for data collection. I thank for his contributions to constructing the experiment models including the wooden ankle mockup, SRS socks, and cross-sloped platform.

I would like to thank all of the PIs involved with those and for their guidance throughout this project and their assistance with experiment design/data analysis approach: Dr. Adam Knight, Dr. Harish Chander, Dr. Brian K. Smith, and Dr. R. K. Prabhu.

I would especially like to thank Dr. Burch, lead PI for the project, and Dr. Ball, my academic advisor and PI for the project. Dr. Burch has done an incredible job pushing myself and others to accomplish some great goals over the past few years, and has always been a great source of encouragement when progress was made. Dr. Ball gave me some great

direction during my research efforts, was always helpful and available to me whenever I had questions, and has just been a fantastic person to get general life advice from.

The work presented in Chapter 3 was partially funded by a Mississippi State University (MSU) Office of Research and Development (ORED) undergraduate research grant and a MSU Bagley College of Engineering Working Group grants for the Multi–Sensor Working Group and the Wearables Working Group. The work presented in Chapter 4 and Chapter 5 was funded by the National Science Foundation under NSF 18-511—Partnerships for Innovation award number 1827652. The findings and opinions in this thesis belong solely to the author, and are not necessarily those of the sponsor.

TABLE OF CONTENTS

LIST OF TABLES

LIST OF FIGURES

LIST OF SYMBOLS, ABBREVIATIONS, AND NOMENCLATURE

ADC Analog-to-Digital Converter

AT Athletic Trainer

AHRS Attitude and Heading Reference System

CAVS Center for Advanced Vehicular Systems

DOF Degrees of Freedom

DES Dielectric Elastomer Sensor

DF Dorsiflexion

EVR Eversion

FS Flat Surface

GPS Global Positioning System

HPL Human Performance Lab

I-CORP I-Corporation

IMU Inertial Measurement Unit

IRB Institutional Review Board

INV Inversion

MAE Mean Absolute Error

MEMS Micro Electromechanical Systems

MSU Mississippi State University

NSF National Science Foundation

NWB Non-weight Bearing

PFI Partnerships for Innovation

PSPICE Personal Simulation Program with Integrated Circuit Emphasis

PF Plantarflexion

POC Position and Orientation Configuration

PCB Printed Circuit Board

PGA Programmable Gain Amplifier

R^2 R-Squared

ROM Range of Motion

RMSE Root Mean Square Error

SAIL Sensor Analysis and Intelligence Laboratory

SRS Soft Robotic Sensor

SPI Serial Peripheral Interface

S&C Strength and Conditioning

SME Subject Matter Expert

TSP Tilted Surface Platform

TPU Thermoplastic Polyurethane

WST Wearable Sensor Technology

$^\circ$ Joint angle degree

ΔR Change in electrical resistance

ρ Electrical resistivity

L, w, h Length, width, and height of SRS channel

ΔL, Δw, Δh Changes in length, width, and height of SRS channel

ϵ Strain

C Capacitance

ϵ_r Relative permittivity of dielectric

ϵ_0 Permittivity of free space

A Area of overlapping electrodes on dielectric

d Thickness of the dielectric layer

Y Estimate of sample from motion capture data

α Intercept of prediction model

β Coefficient of SRS

x Sample from SRS dataset

R Resistance

V Voltage

I Current

CHAPTER 1

INTRODUCTION

Wearables can be defined as technologies used to measure various physiological and kinematic parameters by being sported or borne by the user [60]. A common problem identified after conducting 113 interviews from strength and conditioning coaches across all levels of athletic competition identified their two biggest concerns with the current state of wearable technology: (a) the lack of solutions that accurately capture data "from the ground up" and (b) the lack of trust due to inconsistent measurements. Most data solutions seem to capture data that is irrelevant or is not interpreted in a way that is useful to the end user for making decisions. Some wearable devices mentioned were ones that utilized Inertial Measurement Units (IMUs) and Global Positioning System (GPS) technology, noting that the devices were inconsistent, intrusive, and unable to track quick changes of directions [59].

As wearable technology has advanced, gait analysis has become more prevalent for the use of both clinical practice and biomechanical research. Wearables are gradually becoming a more feasible replacement to multi-camera motion capture systems, which have historically been used for gait analysis but are restricted to a laboratory setting, are expensive, and are computationally intensive. As improvements have been made in terms

of form-factor, power efficiency, and cost, wearable sensors have become more useful for ambulatory gait analysis in sports, rehabilitation, and clinical diagnostics. Temporal characteristics can be collected from the data to determine phase of the gait and have the potential to determine if the user has medical problems [99].

1.1 Athlete Engineering Group: Closing the Wearable Gap

The Athlete Engineering Group was sparked out of the experience and insights gained through a series of interviews that were conducted through the National Science Foundation Partnerships for Innovation (NSF-PFI) I-Corps Program. Through having conversations with 113 strength and conditioning coaches (S&CCs) and athletic trainers (ATs) across the country, it was identified that there was a clear gap in the wearable technology being developed and the end user. Many of the interviewees expressed frustrations with the technology being inaccurate, inconsistent, invasive, and unable to communicate data in a clear and meaningful way. This led to the development of a research group that sought to work with athletics at MSU to get more value out of wearable technology, as well as other existing technologies such as motion capture, to help S&CCs and ATs make more informed, data-driven decisions that are useful and intentional.

Further, the group is seeking ways to develop wearable solutions that mitigate the problems commonly seen in most existing solutions today, such as inaccurate data (e.g. IMU drift) and bulky form factor. Included in Athlete Engineering Group is not only the sports athlete, but also the industrial athlete and the military athlete. Wearable solutions are continuing to be developed and investigated in industry and the military, and further research

will be done to determine if devices developed for the athlete can also be applied to these fields.

1.2 Motivation

My research pertains to investigating the use soft robotic sensors (SRS) to determine their feasibility as a substitute for existing motion analysis technologies, which includes restrictive, camera-based motion capture systems and inertial measurement units (IMUs) [60]. SRS output an electrical value (capacitive or resistive) that increases with stretch. Developing a motion analysis application using SRS could result in a solution that is more portable, more affordable, and less invasive than lab-based motion capture systems. Further it has potential to collect kinematic data that is more reliable than IMU data, due to the elimination of drift.

I conducted several studies using resistive-based SRS from Liquid Wire, Inc. to determine the linearity of the sensors in relation with stretch. Linearity of the sensors was also tested under different temperatures to determine if this affected the output of the SRS. A wooden ankle mockup was also constructed to determine the linearity of resistive SRS output in relation to relative ankle joint angle [60]. Once the SRS output was determined to have a strong linear relationship with stretch, another study was done collecting data from 10 participants performing four common foot movements: plantarflexion (PF), dorsiflexion (DF), inversion (INV), and eversion (EVR). For this study, capactive-based SRS from StretchSense™ and a 12-camera Vicon™ motion capture system were used to determine ideal sensor placement and orientation for collecting foot and ankle joint kinematic data

[89] for the aforementioned movements. Feasibility of detecting slips and trips was also investigated using SRS to detect the PF and DF movements [13]. Finally, a gait study was conducted with 20 participants using StretchSense^{TM} to determine how well SRS perform when used to predict foot-ankle kinematics while the participant is walking on a flat and cross sloped surface [88].

This thesis is organized as follows: Chapter 2 discusses the anatomy of the foot-ankle complex, the gait cycle, description of SRS, motion capture, data pre-processing approaches, and data analysis/modeling approaches. Chapter 3 discusses work accomplished for the linearity study. Chapter 4 discusses work accomplished for the placement study. Chap 5 discusses work accomplished for the gait study. Chapter 6 summarizes the conclusions and lists potential future work.

This thesis contains work from the following publications:

T. Luczak, D. Saucier, R. F. Burch V et al., "Closing the Wearable Gap: Mobile Systems for Kinematic Signal Monitoring of the Foot and Ankle," Electronics, vol. 7, no. 7, p. 117, Jul. 2018, doi: 10.3390/electronics7070117 [60].

D. Saucier et al., "Closing the Wearable Gap—Part II: Sensor Orientation and Placement for Foot and Ankle Joint Kinematic Measurements," Sensors (Basel), vol. 19, no. 16, Aug. 2019, doi: 10.3390/s19163509 [89].

D. Saucier et al., "Closing the Wearable Gap—Part IV: 3D Motion Capture Cameras Versus Soft Robotic Sensors Comparison of Gait Movement Assessment," Electronics, vol. 8, no. 12, p. 1382, Dec. 2019, doi: 10.3390/electronics8121382 [88].

CHAPTER 2

BACKGROUND

This chapter discusses background on anatomy of the ankle joint complex, the gait cycle, motion capture and SRS technologies, hardware used to measure SRS, and data pre-processing and analysis methods. I will first explain some basic concepts regarding kinematics of the foot and ankle to provide a foundation for what I am seeking to measure with SRS.

2.1 Foot and Ankle Kinematics

Kinematics is the study of motion without regard to the force creating said motion. Joint angles are studied within kinematics to measure the angle between two adjacent segments along a planar movement [10]. There are three planar movements that occur at the ankle joint complex. These include plantarflexion and dorsiflexion occurring in the sagittal plane; abduction and adduction occurring in the transverse plane, and inversion and eversion occurring in the frontal plane. Figure 2.1 illustrates these movements. Those motions occur across two primary joints of the ankle. The subtalar joint connects the calcaneus (heel bone) to the talus and contributes to the overall triplanar movement, but predominantly contributes to the inversion and eversion movement. The tibiotalar joint connects the lower leg and talus and functions primarily as a ”hinge”, contributing mostly to the

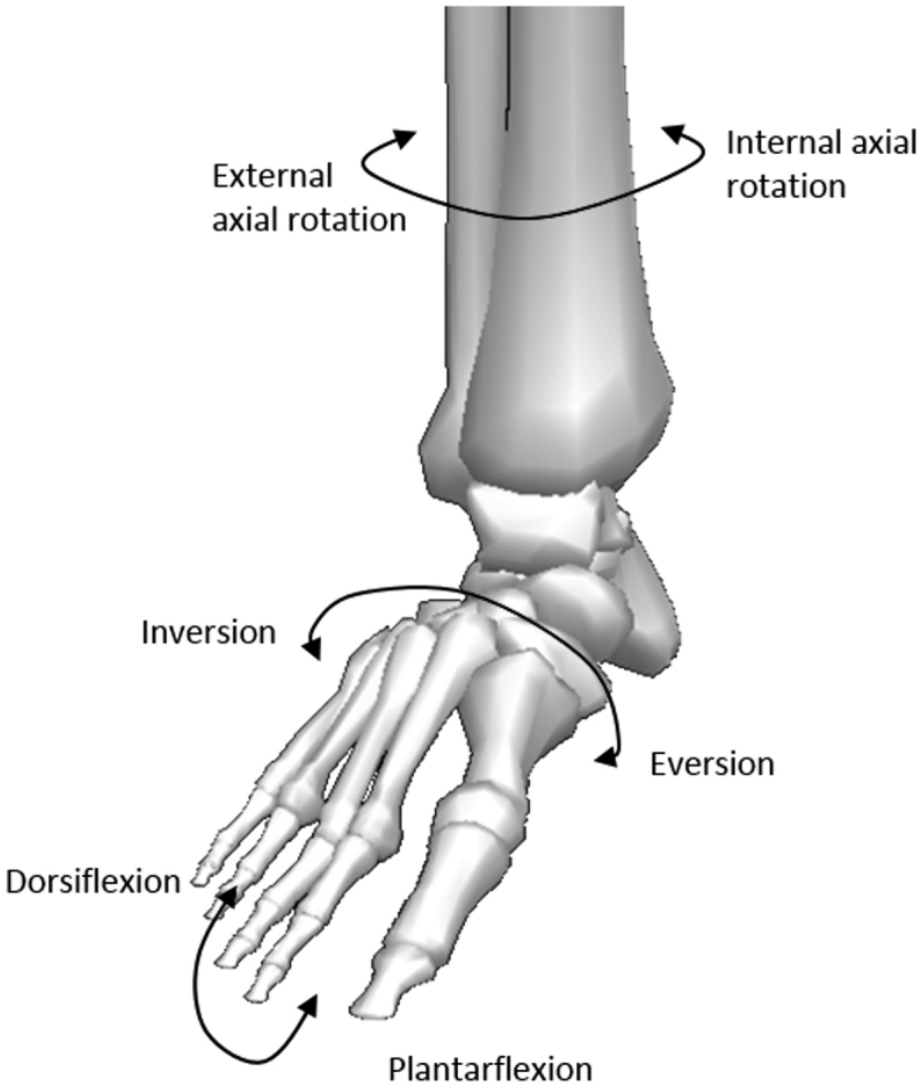

Figure 2.1: Diagram illustrating three planes of motion of the ankle joint complex from [11]. External axial rotation corresponds to abduction and internal axial rotation corresponds to adduction.

plantarflexion and dorsiflexion movements. The three planar movements occur in combination across both the subtalar and tibiotalar joints to create three-dimensional motions called supination and pronation [73].

Pronation and supination are terms used to define the position of the plantar surface of the foot, commonly known as the sole. Plantarflexion, inversion, and adduction occur simultaneously during supination, causing the sole of the foot to face medially (towards the midline of the body). On the other hand, dorsiflexion, eversion, and abduction occur simultaneously during pronation, causing the sole of the foot to face laterally (away from the midline of the body) [11]. The total range of motion (ROM) in the sagittal plane is considered to be between $65°$ and $75°$, with $10°$ to $20°$ occurring in dorsiflexion, and the remaining $40°$ to $55°$ occurring in plantarflexion [97, 35]. The total ROM in the frontal plane is roughly $35°$ with $23°$ of inversion and $12°$ of eversion [97]. One distinction to note is that movement in the sagittal plane becomes restricted to $30°$ when walking [73]. These movements occur naturally during the human gait cycle. Pronation functions primarily to absorb the shock of foot contact with the ground and stabilize the body, while supination propels the foot off of the ground and moves the body forward for the next step. [10].

2.2 Gait Analysis and the Gait Cycle

Gait analysis is the systematic study of human locomotion. It involves the use of various technologies to collect, analyze, and assess data regarding kinematic and kinetic parameters, gait phases, and musculoskeletal functions. Various types of technologies have been used to perform gait analysis, being standardized mainly by multi-camera motion

capture systems. However, the motion capture approach is restricted to an isolated lab environment, is costly, and is encumbered with a lengthy calibration process. Wearable sensors are now being investigated to overcome these issues a provide a low-cost, portable solution that effectively functions as a motion capture system outside a of a laboratory setting [99].

The gait cycle of human locomotion is a periodic movement that can be broken down into the following eight phases: initial contact (or foot strike), loading response, midstance, terminal stance, pre-swing, initial swing, mid-swing, and terminal swing [84]. The first five phases comprise the stance portion of the gait cycle, while the remaining three phases comprise the swing portion. These phases can be further divide based on which legs are in the stance or swing phase. If both legs are in the stance phase, then the body is considering to be using bipodal or double support, whereas if one leg is in the stance phase while the other is in the swing phase, then unipodal or single support occurs [10]. Figure 2.2 provides an illustration for this. The gait cycle is generally considered to be the period of time from one foot making initial contact with the ground until that same foot makes initial contact with the ground a second time [10].

When explaining the various phases, the ”primary foot” will be referred to as the first foot to make initial contact, thus marking the beginning of the gait cycle. The other foot will be referred to as the ”opposite foot”. The stance phase begins with initial contact, which occurs when the primary foot strikes the floor. This can be any part of the foot, but the heel will commonly be the first part of the foot that makes contact with the ground [1]. Once the primary foot is flat on the ground, the loading response begins, where the primary

foot absorbs the shock from landing, and continues until the opposite foot is lifted off the ground for swing. Midstance takes place while the opposite foot advances past the primary foot, and continues until the opposite foot is aligned over the primary forefoot. Terminal stance begins when the heel of the primary foot is lifted off the grounded and continues until the opposite foot makes contact with the ground. Pre-swing begins with the opposite foot making contact with the ground and ends with the toe-off, or lifting, of the primary foot [84, 99, 1, 10].

Following pre-swing, the swing phase begins with toe-off of the primary foot, swinging forward, and continues until the primary foot is in line with the opposite foot. Mid-swing begins when both limbs are aligned and continues until the tibia (shank) of the opposite stance limb is vertical, while the primary foot continues to move forward. Finally the terminal swing takes place as the swing shifts from the opposite tibia being vertical until the second primary foot strike, or initial contact [99, 1].

2.3 Motion Capture

Three-dimensional motion capture has become the ”golden standard” research tool for collecting kinetic and kinematic data of human motion [126]. However, It is generally quite expensive and is restricted to an indoor laboratory setting . Using a set of infrared cameras and a set reflective markers mounted to a subject, the system can determine the position of certain parts of the body and can infer key information about the subject such as joint angle data of various limb segments. Force plates can be used in addition to motion capture technology to determine ground reaction forces occurring at the left and right

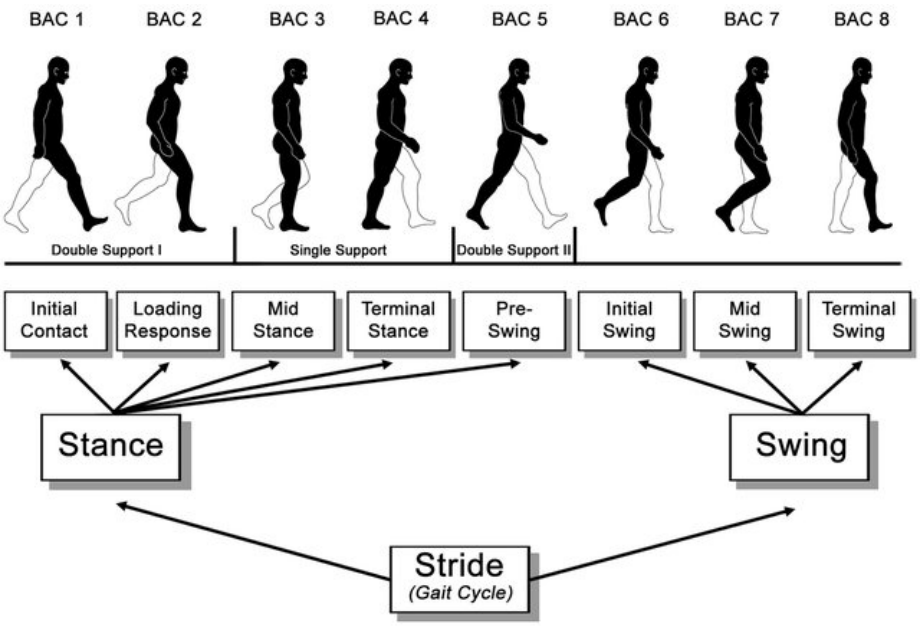

Figure 2.2: Diagram illustrating the eight phases of the gait cycle [83]

legs of the subject. For my thesis, several experiments were conducted using the motion capture system in the Human Performance Lab (HPL) in the Center for Advanced Vehicular Systems (CAVS). This system consisted of 12 Vicon™ Bonita optical cameras, and MotionMonitor™ was used to interpret the motion capture data to kinematic data. Marker clusters were mounted to the limb segments to use for tracking participant movement. Motion capture has been used commonly in studies for validating other technologies in their ability to accurately perform motion analysis [27, 48, 67, 104].

2.4 Soft Robotic Sensors

SRS, also known as stretch sensors, are sensors that can be used to measure deformation such as tension or bending. The sensors are made out of material that is soft and flexible,

and produce an output that is either resistive or capacitive that changes with deformation of the sensor. They can be used to measure movement changes and body posture [111, 40]. Research has been conducted studying the use of soft robotics for the hands/fingers [37, 79], wrist [40], upper body [48], and legs [67, 104]. For my research, I am specifically investigating the application of SRS in the measurement of the ankle joint complex to determine kinematics for the sagittal and frontal planes. I have created a model where four movements are represented by SRS. These four movements include PF, DF, INV, and EVR. Due to the limited movement (5° ROM [10]) of abduction and adduction when walking, I did note measure this plane of movement for these experiments.

2.4.1 Resistive SRS

A common type of resistive SRS seen in recent literature is created using eutectic gallium indium (eGaIn), also known as "liquid metal" [48, 67, 81]. This liquid metal is embedded into an elastomer, which, when stretched, lengthens in the direction being stretched and contracts in the transverse direction. While overall length is increasing, the cross-sectional areas of the sensor channels decrease. Poisson's ratio characterizes the relationship between the stretching and contraction [81, 67]. As a result, the elastomer's channels are proportionally deformed, causing an increase in the electrical resistance through the liquid metal path based on the relationship described in Equation 2.1. For this equation, ΔR represents change in electrical resistance, ρ indicates electrical resistivity of the liquid metal,

L, w, and h are length, width, and height of the channel, and ΔL, Δw, and Δh represent the changes in length, width, and height.

$$\Delta R = \rho \left[\frac{L + \Delta L}{(w + \Delta w)(h + \Delta h)} - \frac{L}{wh} \right] \tag{2.1}$$

Using v to represent Poisson's ratio of the elastomer material and ϵ to represent strain, Δw and Δh can be replaced with -$v\epsilon w$ and -$v\epsilon h$. Further, ϵ can replace $\Delta L/L$. Equation 2.2 shows the original equation simplified with the aforementioned replacements.

$$\Delta R = \frac{\rho L}{wh} \left\{ \frac{(1 + 2v)\epsilon - v^2\epsilon^2}{(1 - v\epsilon)^2} \right\} \tag{2.2}$$

Finally, since resistive SRS are constructed using an elastomer material, Poisson's ratio can be determined, setting v = 0.5, allowing us to finally simplify the expression to Equation 2.3 [67, 81].

$$\Delta R = \frac{\rho \epsilon L(8 - \epsilon)}{wh(2 - \epsilon)^2} \tag{2.3}$$

Circuit design for resistive SRS is generally simpler to implement than for capacitive SRS. Resistor dividers and wheatstone bridges are commonly used to measure this type of sensor since it is essentially a variable resistor. A constant current source can be supplied to voltage dividers as well to create a more linear change in voltage when being measured with a resistor divider [67]. Further, an analog-to-digital (ADC) converter is also utilized to measure the voltage output in a meaningful way. Since the change is resistance for these sensors are generally pretty small (at most an order of tens of Ohms), operational amplifiers are often used to provide a greater range of readings from the output of the SRS [60].

Though easier to measure from a circuit-design perspective, resistive SRS tend be characteristically more difficult to measure accurately. Non-linearity and hysteresis are often

observed to be worse in comparison to capactive SRS [55, 67, 69]. Some of these issues were observed in the first study using Liquid Wire sensors to determine their linearity. Though the sensors appeared to be mostly linear in the controlled experiments. Hysteresis was noticed the more the SRS were used (i.e. the resistance at rest was higher than when the sensor was initially measured) and non-linearity became more apparent as more robust experiments were performed.

2.4.2 Capacitive SRS

Capacitive SRS have found better success with achieving an electrical output that is both highly linear and nonhysteretic. A study from NASA investigated the use of six different types of stretchable sensors, and while some of the resistive-based sensors produced modest results, the capacitive sensor from StretchSense surpassed the other sensors by a significant margin. For example, the creep test lasted on the order of tens of hours for the StretchSense SRS before slight hysteresis was observed, whereas the other sensors were only stretched for minutes or even seconds before hysteresis occurred [55].

The most prevalent type of capacitive SRS in recent years is the dielectric elastomer sensor (DES). This usually consists of a combination of an elastomer dielectric and elastomer electrode layer depending on how the sensors are manufactured. Most work involves using silicone as the elastomer layer [40, 104].

Though capacitive SRS provide a more consistent output than resistive SRS, they are much more difficult to accurately measure. The DES can be characterized as an electrical circuit with a variable capacitor in series with a variable resistor, which all change as

deformation of the DES occurs. Capacitance is better to measure due to its high sensitivity to the change in area of the electrodes, whereas the resistance of a DES is easily influenced by temperature and electrode quality [75]. The capacitance can be characterized with Equation 2.4, where ϵ_0 is the dielectric's vacuum or permittivity of free space, ϵ_r is the dieletric's relative permittivity, A is the area of the overlapping electrodes, and d is the thickness of the dielectric layer [40, 47, 117]. The drawback to measuring capacitance from a DES is that significant electrode resistance causes the meter to incorrectly measure the capacitance [30]. In some cases the capacitance isn't even measured, and instead voltage is measured to at least get a metric that changes with sensor deformation without diving into complex capacitance sensing methods [40].

$$C = \frac{\epsilon_r \epsilon_0 A}{d} \tag{2.4}$$

For the purpose of this research, I will not be diving much further in the methodology for measuring capacitive SRS as extensive research has already been done, and an off-the-shelf microcontroller is being used for my experiments to measure capacitive SRS. StretchSense has addressed this as being a difficult problem to solve and advocates for using their measurement unit, which has been optimized over time to mitigate the nuances of measuring the capacitance of a DES [98].

2.5 Data Preprocessing

In order to collect data from both motion capture and SRS and perform analysis using the two measurements methods, several preprocessing techniques are required, which are detailed below.

2.5.1 Data Interpolation

For measuring capacitive SRS, a proprietary Bluetooth-enabled Serial Peripheral Interface (SPI) sensing module from StretchSense™ was used to collect data from the sensors. A companion smartphone application was used with the module to save the data collected over a given period of time. Due to limitations in the Bluetooth implementation, the max sampling rate that could be collected from the module was roughly 25 Hz, despite the SPI sensing module being able to measure up to 1000 Hz. Further, the samples were not collected at evenly spaced time intervals. The motion capture data was collected at either 100 Hz or 200 Hz. In order to resolve the difference in sampling methods and the inconsistent sampling of the SRS, an approximation method was used to upsample and interpolate the data collected by the SRS to match that of the motion capture system.

Linear interpolation of the SRS data involves curve fitting using linear polynomials to infer new data points inside a range of discrete values defined in a sequence of data. Given two known data points (x_0, y_0) and (x_1, y_1), a linear interpolant is determined as a straight line drawn between these points. For a given value x to be interpolated between the interval (x_0, x_1), y can be determined with Equation 2.5. Solving for y results in Equation 2.6. A complete linear interpolation of a dataset is the result of the concatenation of the linear interpolants determined between each pair of data points. While this approach enables the comparison of the two datasets, it does introduce some error due to the polynomial nature of the output that occurs, based on Rolle's theorem [95, 110].

$$\frac{y - y_0}{x - x_0} = \frac{y_1 - y_0}{x_1 - x_0} \tag{2.5}$$

$$y = \frac{y_0(x_1 - x) + y_1(x - x_0)}{x_1 - x_0} \tag{2.6}$$

2.5.2 Cross-correlation

Once the difference in sampling rates are reconciled, there is usually still a time delay that exists, as the devices did not always begin recording at the same time with two humans synchronizing the start of a trial. Cross correlation is a method that can solve this issue, where one dataset is essentially "slid" over the other to determine the optimal point at which the two datasets match. Equation 2.7 defines this function, where f and g represent continuous functions (in our case, SRS and motion capture), $f[m]$ denotes the complex conjugate of $f(t)$, and τ represents displacement or lag [87, 109].

$$(f * g)(\tau) \triangleq \sum_{m=\infty}^{\infty} f[m]g[m+n] \tag{2.7}$$

The maximum value of the cross-correlation function can be used to determine the point in time where two sequences are best aligned. Equation 2.8 describes collecting the arg max of the cross-correlation function to find the time delay between two datasets [87, 109]. Note that for this expression, $*$ represents correlation, rather than convolution.

$$\tau_{delay} = \arg\max_{t \epsilon \mathbb{R}}((f * g)(t)) \tag{2.8}$$

One dataset is shifted to match the other based on the location of the maximum value, and any excess data points are trimmed. For example, if motion capture began recording before SRS, then values at the beginning of the motion capture would be removed based on the delay calculated. Following this, if one measurement stopped recording after the other one did, then those additional values are removed as well.

In the case of matching SRS data to motion capture data, the two datasets are aligned based on the SRS that best captures the motion being measured. When performing isolated movements in the sagittal plane, the PF and DF SRS are used for cross-correlation, while isolated movements performed in the frontal plane are aligned with the INV and EVR SRS. Prior to performing cross-correlation, when PF and EVR are being evaluated, their datasets are inverted due to their stretch correlating to an inverse movement of the planar movement. In other words, the PF and EVR SRS are positioned to measure joint angle values in the negative plane for the sagittal and frontal movements, respectively. If triplanar movement such as supination or pronation is occuring, then PF and DF are used for cross-correlation, as the positioning of the INV and EVR SRS are coupled to both planes of movements and therefore sensitive to both planes of movement.

2.5.3 Filtering

Filtering methods were used to mitigate noise in the motion capture data and aliasing in the SRS data. For the motion capture data, a 15 Hz low-pass Butterworth filter was used to smooth the data. This particular filter was chosen due to its ability to flatten the frequency response in the passband as much as possible [108].

One issue that came about with the approximation of the SRS data was that some samples were aliased due to the low sampling of the StretchSense Bluetooth module. In other words, certain data points were sometimes interpolated between values that were the same, therefore interpolating the new data point to the same value. This resulted in SRS data that possessed a ”stair-step” appearance when plotted and revealed an issue that

impacted the accuracy of its ability to predict kinematic data. However, when filtering this data, it was important to preserve the peak responses that occurred in the SRS data. The Savitzky-Golay filter was chosen to smooth this data as it is particularly effective at preserving minimum and maximum values [4].

2.6 Data Analysis

Once the data was pre-processed, analysis of the data was performed to evaluate how effective the SRS were at modeling foot and ankle kinematic data. Several metrics were used to determine the linearity and accuracy of the model including R-Squared (R^2) values, Root Mean Squared Error (RMSE) values, and Mean Absolute Error (MAE) values.

2.6.1 Linear Modeling

In order to use SRS data to predict motion capture data, a linear model should be developed to capture the relationship between the two datasets. For my implementation this is done using an ordinary least squares fitting method, which finds the best fitting line that minimizes the sum of the squared residuals. An example of such a model can be observed in Equation 2.9 where Y_i is the estimate of the i'th sample from the motion capture data, x_i is the i'th sample from the SRS, and β is the coefficient of the SRS. In this case only a single sensor is used to predict kinematic data from one plane of motion recorded from the motion capture system. Prior to modeling, the PF and EVR SRS output is inverted to create a positive relationship between the SRS and the motion capture system. Movement in the sagittal plane is predicted with models generated from the PF and DF SRS, while

movement in the frontal plane is predicted with models generated from the INV and EVR SRS.

$$Y_i = \alpha + \beta x_i \tag{2.9}$$

2.6.2 Multivariable Linear Modeling

When triplanar movement occurs, linear modeling must be performed while factoring in output from all SRS in order to get an accurate position, due to the coupling of the planar movements to the same SRS. In order to generate this model, the same principle is applied as done for the single linear model, except that multiple predictor variables are used in the model, each having their own coefficient. This can be observed in Equation 2.10. The difference is that $x_i^{(1)}$ now represents the i'th sample from the j'th SRS and β_j is the coefficient of the j'th SRS.

$$Y_i = \alpha + \beta_1 x_i^{(1)} + \beta_2 x_i^{(2)} + \beta_3 x_i^{(3)} + \beta_4 x_i^{(4)} \tag{2.10}$$

CHAPTER 3

LINEARITY

This chapter is based on publication [60].

3.1 Introduction

While improving athletic performance is a common goal of Strength and Conditioning (S&C) coaches across all levels of competition, the question of optimization of performance is still subject to trial and error. Quantifying training protocols is one method to evaluate and validate performance programs. Traditionally, optical motion capture of biomechanical data collection is considered the gold standard for identifying kinematic and kinetic parameters [27] and is generally confined to a research laboratory or lab-like environment due to the equipment requirements. Unfortunately, high costs and limited access to these research environments reduces the opportunity for improving all athletes through technical analysis [66]. One promising technological advancement that has seen increased exposure in research and competition is wearable sensor technology and the opportunity to measure near real-time kinematics on the playing field [12]. Measuring various physiological and kinematic parameters is now accessible to the average athlete compared to the human activity recognition devices from twenty years ago [52, 26]. Numerous commercially

available products utilize micro electromechanical systems [22] (MEMS), accelerometers, and gyroscopes to capture biomechanical measures outside the lab [27].

One of the benefits of using MEMS devices is that they offer a lower-cost alternative to traditional motion capture solutions. Using an inertial frame, the relative orientation of limb segments can be calculated from accelerometer and gyroscope data [17]. One commonly used type of MEMS is the inertial measurement unit, or IMU, and it is found in most technologies where some form of movement information is captured. However, several recurring issues are seen in IMU-based motion capture systems including distortion and drift [27], and challenges in how to consistently manage calibration [24]. The distortion and drift that affects actual sensor horizontal and vertical data are due to distortions in non-homogeneous magnetic fields, often caused by building construction materials and magnetic interference [27, 76]. To reduce noise, improved anatomical models and static calibration in defined positions have been developed [27, 17]. However, measurement errors still occur due to skin and segment speed of movement and axial segment rotation [57]. According to Kavanagh et al. [46], the separation of limb segment resultant acceleration could not be identified within the sensor data, resulting in the difficulty to obtain accurate measurements. Additionally, external devices are often incompatible with activities that involve contact and may require frequent adjustment and re-calibration [61] making them impractical for use in real-world environments.

In human movement, the neuromuscular system senses strains, positioning, and stretching of its proprioceptors and muscular system in order to coordinate limb segment movement [18]. A body network sensor system that mimics strain and stretch around the joints

may offer an alternative to using stiff, circuit board-based IMUs in capturing human limb movement. Given calibration and consistency challenges that exist with IMUs used in the athletic wearable market today, a potential solution may lie in the use of a different kind of sensor, or sensors developed for a different purpose, such as SRS. Totaro et al. custom designed soft sensors and integrated them into garments for precise movement validated in lower limb joints [104] but this research did not utilize "off-the-shelf" sensors and therefore are limited for future, real-world environment use cases. Other recent studies utilized more commercialized soft robot sensor solutions found in exoskeletons technologies for less complex movements not located around the foot and ankle [40, 77]. For the purposes of this study, SRS can be identified as silicone–textile (or other soft materials) layered with liquid conductive material and generally identified as resistive or capacitive [3, 58]. As these sensors are stretched, their resistive or capacitive values increase. At the beginning of this research, there were two primary SRS solutions available to test. Liquid Wire is a resistance-based sensor and StretchSense^{TM} is a capacitive-based sensor, both of which provide increased output values when stretched past their initial resting lengths. Several advantages for using SRS such as these include (a) the ability to measure biomechanical strain without worry for occlusion errors that typically occur in optical systems and eliminate drift that can occur in MEMS sensors [66]; (b) the realization of small changes in electromechanical specifications during loading and unloading; and (c) the reduction of interference as observed by the wearer [67]. In addition, SRS inherently offer "stretchability", which allows the sensors to cover arbitrarily shaped joints that occur on the human body [118].

The purpose of the research described herein is to take a new type of sensor, SRS, and determine if this solution can be re-purposed for motion capture via a customized wearable technology application. The motivation behind this idea being to mitigate or completely remove the problems described regarding IMU-based wearable solutions. Before any solution design and prototyping based around this sensor solution was initiated, the researchers identified critical questions that needed to be addressed by subject matter experts (SMEs): (a) There are known issues with data consistency and reliability with wearable technology (as previously defined) but what do actual SMEs of the technology think? (b) What are the gaps that SMEs identify as being the biggest opportunities for wearables?

3.1.1 Interviews—Two Concerns

In order to address the first question regarding wearable industry gaps, this research team sought out SMEs who were not only familiar with the intended (and actual) use of the technology but who were also knowledgeable of the "state of the art" of the wearable market. As a result of securing regional NSF I-Corporation (I–Corp) grant funding, the researchers conducted a series of nearly three-dozen, hour-long interviews with S&C coaches and athletic trainers (AT) from around the country in all sports at the collegiate and professional levels for both men and women competition. These interviews were conducted to establish the need and use of wearable technology to improve athletic performance and manage athletic activity. The primary questions posed to the interviews were (a) "What are the gaps in the current generation of wearable technologies available to you today?" and (b) "If you could design a wearable solution, what information would it capture for you in

order to assist in making critical decisions about health and safety?" Two primary concerns were repeated by the interviewees. The first concern was that current data from wearable sensors could not be trusted due to consistent inaccuracies and lack of transparency with generalized correlations. The second most consistently identified gap was that data captured "from the ground up" was desired but was either missing or delivered improperly in current wearable technological solutions designed for athletic competition and movement evaluation. The term "from the ground up" highlights a desire on the part of the S&C coaches and ATs to have data collected at the point where the athlete comes in contact with the ground, the foot and ankle.

3.1.1.1 Rebuilding Trust

The first gap identified through the I–Corp interviews, the issue of trust, is a major concern as these S&C coaches and ATs are responsible for making decisions about the health and safety of athletes. Training and rehabilitation protocols directly influence athletes' functional health beyond competition. Backing the concerns identified by the interviewees, multiple researchers have expressed concerns about the efficacy of sensors in rehabilitation use due to inaccuracies [5, 9], and the inability of users to successfully manage the number of false positives that can occur through wearable sensor use often results in poor compliance [5]. To overcome inaccuracies found in wearable technology, researchers have used a variety of different and frequent calibration procedure methods [53], extra sensors, and substituted ultra-wide band for magnetometers [24]. As seen in a study of three commercially available Attitude and Heading Reference Systems (AHRS) [53], relative accuracy,

which can be related to human joint angle measurement, deviated from one degree in a 30 s time segment to over 16 degrees in repeated two minute dynamic segments compared to the gold standard of optical motion capture. Resetting of the reference points for the sensors during the trials did improve accuracy; however, constant re-calibration can occur in the lab and be tolerated but this frequent level of adjustment is neither practical nor acceptable for practitioners who would need to stop training or practice to re-calibrate wearable devices.

From the corroborated output amassed during the I–Corp interviews, the number of step counts by Mississippi State University (MSU) men's and women's basketball teams captured during the 2016–2017 season recorded higher than normal step activity during practices. Further investigation into the data revealed that the dribbling motion of the basketball by the player's arms and hands were being counted as steps and work performed. Other inaccuracies also occurred with the MSU football team. During a spring training practice in 2017, one player registered as taking a few hundred steps and traveling 10 miles, which is obviously not physically possible. At most, average football players in an average practice will travel between one and two miles depending on the position played, but not 10 miles. Additional evidence of inaccuracies has led S&C coaches at universities of similar sizes and athletic budgets as MSU to completely stop using any type of wearable technology. These peer institutions are recommending that other university athletic programs do the same and terminate wearable use for health and safety assessments associated with practice and training events.

3.1.1.2 From the Ground Up

The second piece of valuable information gained from the S&C coaches and AT interviews regarding wearable gaps revealed the need for information to be captured "from the ground up". According to responses from the I–Corp interviewees, current wearable technology does not provide accurate ground reaction force and ankle complex movement data. Determining ankle complex movement (especially in near real–ime to aid in health and safety-based decision making) has many benefits to both the athletic and rehabilitation industries, as the foot and ankle mobility influence total human movement [42]. Repeated lateral movement or excessive movement beyond normal range of motion of INV can lead to ankle sprains [38]. In addition, high and repeated forces occurring at the foot and ankle can be used to infer what happens at the knee and hip, which can lead to early fatigue and negatively alter postural control, resulting in biomechanical compensations that may cause injury [34]. A review of currently available wearable solutions further accentuates this ankle data gap. While a few solutions capture some information at the foot and ankle level, none of them capture absolute joint angles—meaning, no solution can give exact ankle movement values. In fact, few, if any, wearable solutions provide more than inferred joint angle data (ankle or otherwise) because angles are assumed based on limb segments. Devices proven to be inaccurate due to drift and other inconsistencies are also using inferences to make assumptions about generalized joint movements. The interviewees' concerns about both trust and a lack of data captured "from the ground up" come full circle based on information shown in Table 3.1. Thus, the need to develop wearable technology differently is clear and further emphasizes the need to utilize a technology ca-

pable of consistently capturing the strains and stressors at the ankle complex in order to provide data that may not be visually noticed by the S&C coaches.

Table 3.1 is an analysis of many of the movement-calculating wearable solutions available identified in the I-Corps interviews by S&C coaches as either having been used in the past, in use today by their institution or, at a minimum, of interest for potential consideration. Since many of these wearable technologies are new solutions and have not been validated in literature, much of the information had to be extracted from manufacturer websites as well as news and sports-related articles. In some cases, true capability and functionality were not clear; therefore, the authors had to default to promotional material claims and intellectual property definitions via patents. Much of the information about the devices' true functionality and data capturing granularity is vague at best, which is one of the reasons highlighted in the interviews for why a lack of trust among the users of the technology exists. While compiling Table 3.1 further emphasized the lack of trust gap, the completed version of the table also highlights the second gap, a lack of absolute measurements for any joint, including the ankle complex.

3.1.2 Dynamic Range of Motion and Sensor Placement

Due to the intricacy of the ankle complex, precise placement of sensors are required to obtain accurate kinematic data during movement. Ankle complex rotational components can be found within the talocrural, subtalar, and inferior tibofibular joints [38]. Given the anatomical design of the ankle joints, movement of the foot during open kinetic chain in PF and DF do not occur in a single sagittal plane [116]. During PF, the foot moves 28 degrees

Table 3.1: Wearable solution capability comparison. R = RFID Tags. T = Total Distance. Z = Z-axis only. A = Average Value. DP = Developmental Platform. H = Hydrocell Technology. CF = Conductive Fibers. GPS = Global Positioning System.

		Kinematic Measures					Kinetic Measures				Hardware				
		Symmetry	Step/Jump Count	Inferred Joint Angles	Absolute Joint Angles	Limb Segments	Intensity& Load	Ground Reaction Force	Shock/Impact Force	Pressure	Accelerometers	Magnetometers	Gyroscopes	GPS	Dielectric Elastomers
Catapult [63, 29, 105]	IMU	×	×				×		×		×	×	×	×	
Zephyr [123, 44, 49, 36]	IMU		×				×		×		×			×	
IMeasureU [82]	IMU	×	×	×		×	×		×		×	×	×		
Zebra [120, 119, 101, 16]	RFID		T				×				R				
[86, 103, 122]	RFID		T				×				R				
STATSport [96, 121]	IMU		×				×		×		×	×	×	×	
ADPM [6]	IMU	×	×	×		×	×		×		×	×	×		
TekScan[85]	Insole		×				×		×	×					×
Shimmer Sense [2]	DP		×	×		×	×		×		×	×	×		
zFlo-Motion [71]	Insole		×				×	Z	×	×	×				×
Novel Pedar [41]	Insole & DP		×				×		×	×					×
DorsaVi [14]	IMU			×		×		A	×		×	×	×		
BioStamp [65]	IMU & R&D		×	×		×			×		×		×		
Heddoko [21]	IMU Garment		×	×		×					×	×	×		×
GaitUP [91]	IMU		×	×		×			×		×	×	×		
Motus [106]	IMU		×	×		×	×				×		×		
Notch [74]	IMU & DP			×		×					×	×	×		
Noitom [56]	IMU & DP			×		×					×		×		
Xsens[125]	IMU	×	×	×		×	×		×		×	×	×		
G-Vert [62]	IMU	×	×				×		×		×		×	×	
LegSys [72]	IMU		×	×		×					×	×	×		
paroTec [15]	Insole	×	×				×		×	×					H
Sensoria [23, 68]	CF	×	×					×	×	×	×				
[94, 64]	CF	×	×					×	×	×	×				

in the sagittal plane, one degree in the transverse plane, and four degrees in the frontal plane [38]. Likewise during DF, there are 23 degrees of movement in the sagittal plane, nine degrees in the transverse plane, and two degrees in the frontal plane [38]. Unlike previous research on comparisons of IMUs for optimal motion capture which both ignore internal and external rotations and INV and EVR [92], this study looks at the viability in using SRS to capture all movement in all three planes.

An important aspect of this investigation is the consideration for placement of these sensors in order to optimize measurements of complex ankle movements. Previous work by Mengüç et al. [66] has evaluated the sensor placement at the posterior part of the ankle and heel, extending from the distal aspect of the gastrocnemius muscle complex down to the calcaneous, which has shown positive results in sagittal plane movements (coefficient of determination 0.9680). To capture tri-planar ankle joint movement, one sensor was placed parallel to the distal 1/3 aspect of the fibula, overlaying the lateral malleolus to capture INV and EVR. Second, vertically in–line with the distal 1/3 aspect of the tibia onto the superior aspect of the talus and a third sensor was positioned perpendicular to the 23 degree axis of INV [38]. This research provides a starting point for where sensors should be placed in order to effectively capture full range of ankle motion.

With a clear goal identified (capture data "from the ground up") and a potential replacement IMU sensor direction found, the aim of this study is to evaluate the use of resistive SRS at the ankle complex movement level. Determining ankle complex movement in near real-time has many benefits to both the athletic and rehabilitation industries, as the foot and ankle mobility influence total human movement [42]. As repeated lateral movement or ex-

cessive movement beyond normal range of motion of INV can lead to ankle sprains [38], applying resistive SRS at the ankle joint complex may provide information to coaches, trainers, and therapists in preventing over-use injuries and validate proper ankle rehabilitation training exercises. The goal of this paper is to show that SRS have the potential to usher in a new type of wearable that is not limited by the difficult challenges created by IMUs such as drift. Liquid Wire sensors were selected for this study given their resistive properties, the researcher's access to different substrate types, and the ability to custom order sensors with specific resting resistances and lengths. Based on the goals and limitations above, the contributions of this paper are as follows:

- Liquid metal sensors (specifically those manufactured by Liquid Wire [54]), which are designed for soft-robotics applications, are experimentally shown to be suitable for capturing ankle complex movements for DF, PF, INV, and EVR.
- A simple microprocessor-based computing unit prototype designed to accurately measure the Liquid Wire sensors resistances is provided.
- Liquid Wire sensors, which vary their resistance under stretching, are experimentally shown to provide a linear relationship versus stretching distance and temperature.
- Linear regression models were used to relate the resistance measurements into ankle angle measurements.
- A detailed summary of the state-of-the-art in wearable solutions is provided which shows that there currently is not another wearable solution capable of making ankle measurements (Table 3.1).

The remainder of this paper is organized as follows. Section 3.2 provides information on experimental materials and methods. Section 3.3 discusses experimental results. Section 3.4 draws conclusions and lists the researchers' future work pursuits.

3.2 Materials and Methods

This section discusses materials and methods for (a) testing the Liquid Wire sensors; (b) testing the dynamic range of motion; and (c) estimating angles from the Liquid Wire sensors. Results and conclusions from these tests are discussed in Sections 3.3 and 3.4, respectively.

3.2.1 Liquid Wire Testing

In order to prove that the Liquid Wire sensors are a viable tracking solution, the researchers conducted several experiments to verify that the sensor output changed linearly with stretched length, regardless of temperature, and that the sensor could be feasibly utilized in a microcontroller-based system.

3.2.1.1 Testing Goals

The goals of the Liquid Wire testing were to (a) validate that the Liquid Wire sensor is linear in resistance versus stretched length; (b) validate that the Liquid Wire sensor is linear in resistance versus stretched length at various temperatures; and to (c) validate that the Liquid Wire sensor's resistance could be accurately measured in a microprocessor-based solution.

3.2.1.2 Equipment

Test equipment is shown in Table 3.2. Table 3.3 lists the bill-of-materials for the computing unit.

Table 3.2: Test Equipment for Liquid Wire Testing.

Component/Purpose	Manufacturer	Model
Clamps—hold test article	Irwin	Quick-Grip 3″ clamps
Drill Press—stretch test article	Irwin	4″ Drill Press Vise
Micro-Ohm meter—validate computing unit	Agilent/Keysight	34420A
Digital multimeter—validate computing unit	Fluke	179
Liquid Wire sensors—test articles	Liquid Wire	Various
Hand-held temperature sensor—monitor test article temperature	Etekcity	1080
Ankle complex model—test sensor linearity	Custom	Ankle test fixture
Blow dryer—heat test article	Conair	146RX
Digital Caliper—measure test article stretch	Tritan	0344621
DC Benchtop Power Supply—power circuit for testing	Extech	382213

Table 3.3: Equipment bill of materials for the prototype computing unit.

Manufacturer	Model	Description
Arduino	Uno R3	Microprocessor
RexQuails	RQ-RK-001	Resistors
CTYRZCH	4330118083	16 Bit I2C ADS1115 4-channel Analog–to–Digital Converter Module
Jameco ValuePro	20812	Solderless Breadboard
Elenco	JW–350	Pre–formed Jumper Wire Kit
Elegoo	EL–CP–004	Breadboard wire set for Arduino
Cable Matters	200001–BLK–10x3	USB 2.0 A–to–B Printer Cable, 10 feet

3.2.1.3 Test Procedure

An apparatus was constructed to take measurements from the Liquid Wire sensors at various stretched lengths. In order to stretch the sensor in a stable and consistent manner, an IRWIN four-inch drill press vise was mounted on top of a table. Two IRWIN QUICK–GRIP three-inch clamps held down each end of the Liquid Wire sensor to an end of the vise. Care was taken to not over–tighten the clamps so as to not damage the test article. A digital caliper was used to measure the length of the segment of sensor being stretched. A screw located on one side of the vise was used for adjusting one side of the vise and was used to consistently stretch the Liquid Wire sensor. Figure 3.1 shows the test fixture in the Sensor Analysis and Intelligence Laboratory (SAIL) facility. The Liquid Wire sensor is the dark band highlighted near the bottom of the figure. The caliper measuring the sensor length is also highlighted. By turning the vice screw, the sensor length can be carefully adjusted.

Linearity Testing For the first experiment, two benchmark methods for measuring resistance were used to determine if there is a linear relationship between resistance and stretch length. The methods used were: (a) a Micro-Ohm Meter, which is the lab standard in measuring resistance; and (b) a Wheatstone bridge circuit, which is a very accurate and common circuit used for measuring resistance. These two methods were evaluated and compared against each other to decide which one would be used for the remaining experiments. For the first method, an Agilent Micro-Ohm Meter was connected directly to the Liquid Wire sensor to measure its resistance. The Liquid Wire sensor was mounted on the

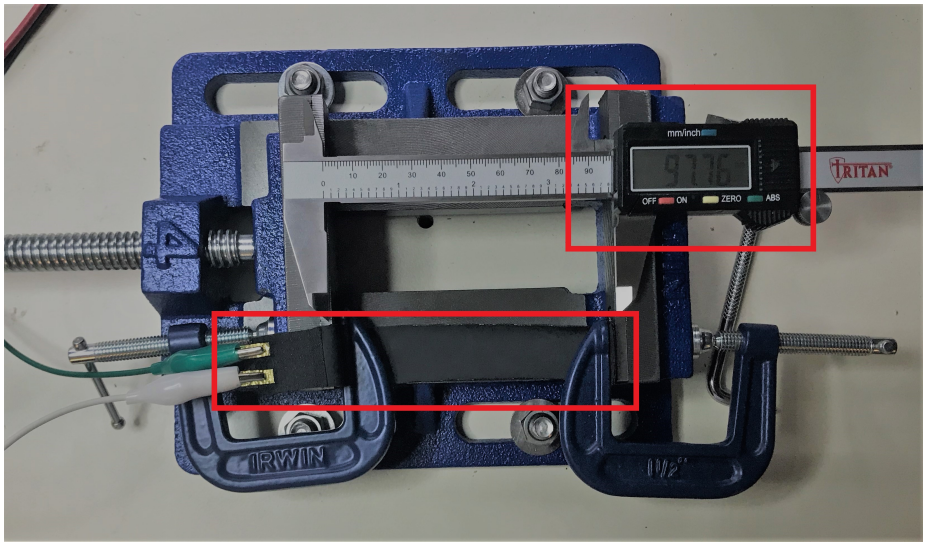

Figure 3.1: Picture of Liquid Wire test fixture. Liquid Wire sensor and digital caliper highlighted.

testing apparatus, and the screw was turned in 180° intervals. At each interval, the resistance and length of the sensor was measured. This was done until the sensor was stretched to approximately 20 mm longer than its original length.

The same process was then repeated for the Wheatstone bridge circuit. For this method, three 10 Ω resistors were soldered together. Care was taken to identify these resistors as R_1, R_2, and R_3, similar to the schematic shown in Figure 3.2. The Micro-Ohm meter was used to record precise measurements of the three resistors to be used in calculations. Alligator clamps were used to connect the Liquid Wire sensor to R_2 and R_3. A power supply (V_{supply}) was connected and set to 0.5 V to reduce current draw through the resistors. The positive end was connected to the node between R_1 and R_3, and the negative end was connected to the node between R_2 and the Liquid Wire sensor. A multimeter was then connected at

the node between R_1 and R_2 and the node between R_3 and the Liquid Wire sensor, and these nodes are labeled as V_{12} and V_{34} in Figure 3.2, respectively. A voltage measurement $V_{measured}$ was taken from the multimeter to determine the difference between these two nodes. These values were used to determine the resistance with Equations 3.1 and 3.2, where all resistances have units of Ohms. The complete derivation for these equations can be found in Appendix A.1.

$$\alpha = \frac{V_{measured}}{V_{supply}} + \frac{R_2}{R_1 + R_2} \tag{3.1}$$

$$R_{LiquidWire} = \frac{R_3 * \alpha}{1 - \alpha} \tag{3.2}$$

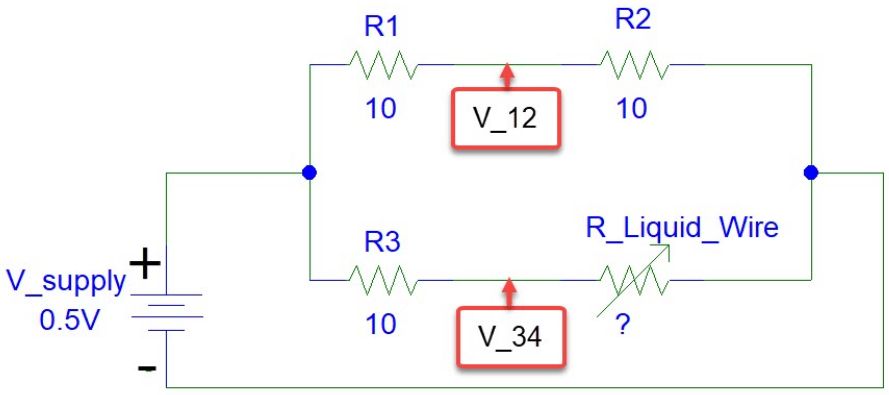

Figure 3.2: Schematic diagram of Wheatstone bridge circuit. Resistances are in Ω.

The benefits of using the Micro-Ohm Meter is its level of precision and the ease of setup as circuit construction was not required to get sensor measurements. Moreover, measurements from this very accurate device were used to validate the prototype computing

unit's measurements. However, this method was not without issue. Due to the way the device calculated the sensor's resistance, there was inherent drift in the measurements. Also, the resistance was updated about once a second, therefore, measuring with this method would not work in a real-time application. The change in resistance was still linear, but it was difficult to get a consistent measurement, since the Micro-Ohm Meter would slightly change the value displayed soon after stretching the sensor. While the multimeter output for the Wheatstone bridge circuit did not provide the same level of precision as the Micro-Ohm Meter, it still provided a more consistent reading for the researcher to record. This was important for consistently collecting data in the remaining experiments.

Results for both of these methods are discussed in Section 3.3.1.1. Based on the issues described related to taking measurements with the Micro-Ohm Meter, the Wheatstone bridge circuit was selected as the method of measurement to be used for the remaining experiments described in this section as well as the static model testing described in Section 3.2.2. During this experiment, the researchers noted that the connections to the sensor leads were getting damaged. After consulting with Liquid Wire, the company stated that a sensor would not work reliably and could potentially be damaged if stretched 20% beyond the sensor's original length.

Lastly, a constant current voltage divider circuit was constructed to take measurements. This simply involved a 10 Ω resistor that was placed in series with a Liquid Wire sensor. By supplying a constant current of 0.1 amps and measuring the voltage across the Liquid Wire sensor with a multimeter, Ohm's Law can be applied to determine the resistance.

$V_{measured}$ is defined as the voltage measured from the multimeter. I_{supply} is defined as the current being driven from the power supply. The schematic is shown in Figure 3.3.

$$R_{LiquidWire} = \frac{V_{measured}}{I_{supply}} \tag{3.3}$$

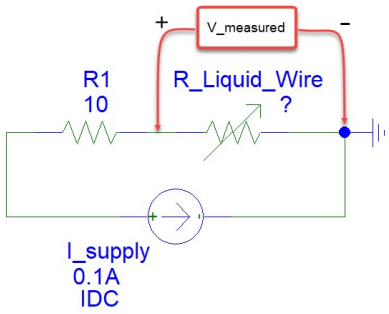

Figure 3.3: Schematic diagram of constant current voltage divider circuit.

Temperature Testing In order to verify that the Liquid Wire sensor output remained linear against stretched length regardless of temperature, the same testing apparatus was arranged as described in Section 3.2.1.3 using the Wheatstone bridge circuit. Two types of Liquid Wire sensors were used, each with a different substrate: one with a TPU (thermoplastic polyurethane) coated proprietary liquid metal, and one with a silicone covering. The different types were chosen for this particular experiment to evaluate whether or not substrate had an effect on resistance at different temperatures. Data was collected for four different stretched lengths of the sensor. This data was first collected with the sensor at

room temperature. Afterwards, a heat gun was used to heat the sensor up to 80°F. A hand-held temperature sensor was used to monitor sensor temperature and make sure that it was maintained at the same temperature. Data was then collected, and the temperature was verified and corrected at each stretched length. This process was completed one last time at 98°F, to simulate the surface temperature of the human body's skin. Results from this experiment are discussed in Section 3.3.1.2.

Microprocessor Testing A microprocessor-based prototype, also known as the computing unit, was constructed to validate the potential for the sensor data to be collected in real-time. This prototype was designed to take measurements from the various types of sensors that were supplied by Liquid Wire, which would also be used for future research experiments (See Future Work in Section 3.4.2). Table 3.4 provides several examples of sensors that were tested, which are also pictured in Figure 3.4. The researchers first designed the prototype using an Arduino Uno R3, an ADS1115 16–bit Analog–to–Digital Converter (ADC) Module, and the previously described Wheatstone bridge circuit. The ADC module was able to pick up small changes in voltage due to its high precision voltage reading, which was useful for increasing sensitivity to changes in stretched length of the Liquid Wire sensor. This module was able to collect even more precise data through the use of its built–in programmable gain amplifier (PGA), which could amplify small signals to provide even more sensitivity to sensor output changes. It essentially replaced the multimeter used in the previous experiments, as it took the difference in voltage measurements between nodes V_{34} and V_{12} and transmitted a corresponding analog value to the micropro-

cessor over I^2C. The Wheatstone bridge circuit and ADC module were powered by the 3.3 V source from the Arduino Uno. Due to the higher voltage supply, the 10 Ω resistors were replaced with 100 Ω resistors to reduce current flow through the circuit. An extra 100 Ω resistor was placed in series with the leg of the Liquid Wire sensor to keep the bridge closer to being balanced. The microprocessor communicated with a laptop over a serial connection and provided output that indicated the current resistance of the Liquid Wire sensor.

Table 3.4: Liquid Wire Testing Article Specifications.

ID	Substrate	Length (mm)	Resting Resistance (Ω)
A	Thermoplastic Polyurethane	202	30.0
B	Thermoplastic Polyurethane	209	44.1
C	Silicone	165	6.0
D	Thermoplastic Polyurethane	107	13.6

While testing the prototype with different sensors, the researchers encountered an issue with reaching a peak amplified voltage due to the differences in resting resistances (resistance measured without stretching) between the Liquid Wire sensors. These resting resistances ranged from roughly 5 Ω to 45 Ω. To prevent this issue, either the gain of the amplifier had to be reduced or the values of the resistors in the Wheatstone bridge had to be increased. Furthermore, this would come at the expense of losing levels of voltage mea-

surements, also known as bins. In practical terms, when correlating sensor readings to joint angles, the prototype would lose precision when estimating angles in future experiments if the circuit was not physically changed. Due to this issue, the researchers investigated replacing the Wheatstone bridge circuit with a voltage divider circuit, which was determined to be a simpler and more flexible method for measuring sensors of varying resistance. An added benefit to the voltage divider circuit was that four sensors could be measured at the same time instead of two, since the ADC module would only need to measure the voltage measured at one node V_1 in Figure 3.5.

The data shown in Figure 3.6 taken from Personal Simulation Program with Integrated Circuit Emphasis (pSPICE) provides further justification for this design choice. The simulation performed shows the range of bins that correlate to the given range of resistances that was stated previously. The simulated Wheatstone bridge circuit used 100 Ω resistors at each leg with a variable resistor in series with one of the legs to emulate the Liquid Wire sensor. An instrumentation amplifier was connected to nodes V_{34} and V_{12} to emulate the PGA functionality of the ADC module taking a differential measurement. The simulated voltage divider circuit used a 150 Ω resistor in series with a variable resistor. A non-inverting operational amplifier was connected at node V_1 between the 150 Ω resistor and the variable resistor to emulate the PGA functionality of the ADC module taking a single-ended measurement. In simulation, the gain was set to 4 volts per volt (V/V) for both circuits. At a range of 5 Ω to 40 Ω for the variable resistor, the voltage divider circuit provided 74,421 bins for measurements, while the Wheatstone bridge circuit provided 57,856 bins. When factoring in that the Wheatstone bridge loses linearity in measuring

voltage around 32 Ω, the realistic amount of resolution provided is closer to 50,390 bins. The fact that the circuit provides less resolution and still fails to take reliable measurements after a certain threshold indicates that the voltage divider circuit is the better choice for the prototype. A picture of the computing unit and a block diagram describing the design are shown in Figure 3.4. The design change for the computing unit's circuit design is depicted in Figure 3.5.

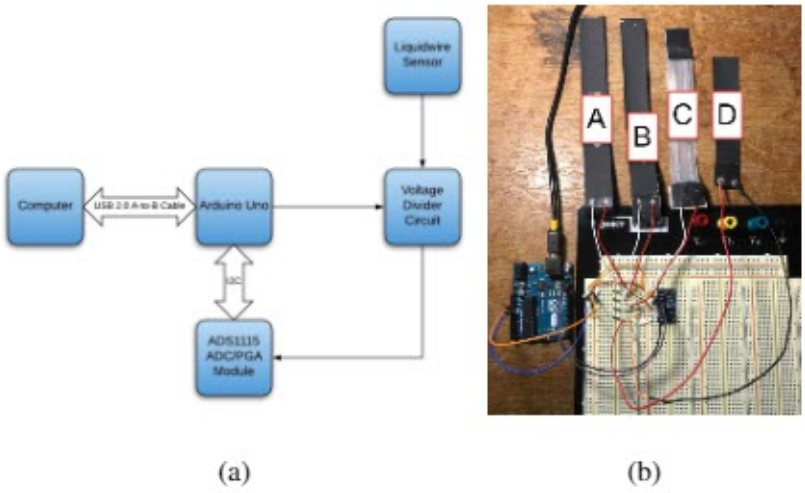

Figure 3.4: Microprocessor prototype. (**a**) Computing Unit block diagram; (**b**) Computing unit with various Liquid Wire sensors connected.

After re-designing the prototype, the voltage divider circuit replaced the Wheatstone bridge circuit to validate the accuracy of the computing unit. The same test procedure described in Section 3.2.1.3 that was used for validating linearity of the Liquid Wire sensor was conducted using the computing unit as a method of measurement. The data collected

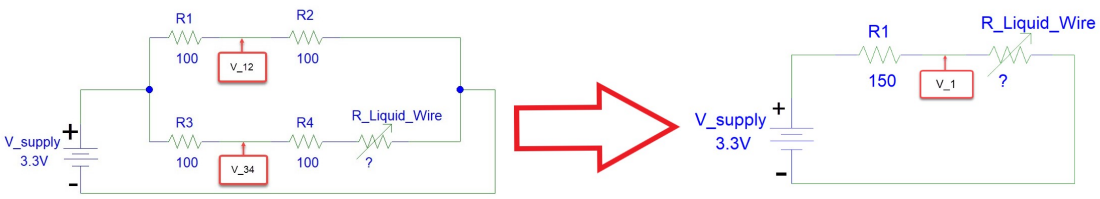

Figure 3.5: Computing unit circuit design change from Wheatstone bridge to voltage divider.

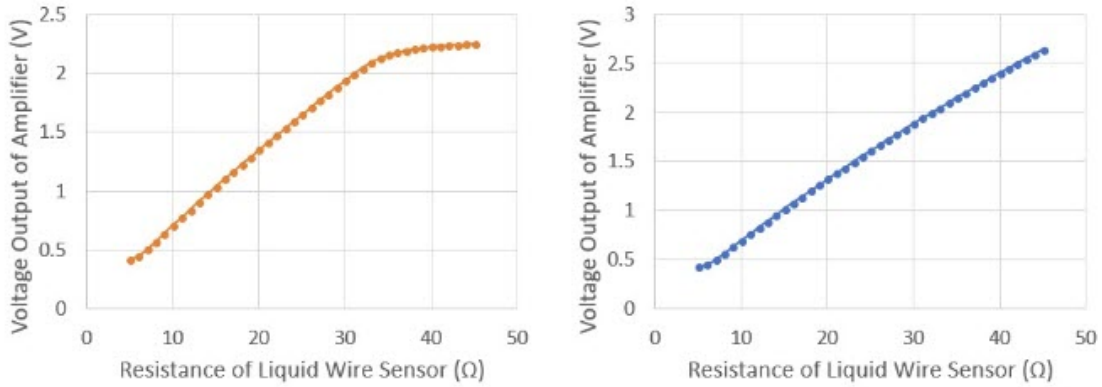

Figure 3.6: Comparison of range of voltage levels (bins) that can be used for taking measurements at various sensor values. Note that sensitivity of change decreases for the Wheatstone bridge at about 32 Ω. (**a**) Wheatstone bridge measurement range; (**b**) Voltage divider measurement range.

from the computing unit was compared to data collected with the Micro-Ohm meter to validate accuracy. Results are discussed in Section 3.3.1.3.

3.2.2 Static Model Testing

The human ankle complex is comprised of three joints: the talocrural joint, the subtalar joint, and the distal tibiofibular joint, which is a syndesmosis joint [38]. This allows the foot and ankle to move in multiple planes of motion as needed for walking, running, and athletic movements. Modeling of the ankle complex has provided basic descriptions of foot movement in PF, a downward movement of the foot; DF, an upward movement of the foot; EVR, an outward movement of the bottom of the foot; and INV, an inward movement of the bottom of the foot. Using these four measures of ankle complex movement has been shown to be effective in studying the differences in passive and active joint movement [42].

To understand the sensor output's relationship to the ankle joint movement, a model of the human ankle was constructed of $2'' \times 4''$ pine and $3/8''$ rubber flooring material securely screwed into the wood, allowing for angular rotation in the sagittal and frontal planes as derived from a previous model used in the literature [28]. The sensor was then attached to the model using toupee double sided tape and reinforced with an overlapping elastic band to secure and create two anchor points. Upon attachment, the sensor was stretched slightly. To measure the degrees of PF and rotation, two smartphones were calibrated using a carpenter's bubble level running the RIDGID Level iOS application. The smartphones were securely attached to the model via elastic bands and phone mount. An electronic goniometer was used to validate the measurements from the smartphone. Using smartphones

allowed for validation of accurate measure for the degrees of movement compared to the hand placement of the electronic goniometer on the model for each change in position. The movement of the model foot was performed by one experimenter while a second experimenter read and recorded the voltage output from a multimeter. A TPU-based sensor and a silicone-based sensor were used for this study. Markings on the model allowed for consistent placement of the different Liquid Wire sensors.

3.2.2.1 Testing Goals

The goals of the model testing were twofold: (a) to capture changes in resistance of the Liquid Wire sensors relative to simulated ankle complex movement and (b) to evaluate the different substrates in capturing simulated ankle complex movement. Previous bench testing provided insight into the linearity of the Liquid Wire sensors; the focus of this portion of the study is on consistent linearity occurring in simulated joint rotation.

3.2.2.2 Equipment

The ankle model was constructed of a 1/2″ wooden base with a vertical wooden 2″ × 4″ spine screwed to the base. Two additional 2″ × 4″'s were used, allowing for the flexible flooring to be securely screwed to the bottom 2″ × 4″. The additional 2″ × 4″ was placed on top of the flooring material and secured by screws into the 2″ × 4″ spine. Another 2″ × 4″ was attached to the top of the flooring material which represented the foot. Images of the model are shown in Figure 3.7. The sensor was connected to a Wheatstone bridge circuit that was arranged as described in the Linearity Testing portion of Section 3.2.1.3.

(a) (b)

Figure 3.7: Pictures of the ankle model mockup. (**a**) Measurements taken with goniometer; (**b**) Measurements taken with smartphone levels.

3.2.2.3 Test Procedure

Two researchers compiled the data onto a Microsoft Excel formatted sheet. After properly applying and securing the sensor with toupee tape and an anchor strap, and mounting the smartphones onto the model, one researcher moved the model's foot and called out the number of degrees of movement. The second researcher then recorded the multimeter output onto the Excel sheet. After recordings were taken, calculations were run based on the previously given Equations (3.1) and (3.2) to determine the resistance of the Liquid Wire sensor.

3.3 Results and Discussion

This section discusses the results of the Liquid Wire TPU and Silicone sensors conducted in Section 3.2 (a) the bench testing on linearity; (b) temperature testing; and (c)

changes in resistance during a static positioning representing PF, INV, and EVR on the ankle model.

3.3.1 Liquid Wire Testing Results

The following three subsections discuss the results gathered and their relevance to the testing goals (a), (b), and (c) as defined in Section 3.2.1.1.

3.3.1.1 Linearity Testing Results

The results in Figure 3.8 address testing goal (a) of Section 3.2.1.1, which was to validate that the Liquid Wire sensor was linear in resistance versus stretched length. Linearity in stretched length was evident for both the Micro-Ohm Meter and the Wheatstone bridge circuit. Figure 3.8 depicts linearity test data collected for each method as well as their coefficient of determination values.

3.3.1.2 Temperature Testing Results

Next, testing goal (b) of Section 3.2.1.1 was addressed, which was to validate that the Liquid Wire sensor was linear in resistance versus temperature. Based on the data gathered, temperature did not have a drastic effect on the linearity of strain on the Liquid Wire sensors. However, one interesting result was that temperature did appear to have an effect on the TPU sensor's resistance overall, as the values measured increased with temperature. Based on the data collected from the silicone sensor, there appeared to be minimal correlation with resistance and temperature. This finding is important when considering tying resistive values to the tracking of movement on the human body. If the TPU sensor is

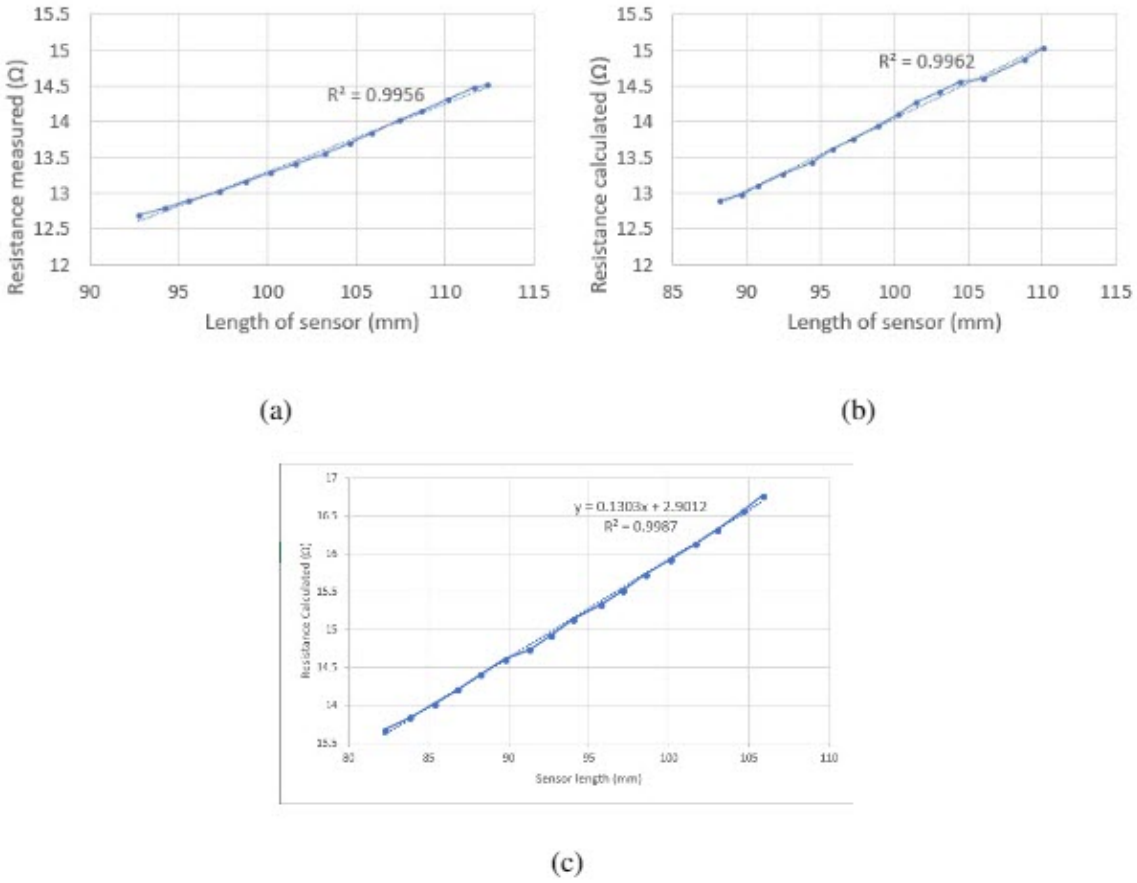

Figure 3.8: Data collected for linearity testing for resistance versus the stretch length. (**a**) Micro-Ohm Meter results; (**b**) Wheatstone bridge results. (**c**) Constant Current results.

used, extra temperature sensing may be needed to correct an increase in resistance value if the sensor's temperature is affected by the human's surface body temperature. Results are shown in Figure 3.9.

3.3.1.3 Computing Unit Testing Results

Finally, the computing unit prototype was compared against a Micro-Ohm meter to satisfy testing goal (c). The prototype constructed for taking measurements of the Liquid Wire sensor proved to be a viable solution. An average percent error of 1.55% was calculated between the measurements taken from the computing unit and the Micro-Ohm meter. This could have been due to the calculations performed by the microprocessor, or from researcher error when resetting the linearity testing apparatus. Results are shown in Figure 3.10. These results show that the computing unit is very close to measurements of a high–accuracy, laboratory unit.

3.3.2 Estimating Angles from Liquid Wire Measurements Testing Results

To test the linearity of both the Liquid Wire TPU and Silicone sensors, the model was moved and held at specific, static degrees representing human ankle complex PF. This resulted in the degree of PF as the independent variable and sensor resistance as the dependent variable. Using a regression analysis comparing the change in sensor resistance when stretched due to changes in increasing ankle model's PF resulted in the development of two mathematical models. The significance level was set at $\alpha = 0.05$ for all of the analyses. The Fit Regression Model analysis (MiniTab18 Statistical Software, USA), revealed the regression models for the Liquid Wire TPU (Equation (3.4)) and Liquid Wire silicone

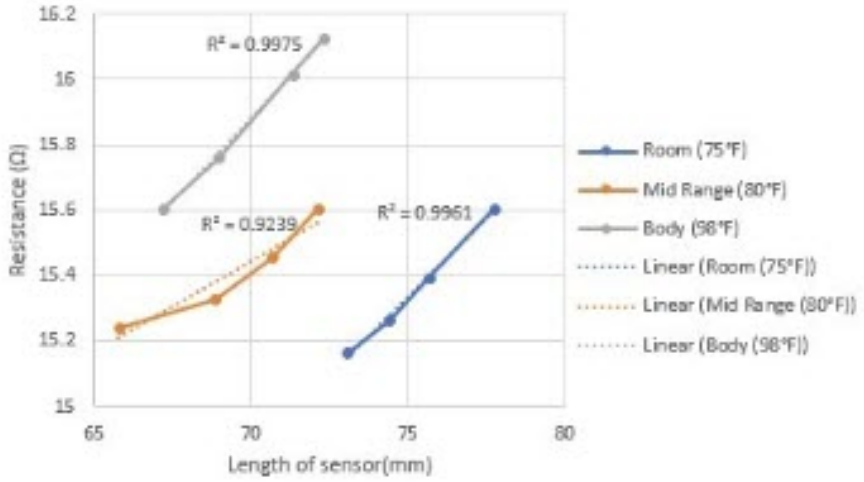

(a)

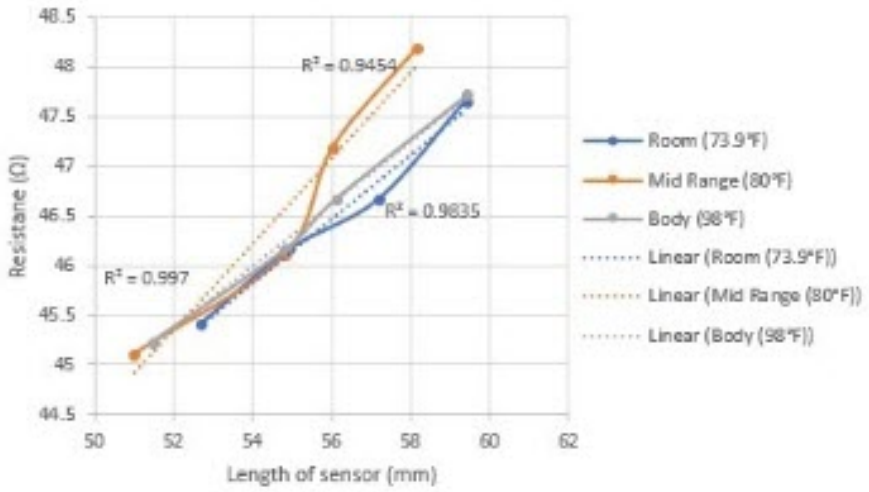

(b)

Figure 3.9: Data collected for temperature testing for resistance vs length stretched. (**a**) TPU; (**b**) Silicone.

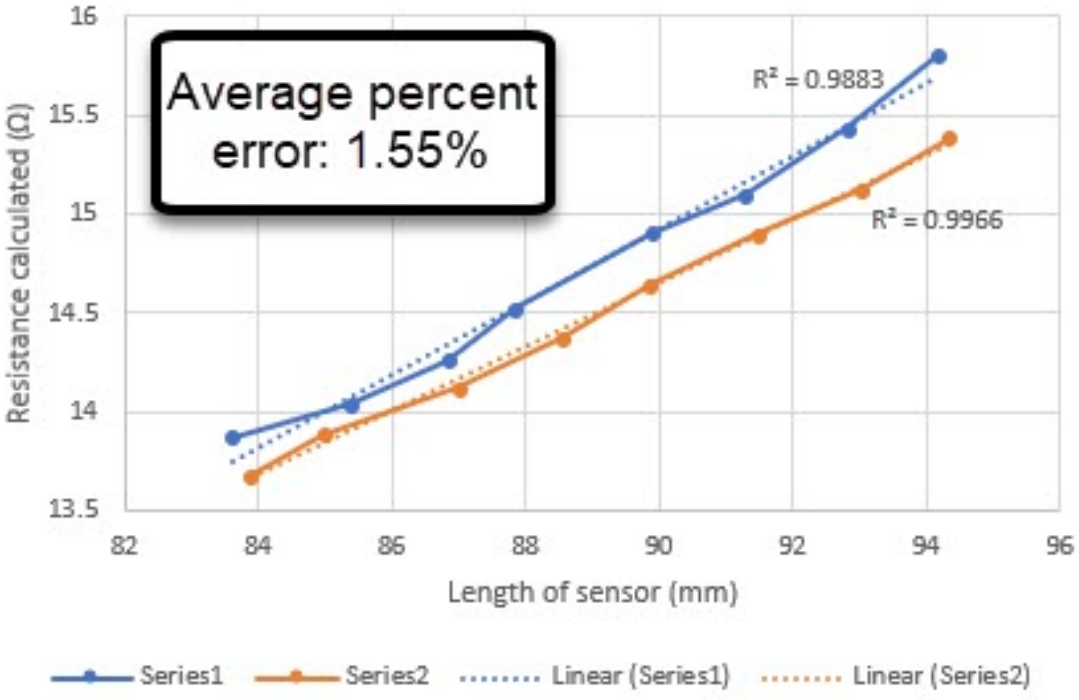

Figure 3.10: Comparison of Computing Unit and Micro-Ohm meter measurements collected.

sensor (Equation (3.5)), which produced linear models with coefficients (p–value ¡0.001). Thus, the model provides the expected value of sensor resistance in Ohms when varying degrees of D, which is angle of PF in degrees. R_{TPU} is the resistance estimate for the TPU sensor, and R_{SIL} is the resistance estimate for the silicone sensor, respectively. The rotational aspect of the model resulted in almost equal changes in resistance of the sensors. This provided insight into the requirement of using multiple sensors to assess ankle INV and EVR. Due to the symmetry of the change (Figure 3.12), it would not be possible for the software to determine whether the change in resistance was INV or EVR. In future human trials I will assess changes in degrees of ankle complex movement from specific ranges of sensor resistance. Measurement results of the Liquid Wire sensor are shown in Figure 3.11 and Figure 3.12.

$$R_{TPU} = 10.9831 + 0.01142D \tag{3.4}$$

$$R_{SIL} = 6.2922 + 0.05194D \tag{3.5}$$

3.4 Conclusions

The purpose of this research was to find a way to mitigate some of the concerns regarding wearable technology identified by the SMEs interviewed in response to the NSF I–Corp project. The first noted concern was the lack of wearable solutions that capture data "from the ground up" and provide meaningful data about the ankle complex. The researchers addressed this concern by focusing on a sensor-based solution that could accurately capture movement of the ankle complex. The second concern voiced by the SMEs was their lack of trust for existing wearable solutions. The identification of this trust issue is accompa-

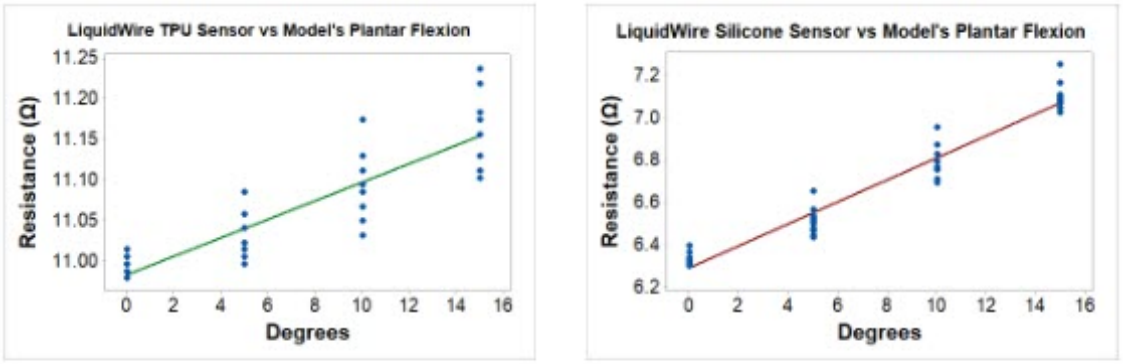

(a) (b)

Figure 3.11: Liquid Wire TPU and Silicone sensor measurements and model results. (**a**) Change in resistance of TPU sensor relative to angle of PF on model during multiple static testing trials. (**b**) Change in resistance of silicone sensor relative to angle of PF on model during multiple static testing trials.

nied by research in literature as there are known concerns with IMU drift and the need for calibration of wearable equipment. To address this concern, the research team investigated liquid metal sensors to determine if they would be an appropriate measurement option in future wearable solutions. The researchers wanted to learn if liquid metal sensors could be utilized to capture absolute joint angles as opposed the inferred joint measurements that are present in most wearable solutions available during the time of this study. For this reason, Liquid Wire sensors were selected.

In order to test the Liquid Wire sensors, basic tests were performed to validate the linearity of the sensors using two methods: (a) Micro-Ohm Meter and (b) Wheatstone bridge. The results of both methods concluded that the Liquid Wire sensors show a linear correlation between the increase in stretch of the sensor and the increase in resistance. Linearity of

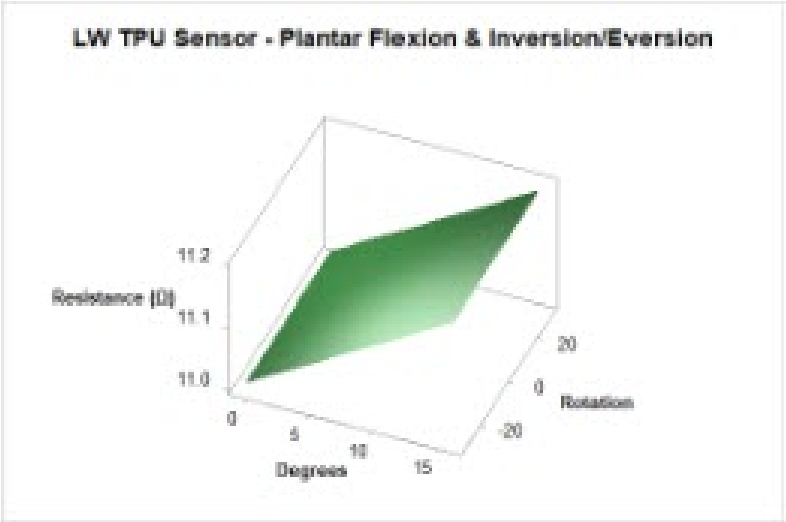

(a)

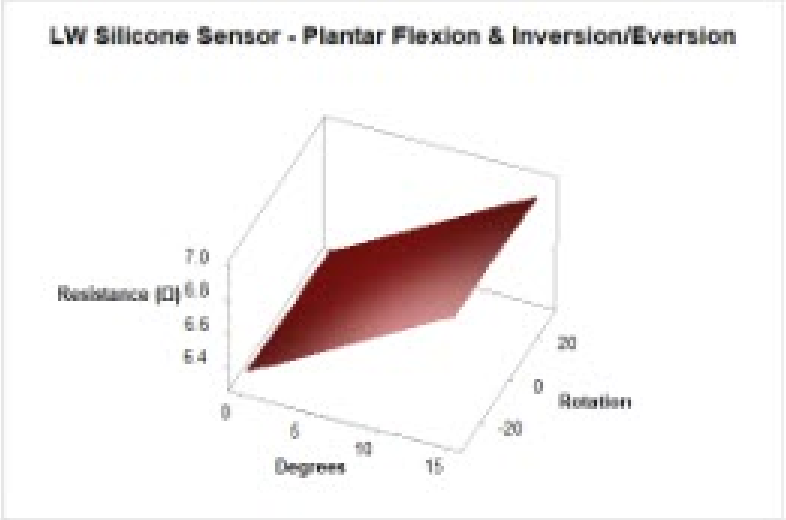

(b)

Figure 3.12: Liquid Wire TPU and Silicone sensor measurements and 3D surface plot results. (**a**) 3D surface plot results of PF, INV, and EVR with single TPU sensor. (**b**) 3D surface plot results of PF, INV, and EVR with single silicone sensor.

the Liquid Wire sensor was tested across different temperatures with the expectation being that these sensors would be located within adjacent materials, creating additional frictional heat, therefore becoming warmer than room temperature. Also, Liquid Wire sensors comprised of different substrates were tested for linearity at different temperatures with the similar expectation that they must be comfortable to the wearer, as the sensors may be embedded in or on top of material that is in close contact with the skin and therefore different materials may offer different comfort. Linearity remained consistent regardless of temperature or substrate. This is important to know as the the sensor could be closer to room temperature at the beginning of an exercise and closer to body temperature as the exercise progresses so compensating for different resistance values will be important for correctly and consistently correlating ankle complex movement to sensor outputs. For future data collection, a computing unit was built to collect resistance values. This computing unit was validated against a Micro-Ohm Meter to insure accuracy and consistency of the readings. It was determined that the voltage divider circuit is more practical than the Wheatstone bridge at this time, since I don't currently have a consistent resting resistance to work with. Furthermore, using the voltage divider reduced the size of my circuit and allowed me to measure more sensors at the same time with the ADC module, which could end up working in my favor for future product hardening.

To further test Liquid Wire capability in the context of ankle complex movement, a model of the human foot and ankle was constructed to provide a platform on which to attach the sensor and test for very specific human movements such as PF. With the aid of the ankle complex model, both substrates were tested while performing the PF motion and

both TPU– and silicone-based sensors were found to have a significant relationship between the positional change and the resistance values therefore confirming that the Liquid Wire solution is effective for accurately capturing these types of movements.

The results of the study ultimately confirm the researchers' hypothesis that liquid metal sensors, and Liquid Wire sensors specifically, can serve as a mitigating substitute for IMU-based solutions that attempt to capture specific joint angles and movements. The solution that the researchers have begun to design based on this Liquid Wire-based ankle complex wearable concept will be effective in overcoming the primary concerns identified by the SMEs that use wearable technology in athletic and training environments.

3.4.1 Limitations

To the knowledge of the researchers performing this study, this research was the first of its kind; therefore, limitations were identified during the discovery process. First, the Wheatstone bridge circuit used to power the sensors and capture sensor resistance exhibited small levels of noise causing minimal variations in voltage output at the time of data capture readings. Creating a printed circuit board (PCB) for future research will help to solve this problem by reducing the sensitivity of the analog signal to noise. The Liquid Wire sensors themselves did not appear to contribute to the noise in the measurements and so a PCB solution should mitigate this problem.

Second, because a wooden model of the ankle complex was used and not a real human ankle, there were limitations in the ability to capture certain movements such as DF. In order to capture DF, the sensor needed to be fastened to the wooden model in such a way as

to keep the Liquid Wire sensor in a stretched position so that a reduction in resistance could be measured as the "foot" was lifted back and toward the "shin". However, if the sensor's position begins at rest and no stretching is applied to the sensor, then the resistance value will not change and therefore will not be representative of movement changes. Beginning trials with the Liquid Wire sensor in a stretched state posed an issue for the researchers because of the length of the sensor and the rigid nature of working with the wooden model that led to stretching the sensor beyond its 20% stretch limitations. This over-stretching often resulted in a damaged sensor or damaged sensor terminals. For this reason, DF has to be demonstrated by a reverse of the methods used to test PF which prove the capability of the sensor in that it remains linear as the stretch state is removed but is not representative of real DF movements. Furthermore, due to the sensor being set in a stretched state and the method by which it was mounted, there would sometimes be slippage at the point at which it was mounted. Since the sensor output is also sensitive to change based on pressure, this caused variation in the resistance measurements taken at each angle for PF. The researchers believe that the dimensions of the wooden model versus the dimensions of a real ankle complex attribute to these challenges. This measurement was also difficult to make because only one sensor was used, leading to the next limitation.

Third, ankle complex movements are complicated and three–dimensional in nature. Only using one sensor to take measurements limited the movements that could be studied. For example, INV and EVR occur when the foot is turned either inward or outward respectively. A single Liquid Wire sensor is able to determine (through an increased resistance value) that movement at the ankle has occurred when an INV or an EVR movement is

made. However, the sensor cannot differentiate between these two movements. Likewise, when a PF movement is combined with either an INV or EVR movement, there is no way to differentiate between the amount of stretch caused by the PF version verses the other movement. Multiple sensors are needed to identify direction and magnitude of the ankle complex movement.

Lastly, an important lesson learned on the part of the experimenters is the desire for consistent and common resting resistances (resistances when the liquid metal sensor is not stretched) for the Liquid Wire sensors. While all sensors were linear in their movement–to–stretch resistive output, not all sensors held comparable resistance values at rest. Due to the variation in resting resistances, a more flexible circuit was required, but this will add more complexity to the programming for the computing unit to determine resting resistances for the sensors. This was less of an issue as only one sensor was being tested at a time, but as this team moves forward with human trials and multiple sensors to capture the more difficult movements of DF and INV/EVR in addition to PF, a consistent resting resistance is preferred with a known, minimal variance.

3.4.2 Future Work

Additional work has already begun with the Liquid Wire sensors including human trials where multiple sensors with the same resting resistances will be positioned on participants in order to perform static and dynamic movements of the foot and ankle. As the limitations of this study showed, multiple sensors will need to be positioned around the ankle complex in order to capture more complicated movements, but where these sensors should be

placed and how they will be held in place on the participant is a critical discovery. Using machine learning, the researchers will be able to take the resistance values from multiple sensors anchored to a participant and determine the exact position of the foot and ankle. This positioning will then be validated using motion capture and force plate feedback allowing the researchers to identify the capability delta between the SRS solution and the golden standard of human movement analysis. Further, once preferred Liquid Wire sensor placement is identified, a proper gait study on human participants using static and dynamic movement assessment techniques will be used to validate that data "from the ground up" is being properly captured and that precise ankle complex movements are correctly identified. Once the machine learning algorithms are adequately refined for walking movements, product hardening will occur for testing of training-based movements commonly used by athletes outside of the lab in their practice environments.

CHAPTER 4

PLACEMENT

This chapter is based on publication [89].

4.1 Introduction

Biomechanical analyses of human joint range of motion (ROM) have evolved from simple goniometric measures to technologically advanced optical motion capture systems. While motion capture technology aids in the assessment of joint range of motion with gold standard precision measures [27], the use of this technology is primarily confined within a laboratory setting, with limited applicability to changes in joint angles that occur in everyday tasks. Moreover, the financial cost and time consumed are also greater with the use of laboratory-based motion capture equipment. Therefore, there is great demand for alternative solutions to precisely measure joint kinematics outside of a laboratory that have lower financial and time cost requirements and can capture day-to-day real-life scenarios. A wearable device that can measure changes in joint range of motion and limit the negative aspects of motion capture while being precise is a potentially promising solution [12].

Very recently, SRS (liquid metal sensors) that change in resistance when stretched were used to determine if ankle joint movements could be inferred by using a custom-built, rigid-body ankle joint mechanical device [60]. This device mimicked the ankle joint in its ability

to perform ankle joint motions of PF, INV and EVR. A single sensor was placed on the middle of the ankle joint device and all ankle movements were performed passively on the device with data from the sensor recorded for each ankle movement at various degrees of ROM quantified by using an electric goniometer and two smart phones with the RIDGID level iOS application installed [60]. Based on the results of this study, the sensor could provide significant linear models in predicting ankle joint PF. However, the INV and EVR movements were still difficult to predict accurately with only a single sensor being used. It was concluded that there was a significant linear relationship between the positional change of the mechanical device and the resistance values of the SRS for the ankle PF movement. This indicated that the sensor was promising to be a potential "out-of-the-lab" substitute to inertial measurement units (IMU) and motion capture based solutions to quantify human joint kinematics [60]. Utilizing SRS offers the advantage of contouring over the anatomical surface of the human joints, thus mitigating the drift in measurements associated with IMUs. Furthermore, they can be embedded into garments to function as a wearable solution [66, 67, 118].

While SRS were found to be successfully indicative of ankle ROM during PF, INV and EVR, these were still conducted on a mechanical ankle joint device that is far from animate and real-life, compared to the human foot–ankle complex. The human ankle and foot—unlike the mechanical device—has intrinsic properties of living tissues such as skeletal muscles that are responsible for force production to cause joint rotation and bones that act as attachment sites for muscles and as mechanical levers for human movement [25, 38]. One of the major limitations outlined in the previous study was that the ankle joint complex

has three-dimensional movement and thus three degrees of freedom (DOF), with varied ROM for each DOF [60]. More importantly, these DOF rarely occur in isolation in a real-world setting or during activities of daily living but occur as a combination with other DOF of the ankle and foot segment [25, 38]. It was also reported that a single SRS can detect PF, INV and EVR, but it was not capable of differentiating INV and EVR [60], subsequently mandating the need for testing human participants with active movements of the ankle and foot segments. Additionally, the SRS placement and orientation on human participants have not been analyzed yet, which can present additional challenges in data collection and interpretation. Finally, the SRS data used to infer ankle and foot movements need to be validated against the state-of-the-art technology using motion capture analyses. Therefore, the purpose of the study was to analyze various SRS placements and orientations when using more than one SRS, to determine good positional and surface anatomical location of the SRS on the foot–ankle segment that provides the most accurate and precise ankle and foot ROM measurements validated against a 3D motion capture system. The primary contributions of this paper are:

1. The initial work in [60] was extended to human movement.
2. SRS sensor placement was analyzed and optimal sensor placement was determined for PF, DF, INV, and EVR.
3. Linear model analysis results show high levels of goodness-of-fit and low RMSE values, meaning the proposed placements are effective at measuring INV, EVR, PF and DF compared to the gold-standard motion capture solution.

4.2 Materials and Methods

4.2.1 Participants

Ten participants (five males: age, 22–24; height, 170–193 cm; mass, 71–100 kg; foot size, 10–13; and five females: age, 23–25; height, 156–168 cm; weight, 48–66 kg; foot size, 5.5–8) with no history of lower extremity musculoskeletal injuries/surgeries or neuromuscular diseases/disorders were tested. This sample was chosen to test both genders and individuals with small, medium, large and extra-large sized feet. Since this was a preliminary study, the sample size was set at 10 participants, which is consistent with a recent study that examined gait kinematics of the foot and ankle among 10 participants [70]. All participants read and signed an informed consent to participate in the study. The study was approved for human subjects testing by the University's Institutional Review Board (IRB).

4.2.2 Study Design

The study design followed a single day testing protocol with an initial familiarization session that was conducted prior to the experimental testing. All participants visited the Human Performance Lab (HPL) at the University's Center for Advanced Vehicular Systems (CAVS) research center. During familiarization, all participants were briefed on the procedures and provided an opportunity to perform a few trials of the experiment that included simple ankle movements in a non-weight bearing (NWB), high-seated, sitting position (explained further under experimental procedures). Following the familiarization process, the participants performed the experimental testing.

4.2.3 Instrumentation and Participant Preparation

The experimental testing included measurements of ankle joint kinematics using 12 Bonita 10 camera 3D motion capture system (Vicon, Oxford, UK). The SRS used in the current study included the StretchSense^{TM} sensors (Auckland, New Zealand). The motion capture data were sampled at 100 Hz and the SRS data were sampled at 25 Hz. For this study, only the right foot–ankle complex was measured. During testing, each participant was prepared by placing reflective motion capture marker clusters on the right lower extremity for the foot and shank (lower leg) segments. Four SRS were placed on the ankle and foot segment in a predetermined POC, explained further in Section 4.2.4.1.

4.2.4 Movements

The participants started in neutral positions. Figure 4.1 shows the neutral, DF and PF movements in the sagittal plane, and Figure 4.2 shows the neutral, INV and EVR movements in the frontal plane.

4.2.4.1 SRS POCs

Three different POCs were determined based on bony landmarks and movement patterns of the foot–ankle segment. The individual SRS were then labeled based on the movement they were positioned and oriented to measure. The sensors were located in a position that would cause them to be stretched by the corresponding joint motion. The PF SRS was mounted on the dorsal surface of the foot to measure the downward movement of the foot, such as when the toes are pointed towards the ground and the angle between the dorsal surface of the foot and the lower leg increases [25, 38]. The INV SRS was mounted on the

lateral side of the ankle to measure the movement of the sole (bottom of the foot) towards the midline of the body [25, 38]. The DF SRS was mounted on the heel of the foot to measure the upward movement of the foot towards the lower leg (angle between the top of the foot and lower leg increases) [25, 38]. The EVR SRS was mounted on the medial side of the ankle to measure the movement of the sole away from the midline of the body [25, 38].

The PF POCs were determined based on the hallux (big toe) and surface of the top of the foot. The PF SRS was first oriented towards the hallux, then over the middle of the foot, and lastly towards the 5th phalanx. The INV POCs were centered around the lateral malleolus (bony landmark on the lateral side of the ankle). The INV SRS was first positioned anterior to the lateral malleolus, near to the 5th phalanx, then directly over the lateral malleolus, and finally, posterior to the lateral malleolus, close to the heel of the foot. The DF SRS was kept in the same position over the heel for all three POCs, due to the small surface area in which the DF movement could be measured. The POCs for the EVR SRS were determined similarly to the INV POCs, except they were based on the medial malleolus (bony landmark on the medial of the ankle). For the first and third POCs, the EVR SRS was kept parallel with the INV SRS. These POCs are illustrated in Figures 4.3–4.5.

4.2.5 Experimental Procedures

The participant was first instructed to fill out a participation consent form as per IRB protocol. The participant was then given a sock attached with Velcro mounts to place on

(a) (b) (c)

Figure 4.1: Sagittal plane: (**a**) neutral; (**b**) DF; and (**c**) PF

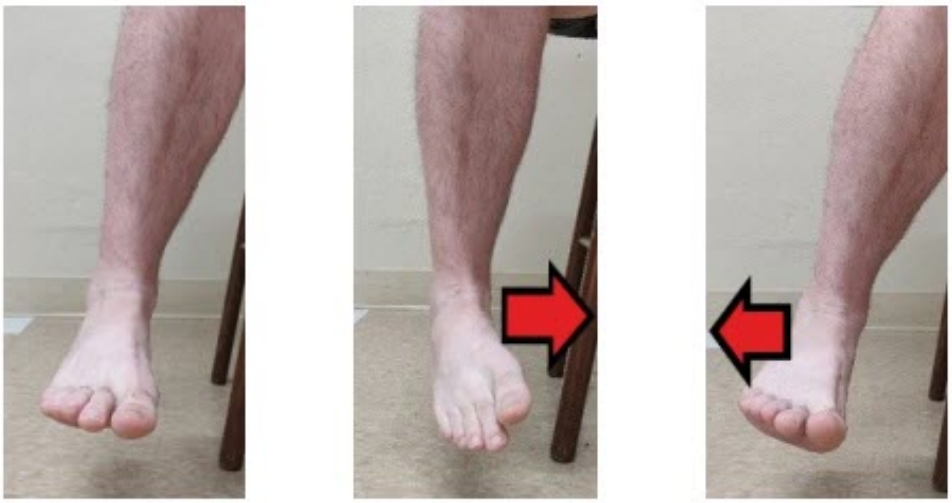

(a) (b) (c)

Figure 4.2: Frontal plane: (**a**) neutral; (**b**) INV; and (**c**) EVR.

Figure 4.3: PF and DF sensor POC positions: (**a**) PF POC 1; (**b**) PF POC 2; (**c**) PF POC 3; and (**d**) DF POC 1; The DF sensor was positioned the same for all three POCs (heel of the foot is pictured).

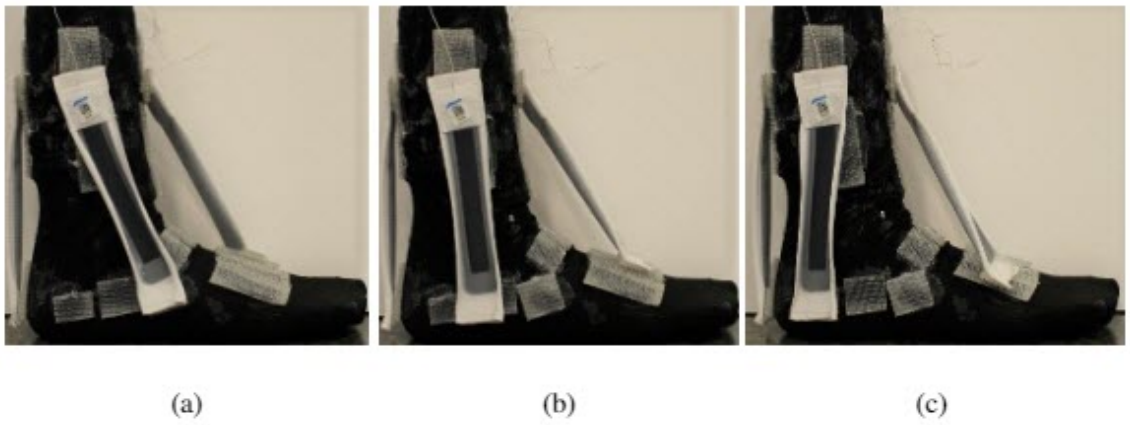

Figure 4.4: INV Sensor POC Positions: (**a**) INV POC 1; (**b**) INV POC 2; and (**c**) INV POC 3.

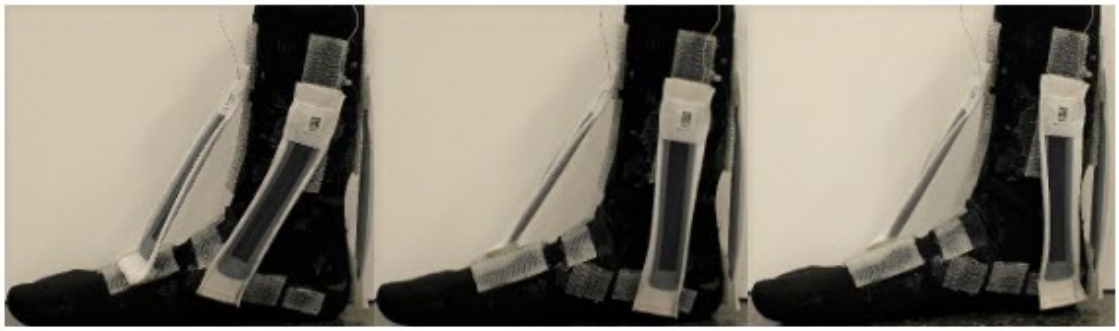

(a) (b) (c)

Figure 4.5: EVR sensor POC positions: (**a**) EVR POC 1; (**b**) EVR POC 2; and (**c**) EVR POC 3.

their right foot. Participants were given either a small/medium or large/extra-large sock depending on their shoe size. Following this, the participant assumed a high-sitting position in an NWB position. For the familiarization process, the examiner aided the participant in a demonstration on how to perform each of the foot–ankle movements, encouraging the participant to perform full ROM (i.e., moving the foot as far as possible). Following this, the motion capture cluster sensors were mounted to the right foot and right shank, and the sensors were calibrated (see Figure 4.6).

A validation step was then conducted, where, in the NWB position, the participant performed full ROM of the ankle three times repeatedly, moving the foot in the specified direction, and then returning to its original position. Each trial began with the participant staged in a neutral position of the ankle (approximately zero degrees of DF/PF and zero degrees of INV/EVR) which was set by the examiner using a mechanical goniometer.

This process was equivalent to one trial and was repeated for each of the four foot–ankle movements (PF, DF, INV and EVR).

Following the validation step, the SRS were mounted to the sock in POC 1, and the four movements were repeated. An example of a participant completing the trial with the sensors in POC 1 can be seen in Figure 4.6. This process was repeated for POC 2 and POC 3 (noting that the DF movement only had one POC). Both kinematic 3D motion capture data and raw capacitance data from the SRS were collected simultaneously for each of the sensor placement trials. Completion of the movement trials for the last SRS POC marked the completion of the testing procedures.

(a) (b)

Figure 4.6: Participant image showing SRS and motion capture sensors: (**a**) front view; and (**b**) side view. The SRS sensing module is circled in red.

4.2.6 Data Analysis

The kinematic data of ankle ROM for each DOF were determined by using the Grood–Suntay angle orientation in the MotionMonitor™ (Innovative Sports Training, Inc., Chicago, IL, USA) software. Raw kinematic data were filtered with a low-pass third-order Butterworth filter with a cut-off frequency of 15 Hz. The raw capacitance values of the SRS were measured using the 10 Channel SPI Sensing Circuit in conjunction with the Bluetooth Low Energy (BLE) module, both made by StretchSense™. The values were recorded using the proprietary StretchSense™ BLE iOS application.

4.2.7 Statistical Analysis

The R language was chosen for formatting and analyzing the dataset, as R automated the analysis and is capable of powerful data visualization. The data for each trial was saved to a file that was named according to participant ID, SRS POC, and movement performed. This naming convention was used to pair each set of motion capture and SRS data files. When comparing data, the SRS positioned to measure PF and DF were matched with the Flexion column recorded by MotionMonitor™, and the SRS positioned to measure INV and EVR were matched with the INV column recorded by MotionMonitor™.

To compare the motion capture data to the SRS data, several preprocessing steps needed to be taken. First, the sampling rates needed to be matched between motion capture and SRS. Due to limitations of the StretchSense™ BLE module, the max sampling rate that could be used was 25 Hz, and after further processing through the StretchSense™ proprietary iOS application, the intervals between timestamps were not always consistent.

To mitigate this, an R approximation function was used to interpolate the SRS values based on the timestamps collected from MotionMonitor™, bringing the StretchSense™ data up to 100 Hz.

After upscaling the StretchSense™ SRS output, the data needed to be aligned over time with the motion capture output, as a slight delay existed due to the need to manually start the data recording on each measurement system. Cross correlation was utilized to determine the proper data time alignment, based on the recommendation of Rhudy [87]. The function was utilized based on the sensors measuring the movement performed (i.e., PF SRS used to align PF movement data), as it would be expected that both datasets would consistently produce three distinct peaks, each peak being representative of the foot movement performed by the participant during each trial. When EVR or PF was being measured, the motion capture data were inverted before performing cross correlation, as these movements were measured in the negative plane when recorded by MotionMonitor™.

Finally, all data points where the motion capture data moved into a negative position or below the trial's starting angle for the participant were dropped. This was implemented due to the sensor's limitation of only being able to capture one direction of the ROM, since the sensor needs to be in tension. For example, if the participant was performing PF but went into slight DF during their foot–ankle movement, the sensor measuring PF would lose tension and record no movement, thus becoming unreliable for measuring a linear change in capacitance. The motion capture Flexion output would record this as a negative flexion value (indicating the participant moved into DF), so these flexion values would be removed. Since the participant began each trial in a position of 0 degrees of flexion, this could be

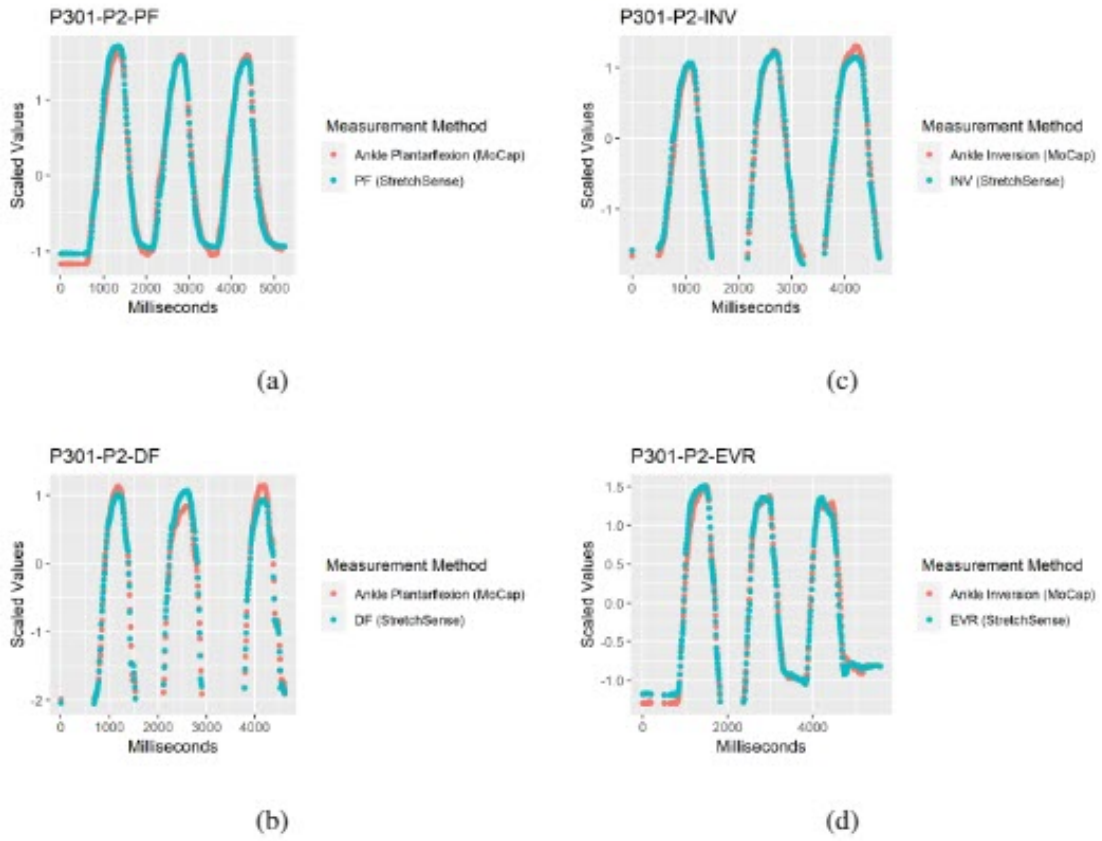

Figure 4.7: Examples of Preprocessed data: (**a**) preprocessed data for PF movement at POC 2; (**b**) preprocessed data for DF movement at POC 2; (**c**) preprocessed data for INV movement at POC 2; and (**d**) preprocessed data for EVR movement at POC 2.

used as a reliable threshold for measurement, as care was taken to ensure there was some tension in the SRS at this position. An example of the preprocessed data is depicted in Figure 4.7. This graph presents scaled versions of the two datasets and was generated for all trials for visual inspection to make sure the data was preprocessed correctly.

Once the data were properly formatted, a linear model was created based on sensor capacitance versus motion capture angle. The R^2 value and root-mean-squared error (RMSE) were then calculated based on the linear model, and a plot of all residual values from the model was created for visual inspection. Figure 4.8 provides examples of this plot, with magnitudes of residuals being double encoded with size and color. Finally, a table was generated, characterizing each of the trials with the calculated R^2 value and RMSE to provide a measure of how well the SRS modeled the motion capture data.

To determine which sensor position configuration performed well at modeling the motion capture data, three metrics were considered: accuracy of angle prediction, consistency in prediction performance, and robustness across participants. Accuracy of angle prediction was determined based on observing which trials resulted in the highest average R^2 value, which indicates a goodness-of-fit of the linear model, and the lowest average RMSE value, which measures how accurately the model predicts the response in units of degrees [33]. Consistency in prediction performance was evaluated based on the standard deviation of the R^2 and RMSE values across all participants for each SRS POC.

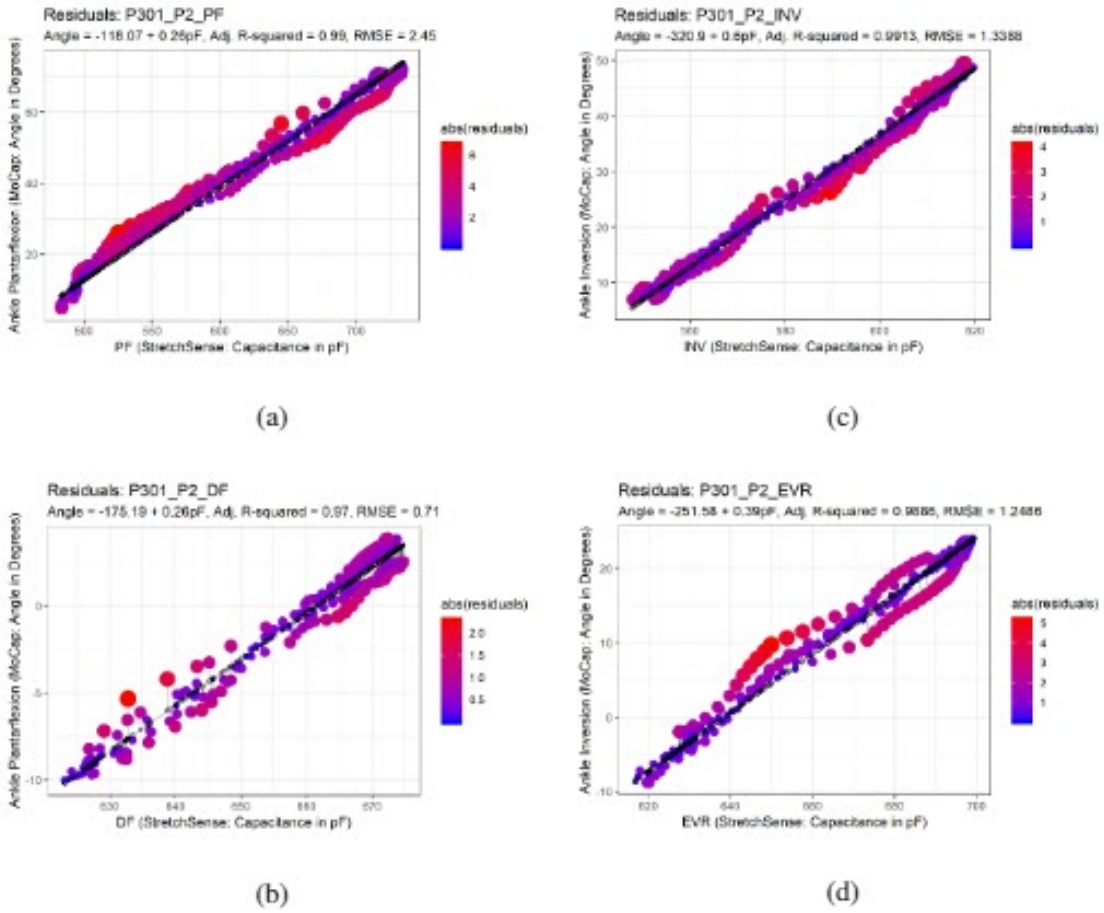

Figure 4.8: Residual plots: (**a**) residual plot for movement at POC 2; (**b**) residual plot for DF movement at POC 2; (**c**) residual plot for INV movement at POC 2; and (**d**) residual plot for EVR movement at POC 2.

4.3 Results

The results for the three aforementioned metrics are summarized in Table 4.1. The best results for each metric for each POC are identified in bold. Figure 4.9 captures the performance of the accuracy and consistency metrics for each POC. The average values are calculated and plotted as single points, and a horizontal line is drawn to indicate the location of the best performing average value. Figure 4.9 also depicts violin plots, which are the curved areas along each POC that gives an idea of the "spread" of the data. These violin plots represent a kernel density distribution portrayed vertically. A greater horizontal width of a curve in the plot indicates a greater portion of participants that produced results near the value on the *y*-axis. For example, in Figure 4.9a, a large portion of participants produced an R^2 around 0.95–0.99 for the INV sensor at POC 2, while participants were more spread out at R^2 values of 0.97–0.65 for the INV sensor at POC 3. When comparing these graphs visually to the standard deviation values in Table 4.1, distributions resulting in the lowest standard deviation values are easily identifiable. Additionally, given that the individual participant data points reiterate the "spread" of the data, the POCs producing the most outliers can be easily identified as well.

To determine which SRS POCs were the most robust, a histogram was created based on which POC produced the highest R^2 value or lowest RMSE value for each participant. The POC that most frequently resulted in the best value was considered the most robust. The motivation for this metric was to get an idea for how well each POC performed against the variety of foot sizes amongst each of the participants. The results of this metric are seen in Figure 4.10 and also recorded in Table 4.1.

The SRS were also evaluated to determine how well they tracked multiple movements beyond the single movement that they were positioned to record. For example, the PF SRS is placed on the top of the foot–ankle to capture the movement, but because the participants also performed INV and EVR movements while the PF SRS was mounted, the PF SRS could be evaluated for other foot–ankle movements; essentially, this assessment was completed to determine if measuring multiple movements with one SRS was feasible. Thus, a new table was generated identifying R^2 and RMSE values for all four SRS for each trial, regardless of the primary movement that was being measured.

In Figure 4.11, the results can be seen for each movement based on the SRS that was observed. The titles for each subgraph indicate the movement that was performed by the participant, while the color of each data point represents the movement that the SRS was originally intended to measure based on the POC. One thing to note on the R^2 graph is that an inverse relationship will also produce a high R^2 value, hence why the EVR SRS produced a reasonably good R^2 value when used to measure the INV movement. As the foot goes further in the INV movement, it can be expected that the EVR SRS would decrease in value, if there is still tension in the SRS.

Lastly, gender and shoe size were compared to see if they influenced the quality of the SRS's measurements. For this study, all females used the small/medium sock, while all males used the large/extra-large socks, so both categories are encoded in the following results. Figure 4.12 presents average R^2 and RMSE values between both genders for each SRS POC.

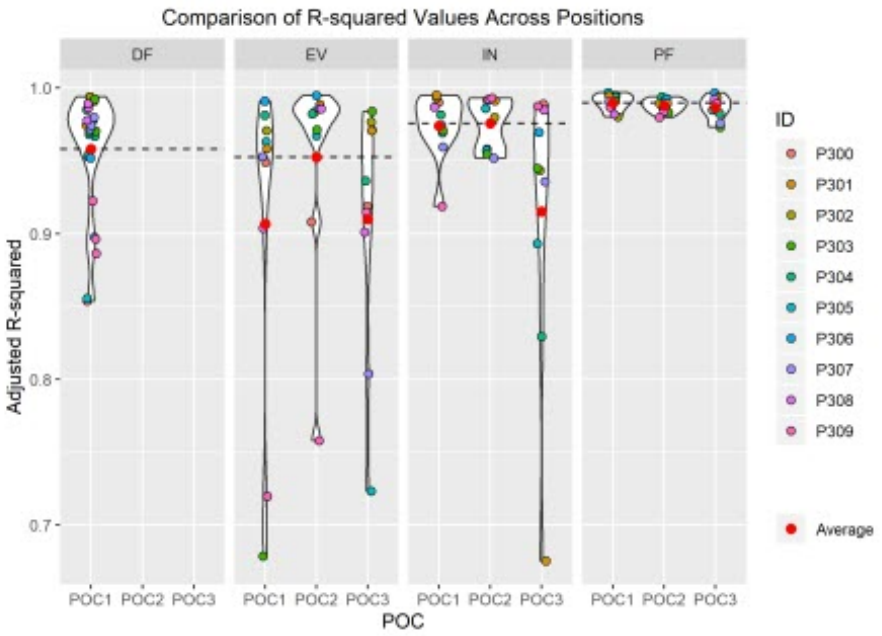

(a)

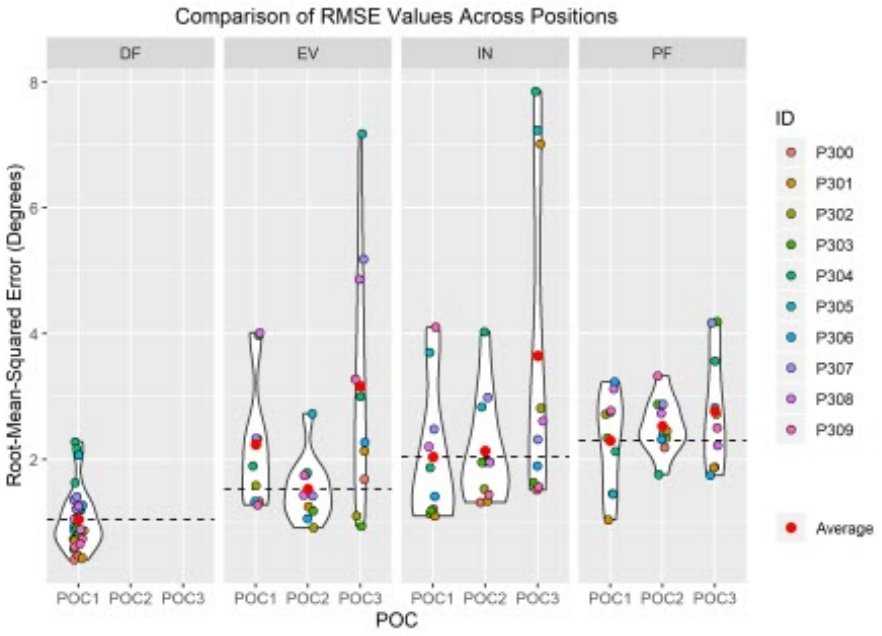

(b)

Figure 4.9: Violin plots: (**a**) R^2 average and Violin plot comparison for all POCs; and (**b**) RMSE average and Violin plot comparison for all POCs.

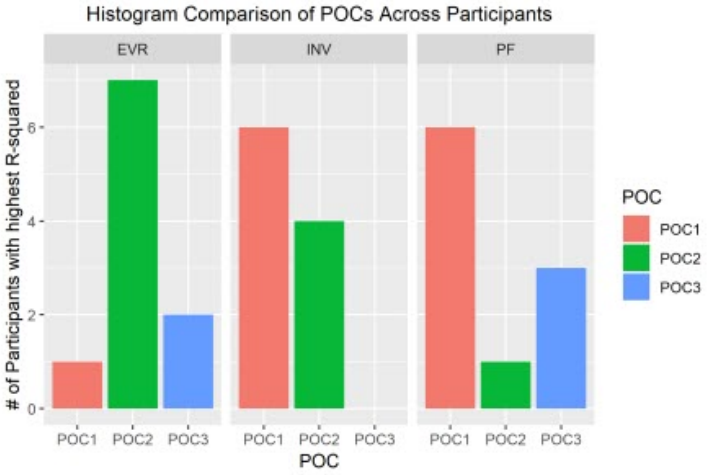

(a)

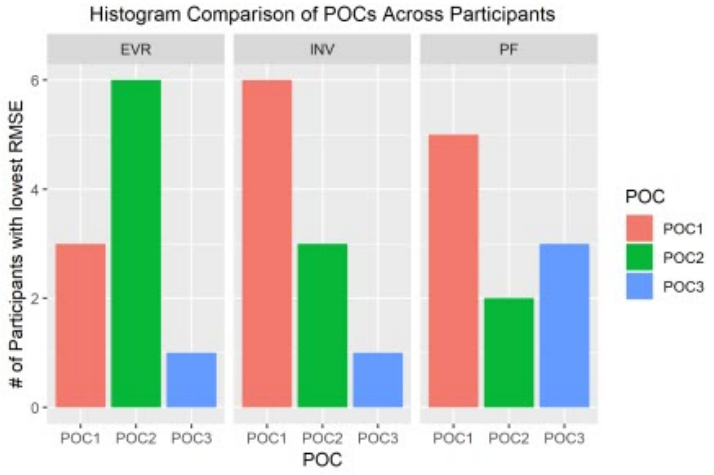

(b)

Figure 4.10: Number of participant counts: (**a**) number of participants where SRS POC resulted in the highest R^2 values; and (**b**) number of participants where SRS POC resulted in the lowest RMSE value.

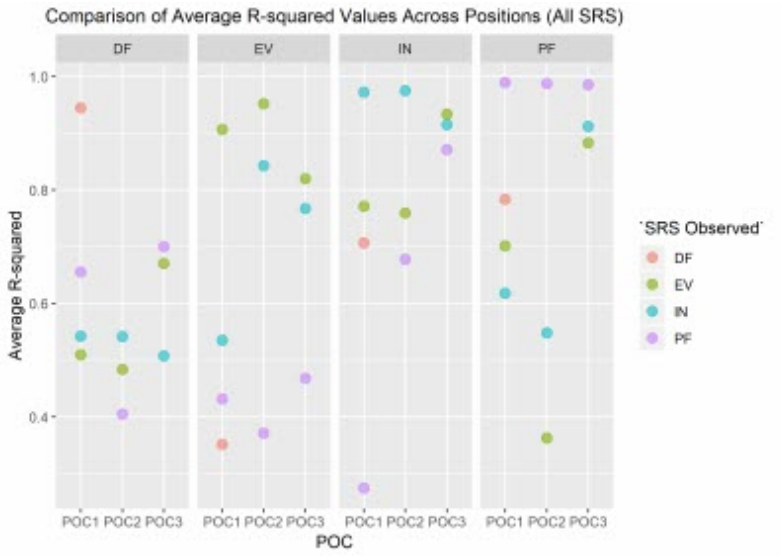

(a)

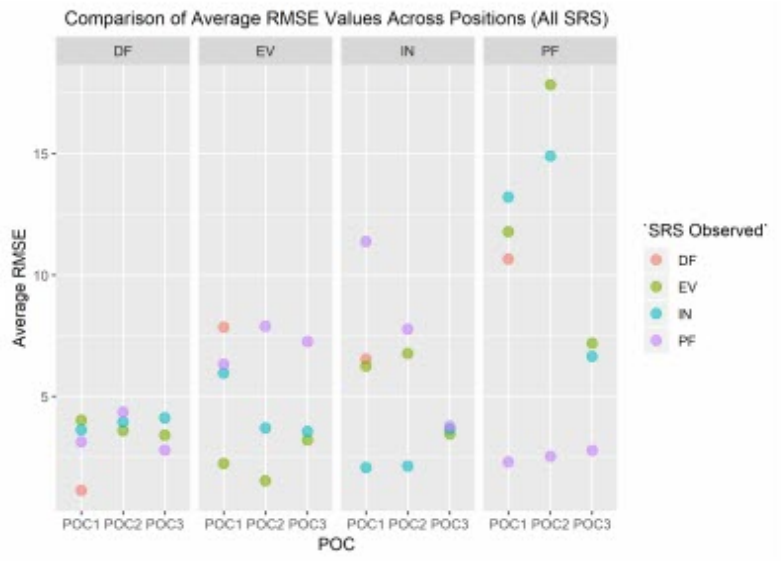

(b)

Figure 4.11: Comparison of R^2 and RMSE values: (**a**) comparison of average R^2 values for all SRS at all POCs; and (**b**) comparison of average RMSE values for all SRS at all POCs. Note that in both comparisons DF only had one SRS POC.

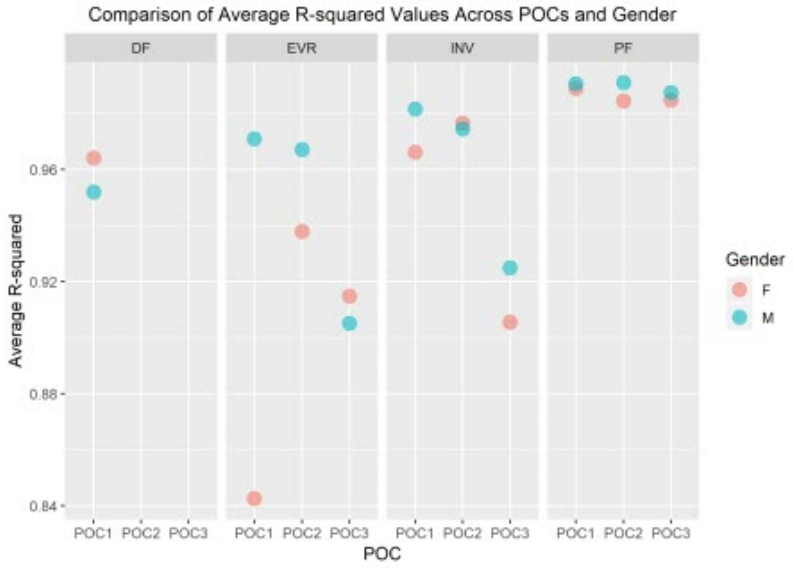

(a)

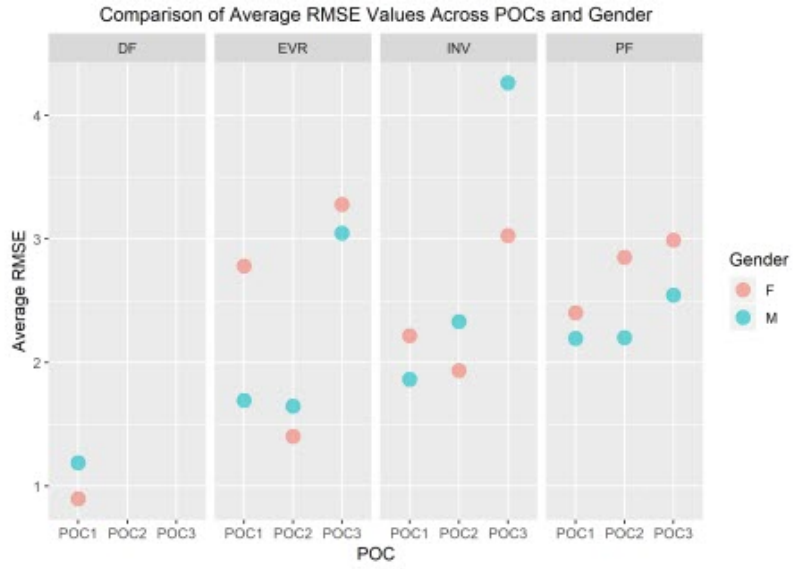

(b)

Figure 4.12: (**a**) Comparison of average R^2 values for all SRS between genders/foot size; and (**b**) comparison of average RMSE values for all SRS between genders/foot size.

Table 4.1: Averages, standard deviations, and participant count of R^2 and RMSE values for all POCs; best POC in bold. * Denotes preferred POC location for each of the four foot–ankle movements. Deg., degrees; Std. Dev., standard deviation.

Movement	Position and Orientation Configuration (POC)	R^2 Average (Figure 4.9a)	RMSE Average (deg.) (Figure 4.9b)	R^2 Std. Dev.	RMSE Std. Dev. (deg.)	Higest R^2 Number of Participants (Figure 4.10a)	Lowest RMSE Number of Participants (Figure 4.10b)
EVR	POC 1	0.9068	2.2378	0.1123	1.0159	1	3
EVR	**POC 2 ***	**0.9525**	**1.5269**	**0.0727**	**0.5186**	**7**	**6**
EVR	POC 3	0.9100	3.1628	0.0845	2.0127	2	1
INV	POC 1	0.9739	**2.0407**	0.0225	1.0939	**6**	**6**
INV	**POC 2 ***	**0.9755**	2.1340	**0.0178**	**0.8838**	4	3
INV	POC 3	0.9153	3.6455	0.0977	2.6128	0	1
PF	**POC 1 ***	**0.9898**	**2.2996**	0.0056	0.7616	**6**	**5**
PF	POC 2	0.9877	2.5274	**0.0046**	**0.4376**	1	2
PF	POC 3	0.9861	2.7679	0.0076	0.9216	3	3
DF	**POC 1 ***	0.9567	1.0568	0.0410	0.4952	N/A	N/A

4.4 Discussion

The purpose of the study was to use a 3D motion capture system of human participants to identify SRS POCs that accurately record the four primary movements of the foot–ankle complex: PF, DF, INV, and EVR. More specifically, the purpose was to examine what combination of four SRS will most accurately measure ankle movements in four directions compared to the golden standard for human movement assessment. Given the complex nature of using a linear solution to accurately quantify movement of a triaxial joint, movement was captured from 10 participants and multiple tests were performed to analyze the SRS capacitance output from multiple positions around the foot–ankle. This section outlines the findings for each of the four individual movements analyzed in this study from most simple POC placement preference to the most difficult.

4.4.1 Dorsiflexion (DF)

DF was the only foot–ankle movement where just one POC placement was tested. Only one POC was needed for this movement because the anatomy on the posterior side of the foot, primarily the calcaneus (heel), only provides one location for POC to accurately measure DF [25, 38]. However, SRS accuracy still needed to be validated against motion capture similarly to how all other SRS POCs were evaluated in order to establish baseline confidence in the solution. DF POC 1 had a high R^2 average above 0.95 over all participants meaning that nearly all values of the SRS correlate directly to the flexion values captured via motion capture (Table 4.1 and Figure 4.9a). Therefore, there is a high level of fit between SRS and motion capture for the DF movement across all participants. Likewise, where a high R^2 average is an indicator of relative measure of fit, a low RMSE average value indicates an absolute measure of fit. DF POC 1 scored a low value for all participants for RMSE average further confirming the SRS measurement's fit to motion capture (Figure 4.9b). PF was the closest comparable movement as Figure 4.11 demonstrates that DF and PF are opposing movements [25]. POC 1 was confirmed to be the proper SRS placement for DF and there was minimal difference in average R^2 and RMSE values between men and women and/or foot size (Figure 4.12).

4.4.2 Eversion (EVR)

The second simplest SRS placement was found to be POC 2 for EVR. Three POCs were tested and six measurements were taken to decide optimal positioning for EVR. All six measurements (Table 4.1) clearly indicate POC 2 as the best location for SRS based data

collected via motion capture. The R^2 average was high, over 0.95, and RMSE average was low indicating good fits for both relative and absolute measures respectively (Figure 4.9). Most participants had the highest R^2 values and lowest RMSE values for POC 2. POC 2 demonstrated the best comparison movement with INV (Figure 4.11), the proper opposing movement to EVR, for both R^2 and RMSE calculations. The comparison of R^2 and RMSE for EVR between men and women participants occurred at POC 2 as well, as observed in Figure 4.12.

While no outliers were removed for this study, there were some notably different data points for EVR R^2 calculations and EVR POC 3 RMSE that needed to be investigated to ensure that POC 2 is absolutely the better SRS placement selection. For a few of the participants, performing foot–ankle movements such as EVR and INV in isolation was difficult because some PF also occurs with INV and EVR movements [25, 38, 39, 102, 107]. The worst case of a participant's inability to disassociate the two movements and perform true INV and EVR movements was captured by participant P03. To confirm that P03's movement should not impact final placement decisions for EVR, the motion capture data were evaluated to understand why the participant's R^2 and RMSE averages were much lower and higher, respectively. Figure 4.13 demonstrates that, as P03's "INV/EVR" movement experienced negative peaks (indicating an EVR movement), their "Plantar flexion" movement peaked showing a correlation between the two movements and thereby confirming that EVR for P03 was not in true isolation. The reason this is important from an SRS placement perspective is that, by moving into PF, P03 reduced tension on the SRS and therefore reduced the capacitance value output indicating that the SRS output would

not demonstrate as strong of an EVR movement as compared to the true EVR movement captured in motion capture, thus further weakening R^2 and RMSE fit.

4.4.3 Plantar Flexion (PF)

SRS placement for PF was not quite as definitive as EVR but was still very compelling as four of six metrics used for evaluation Figure 4.3 indicated POC 1 being the best fit. R^2 average value was extremely high at over 0.98 and RMSE average was the lowest of the three positions for POC 1 (Figure 4.9). While standard deviation of R^2 and RMSE was not the lowest for POC 1, six of 10 participants had the highest R^2 and lowest RMSE for this position (Figure 4.10). DF is the closest opposing movement for POC 1 (Figure 4.12) as expected while POC 1 indicates the best fit for both men and women (Figure 4.13).

4.4.4 Inversion (INV)

Of all the movements, determining the placement for INV was the most challenging, because two POC options, POC 1 and POC 2, appeared to be nearly identical in performance. POC 2 demonstrated the best R^2 average at over 0.97 (Figure 4.9a), but POC 1 was just slightly lower (Table 4.1). RMSE average was lowest for POC 1 (Figure 4.9b), but POC 2 was only slightly higher. Standard deviation adjustments for R^2 and RMSE both indicated POC 2 as the better fit but the total number of participants with the better fit values indicated POC 1 as the optimal location for placement (Figure 4.10). To make a decision as to the best POC for SRS placement regarding INV movements, the research team considered the following three pieces of information: (a) R^2 is often viewed to be the better indicator of fit; (b) the POC selected for EVR (the opposing movement to INV) in

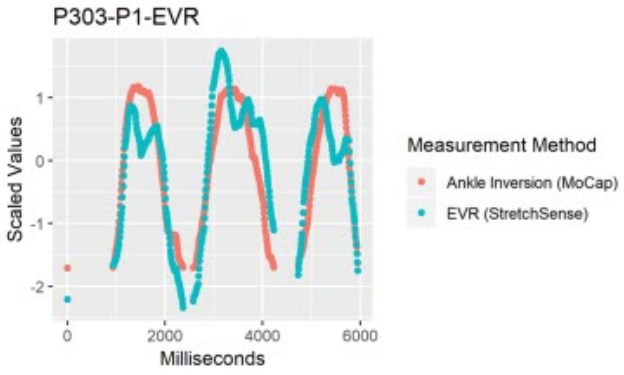

(a)

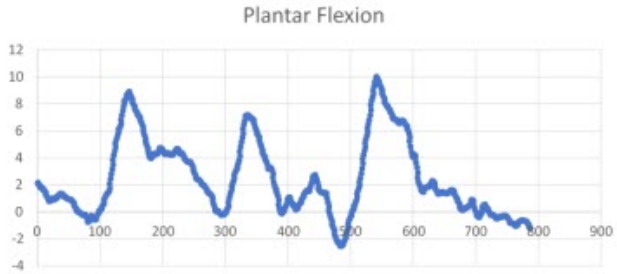

(b)

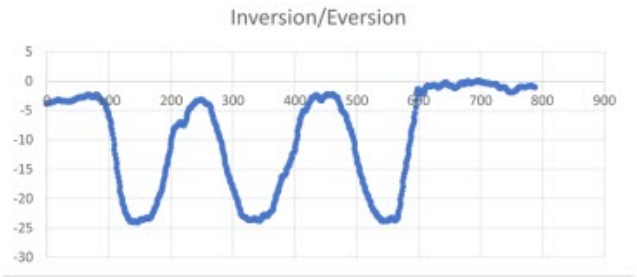

(c)

Figure 4.13: (**a**) Comparison of motion capture and StretchSense^{TM} when EVR movement not performed in isolation. Both datasets scaled and motion capture data inverted to depict relationship between sensing methods. (**b**) Raw motion capture data for PF movement. (**c**) Raw motion capture data for EVR movement (negative values).

order to promote uniformity and sensor placement during wearable design; and (c) picking either POC has limited negative ramifications given that the output for each is so similar. For this reason, POC 2 was selected for INV. these results indicate that both POC 1 and POC 2 provided good results, and that this motion was not as clearly delineated as the other movement cases.

Similar to EVR, some participants had issues isolating their movements to only perform INV without PF. INV is a difficult joint action to perform in isolation [25, 38, 39, 102, 107]. In addition, similar to Figure 4.13, Figure 4.14 shows that, as their "Inversion MoCap" movement experienced positive peaks (indicating an INV movement), their movement also peaked showing the same correlation between the two movements while also reducing stretch on the SRS thereby reducing capacitance value output.

4.4.5 Limitations

As noted in the Discussion Section, a few participants had a difficult time isolating their movements and so PF was performed during INV and EVR trials. This is not an issue for motion capture as the cameras and markers can accurately observe all joint angle movements regardless of the movement type. However, SRS capacitance values are dependent upon consistent tension and stretch that occurs linearly. By performing two movements at once (e.g., PF and INV), the tension was reduced, and capacitance was lowered thus recording "weaker" values and further lowering and raising R^2 and RMSE averages, respectively. This was only an issue, however, because one sensor was being observed at a time. With multiple SRS output being captured simultaneously for all four movements,

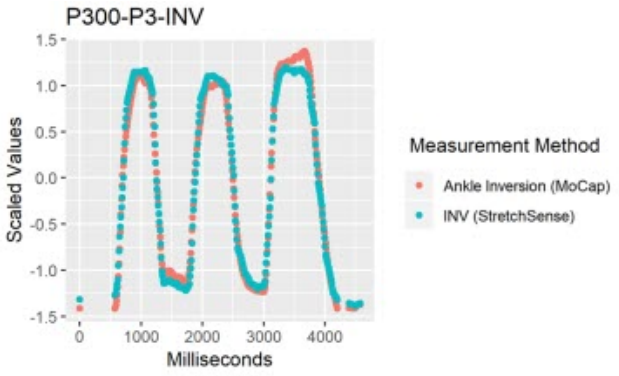

(a)

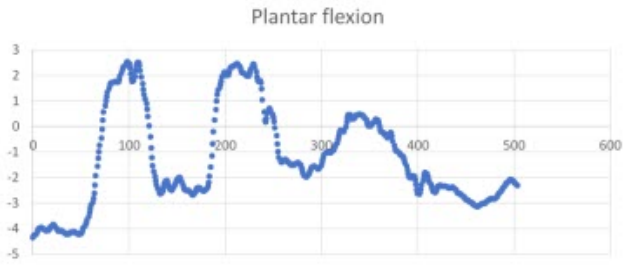

(b)

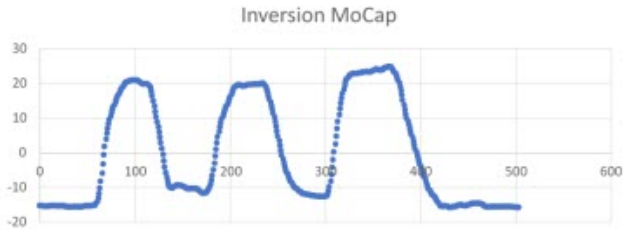

(c)

Figure 4.14: (**a**) Comparison of motion capture and StretchSense^{TM} when INV movement not performed in isolation. Both datasets scaled to depict relationship between sensing methods. (**b**) Raw motion capture data for PF movement. (**c**) Raw motion capture data for INV movement (positive values).

PF would have been captured in addition to INV and EVR. However, this does not solve the issue of a lack of tension in the INV and EVR SRS every time an additional PF movement is performed. Mitigating these issues will likely require additional investigation into the initial "tightness" of the SRS while the wearer is in a neutral position. In addition, because EVR and INV are opposing movements, information about one movement can be inferred from the other. Further, with all four sensors collecting foot–ankle movement data, machine learning solutions can be developed to further enhance robustness of the solution. Utilizing more sophisticated modeling techniques with multiple sensors as inputs, the output angles for each foot–ankle complex motion may become more robust and have lower errors.

In addition, this study used participants with bare feet (i.e., no shoes). From a product development perspective, creating a solution that utilized the capabilities of the SRS while still allowing the users to wear shoes would be the ideal scenario. The intent of this study was to find the best SRS placements in order to accurately quantify foot–ankle movements. While a sensor that conforms to the curvature of the ankle complex on top of the sock is an ideal end state, this study was strictly about validating placement. Creating a fully SRS-integrated, sensor-ladened compression sock is the end goal for this research, but confidence in positioning is necessary prior to incorporation of the technology into the textile materials.

4.4.6 Future Work

With each SRS POC identified, the next logical step is to conduct a study where all four SRS are placed on participants who are performing dynamic movements such as walking while also wearing motion capture markers for continued validation. With walking data, the research team will begin to understand more about the interactions between all four sensors as they collect information on the same movement but from different locations about the foot and ankle. The same validation tests can be performed as an assessment of fit that will be performed against motion capture output. Basic walking movements on a flat surface at a normal pace will need to be observed. In addition, to engage true INV and EVR movements, participants will need to walk on a slightly inclined surface. Further, both feet and ankles will need to be assessed during the same gait movement. Should this SRS solution be verified as an accurate assessment tool for gait, there will be many rehabilitation- [50, 80, 20] and athletic-based [124, 31] opportunities for an off-the-shelf sensor solution that nearly duplicates the accuracy of motion capture yet was originally intended for the use in soft robotics.

Machine learning has been applied to body sensor networks [93], rowing coaching [2], and human gait analysis [100, 45], to name a few. I plan to apply machine learning techniques when linear models are not adequate or to combine multiple SRS inputs into an output, such as estimating INV or EVR angles.

Our current study is a preliminary work on testing the efficacy of the wearable sensors for the foot–ankle complex movements. In this regard, my focus was to assess the performance of the sensors within the first standard deviation, and, hence, the sample size of

ten human subjects. However, in considering the design of wearable sensors for the foot–ankle movements, I plan to test the performance of these wearable sensors that would be applicable for 95% of human subjects (the human subject number would be greater than that implemented in the current study).

4.5 Conclusions

Upon completion of the participant trials, R^2 and RMSE averages were used to determine both relative and absolute fit for the SRS output as compared to motion capture. Robustness was determined by how many participants had the same POC selection for each movement type. Standard deviation for R^2 and RMSE was calculated for each participant as well. In addition, opposing movement comparisons were made for each SRS POC and comparisons between gender and foot size were observed.

Through these many evaluations, SRS POCs that best captured foot–ankle movement were determined with a high level of confidence. POC 1 was selected for both PF and DF and POC 2 was selected for both INV and EVR. With these placements identified, this research team is confident that a true gait assessment that rivals the accuracy of 3D motion capture systems can be performed using only four, off-the-shelf SRS sensors. The solution verified on human participants within this study essentially creates a real-time, continuous, and consistent electric goniometer that a user can wear to accurately assess their movements "from the ground up" [60].

CHAPTER 5

GAIT

This chapter is based on publication [88].

5.1 Introduction

The biomechanical analysis of movement patterns, such as walking gait, is essential to understanding how an individual can maximize movement [114]. A typical gait cycle spans two consecutive events of the same limb, usually with initial contact to an external surface [112]. Throughout one gait cycle, each lower extremity passes through two phases: (a) A stance phase and (b) a swing phase [112]. During the stance phase, five different movement stages with corresponding joint angles are executed: (a) Initial contact/heel strike (0° of ankle and knee flexion/extension, 20° flexion of hip joint), (b) foot flat (5° plantarflexion of ankle, 15° of flexion of knee and hip joints), (c) midstance (5° dorsiflexion of ankle, 5° flexion of knee, 0° of hip), (d) heel off (0° of flexion of ankle and knee, 10–20° of hyperextension of hip), and (e) toe-off (20° plantarflexion of ankle, 30° of knee flexion, 10–20° of hyperextension of hip) [112]. The second stage–the swing phase–consists of three stages: (a) Acceleration (10° plantarflexion of ankle, 30° flexion of knee, 20° of flexion of hip), (b) midswing (0° ankle flexion, 30° flexion of knee and hip), and (c) deceleration (0°

of ankle and knee, 30° flexion of hip) [112]. The ability to capture these joint kinematics is made possible through 3D motion capture and wearable technology.

Biomechanical analyses of gait have become a valuable tool for practitioners to assist in clinical diagnoses, strength and conditioning (S&C) specialists to improve athletic performance, and therapists to promote rehabilitation. To monitor gait, 3D motion capture is considered the optimal system for identifying kinematics and kinetics of the gait cycle [27]. However, 3D motion capture traditionally takes place in a laboratory setting which can hinder the opportunity to analyze a real-life scenario and can be quite expensive due to the costs of required equipment [27], as well as the steep learning curve. Moreover, wearable sensor technology is another option to analyze kinematics during a real-life scenario either in a rehabilitation clinic or on a competitive playing field [12].

Various types of wearable sensor technology (WST) have increased in popularity on the market such as accelerometers, gyroscopes, micro electromechanical systems (MEMS), and inertial measurement units (IMUs) [24, 26, 22]. Being portable, WST allows remote monitoring in real-life environments as opposed to the simulated laboratory setting. In addition to portability, WST is inexpensive when compared to a 3D motion capture system [12]. However, there are several reoccurring problems with several types of WST such as an IMU. According to Filippeschi et al. (2017), IMUs have issues with reducing drifts, magnetic disturbances, and calibration. Due to non-homogenous magnetic fields, mainly from construction building materials and magnetic interference, distortion and drift affect a sensor's vertical and horizontal data [24]. A sensor system that could simulate stretch and strain around the joints may offer an alternative method to gait analysis rather than using

stiff, circuit board-based IMUs [60]. Consistency and calibration issues regularly result from sensors on the market, a potential solution may lie in the form of a different type of sensor, such as stretchable SRS) [60].

Due to the reoccurring issues with wearable technology, the purpose of this paper is to continue the research and development narrative for building a new SRS-based wearable solution that closes the WST gap identified by the practitioners [60]. This paper suggests alternative methods for capturing the human gait cycle in a real-life setting for more precise rehabilitation techniques and improvement of athletic performance. Luczak et al. [60] and Saucier et al. [89] recommend a more accurate technology—stretchable SRS accompanied by liquid conductive material, placed in garments, that can be directly placed on joints to analyze joint kinematics [60, 89]. There are several benefits for using SRS which include (a) the capability to capture biomechanical strain without the occlusion of errors that normally occur in 3D motion capture systems and eliminate drift that can arise in IMU sensors [60]; (b) the realization of small changes in electromechanical specifications during loading and unloading; and (c) limited interference observed by the consumer. In addition, SRS inherently offer "stretchability," which allows the sensors to cover the joints of the human body [89].

5.2 Materials and Methods

In Parts II and III of "closing the wearable gap" paper series [89, 13], both 3D motion capture and SRS were used to assess specific foot-ankle movements. Part II analyzed the four primary foot-ankle complex angles—PF, DF, INV, and EVR—during static move-

ment assessments where each angle was measured separately [89]. Part III captured PF and DF during dynamic slip and trip movements that were both expected and unexpected [13]. For Part IV of this series, all four foot-ankle movements will be captured simultaneously during dynamic gait trials. Therefore, due to similarities in equipment, study design, and discovery intent, much of the layout and wording of this section will originate from the previous papers [89, 13] with modifications to describe (a) the new population of participants and (b) modifications in the methods to shift from single sensors capturing static movements and two sensors capturing dynamic slips and trips to four sensors per leg capturing dynamic gait movements.

5.2.1 Participants

A total of 20 participants (10 males: Height, 168–193 cm; mass, 61–117 kg; foot size, 10–13; and 10 females: Height, 158–168 cm; mass, 50–113 kg; foot size, 5.5–10) with no self-reported history of lower extremity musculoskeletal injuries or surgeries and neuromuscular diseases or disorders were tested. Note that participant foot sizes are indicated using US shoe size measurements. This sample was chosen to examine both genders and individuals with small/medium and large/extra-large sized feet. Since this was a gait assessment study, the sample size was set at 20 participants, which is consistent with recent gait-based literature [70, 7, 32, 8]. The study was approved for human subjects testing under the University's Institutional Review Board (IRB; protocol #17-725). Informed consent was obtained for all participants after fully explaining the protocol along with the risks and benefit involved.

5.2.2 Study Design

All participants were instructed to visit the Human Performance Laboratory (HPL) at Mississippi State University's Center for Advanced Vehicular Systems (CAVS) research center. The study design followed a single day testing protocol with an initial familiarization session that was conducted before the experimental testing. During familiarization, all participants were briefed on the procedures and provided an opportunity to perform a few trials of the experiment that includes a self-paced, regular speed walk on both a flat surface (FS) and a tilted surface platform (TSP). The FS was comprised of four, half-inch thick rubber mats that were 0.91 by 1.52 m in size. The short edge of the mats was aligned such that a rubber walkway of 6.10 m covered the middle section of the HPL floor running south to north from the entrance side to the room to the back portion of the room. A linear walking space of 6.10 m is enough to capture at least three full gait cycles for an average person [115]. Since the FS does not induce INV or EVR at the foot, a TSP was designed and built such that INV and EVR at the foot-ankle complex could be recorded for participants during their self-paced gait cycles. A wooden platform was built to be 1.22 m wide by 7.32 m long, creating a walkway tilted at 10 degrees. The same type of rubber mats used on the floor for the FS was placed on the TSP as not to create a confounding variable between walking on different surface types. The walkway, running parallel to the FS trial area of the HPL, weighed over 54.43 kg and therefore was not susceptible to slippage during a participant trial. The platform surface angle of 10 degrees was validated using the bubble level application (PixelProse SARL Tools) on an iPhone (Apple). The TSP designed for this study was inspired by the dimensions and slope of a walkway built for a railroad bal-

last surface [51] in which similar participant INV and EVR characteristics were studied. Figure 5.1 shows the TSP with rubber mat surface. Following the familiarization process for gait trials on both the FS and TSP, the participants performed the experimental testing.

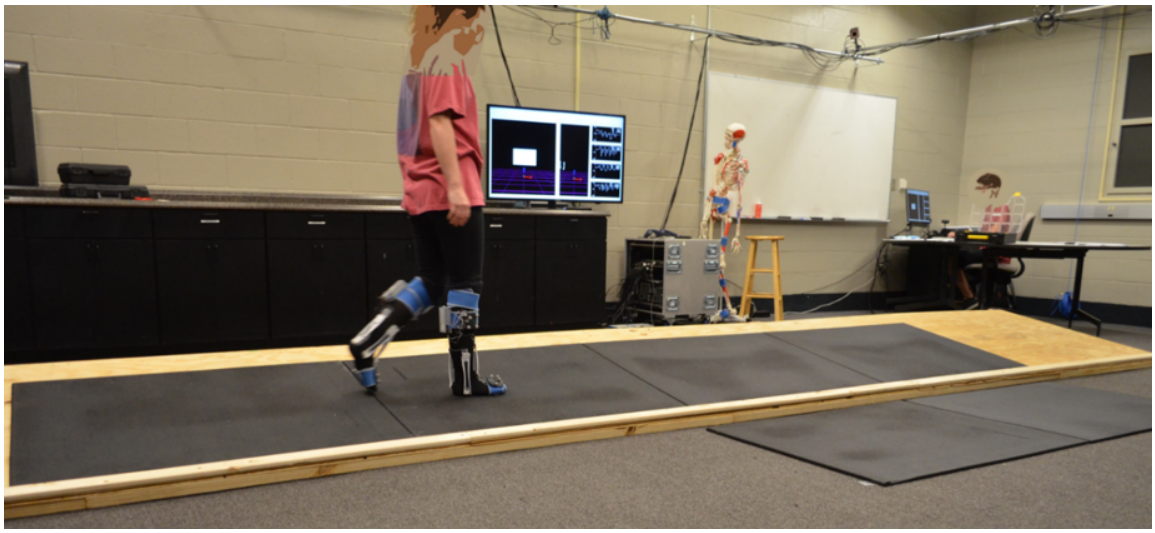

Figure 5.1: A 1.22 m wide by 7.32 m long tilted surface platform or TSP walkway with 10-degree slope for inducing INV and EVR foot-ankle complex movements during self-paced gait trials; includes 6.10 m of covered half-inch rubber mats; simulated participant trial during TSP right-foot INV and left-foot EVR.

5.2.3 Instrumentation and Participant Preparation

The experimental testing included measurements of ankle joint kinematics using 12 Bonita 10 camera 3D motion capture system (Vicon™, Oxford, UK) and eight StretchSense™ SRS (Auckland, New Zealand). The motion capture data was sampled at 200 Hz and the SRS data was sampled at 25 Hz. The MotionMonitor™ (Innovative Sports Training, Inc.,

Chicago, IL) was used in conjunction with Vicon^{TM} to capture, visualize, and assess the motion capture data. For this study, both foot-ankle complexes were measured. During testing, each participant was prepared by placing reflective motion capture marker clusters on the right lower extremity for the foot and shank (lower leg) segments. Four SRS were placed on each ankle and foot segment in a predetermined placement and orientation configuration (POC) identified in Part II of "closing the wearable gap" [89].

5.2.3.1 SRS POCs

Prior to this study, four different POCs were determined based on bony landmarks and movement patterns of the foot-ankle segment. The four POCs used herein were validated using multiple statistical methods including R-Squared (R^2) value and root-mean-squared error (RMSE) in order to respectively assess relative and absolute goodness of fit for the SRS placement against the golden standard of motion capture [89]. SRS POC donning at rest during the start of a TSP trial is demonstrated in Figure 5.2. Figure 5.3 illustrates the POC mounting of all four SRS for a single leg.

5.2.4 Experimental Procedures

Each participant was first instructed to read through a participation consent form and, upon agreement to the expectations of the study methods, sign their approval as per IRB protocol. Each participant was then asked to be seated in a chair-back seat and was given two socks each with four, pre-placed SRS sensors attached to be worn on both feet. Each sock corresponded to a specific leg; researchers ensured the appropriate sock was appropriately placed on the correct leg. Moreover, researchers ensured all participants arrived for

Figure 5.2: SRS placement and orientation configuration or SRS POC placement for the **(a)** left and **(b)** back for a simulated participant at rest prior to a TSP gait trial; SRS POC placement and motion capture marker set placement for the **(c)** left, **(d)** front, and **(e)** right for stimulated seated participant.

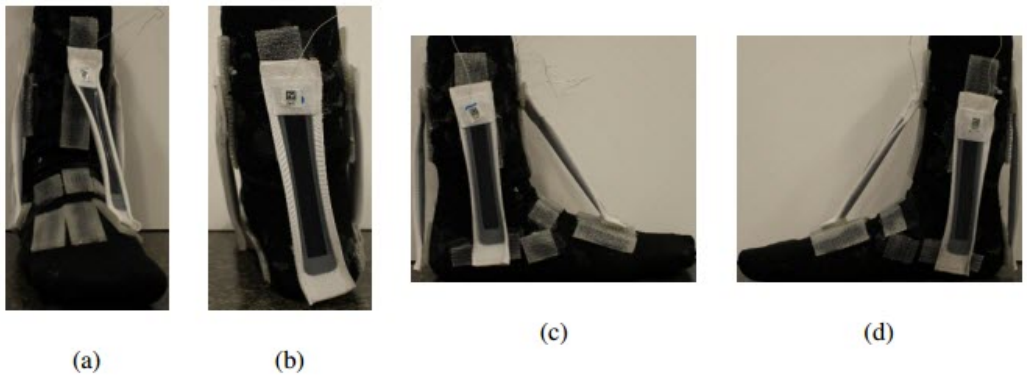

Figure 5.3: **(a)** PF SRS mounted on the dorsal surface and oriented towards the hallux (big toe) to measure the downward movement of the foot; **(b)** DF SRS mounted on the heel of the foot to measure the upward movement of the foot towards the lower leg; **(c)** INV SRS mounted directly over the lateral malleolus (bony landmark on the lateral side of the ankle) to measure the movement of the sole (bottom of the foot) towards the midline of the body; **(d)** EVR SRS mounted directly over the medial malleolus (bony landmark on the medial side of the ankle) [89]

.

the study with their own clean socks to be worn under the SRS donned socks for safety and hygiene purposes. Participants were given a pair of small to medium or large to extra-large socks depending on their shoe size. Following confirmation of proper sock application, the motion capture cluster sensors were mounted to both right and left foot and right and left shanks; following this, each participant assumed a neutral standing position, and the sensors were then calibrated to each participant for 3D motion capture.

A validation step was conducted, where on both the FS and TSP, each participant performed a minimum of two full gait cycles. For both surface types, the researchers confirmed that the 3D motion capture equipment and SRS donned socks were correctly capturing movement data for right and left foot-ankle joints for sensor locations. Upon com-

pletion of all validation steps, each participant was instructed to walk at a self-regulated pace across the 6.10 m of the FS rubber matting resulting in a minimum of two full gait cycles. The participant would then repeat the FS gait cycle for a total of six trials. After the first cycle where the participant began in the south side of the HPL and ended the trial in the north side, the participant was instructed to stand in place, turn around, and begin the next trial by walking from the north side of the room and back to the south. This process was repeated for each participant until all six FS trials were completed and a minimum of three gait cycles were captured per trial.

Upon completion of the six FS trials, six more trials were then captured in the same manner on the TSP across the 6.1 m of rubber matting secured to the platform. Since the TSP sat at a 10-degree incline, as the participants began their trial from the south to north, their left foot-ankle complex would be in an INV state and their right foot-ankle would be in EVR. After the first trial was complete and the participant was asked to stop, turn around, and walk the TSP from the north to south ends of the HPL, their left foot-ankle complex would then be in EVR and their right in INV. This process was completed until six trials (three trials with left leg INV and three trials with right leg INV) each with a minimum of two gait cycles were captured thereby concluding the data collection for each participant. A total of 12 trials (six on FS and six on TSP) were collected with a minimum 24 gait cycles recorded for each participant.

All participants were instructed to begin all gait trials with their right foot. A gait cycle (or stride) begins with the first heel strike of one foot and ends at the following heel strike of that same foot, and includes both the stance and swing phase for each leg [73, 113].

For this study, because participants always started with the right foot, all gait cycles are calculated between right heel strikes.

5.2.5 Data Preprocessing

A similar approach for preprocessing of the data was taken in [89]. Motion capture data was collected at 200 Hz and smoothed with a 30 Hz Butterworth filter. StretchSense^{TM} data was collected at roughly 25 Hz and was approximated and upsampled to 200 Hz to match the sampling rate of the motion capture system. Following this, cross-correlation was used to align the two datasets over time. Each foot was analyzed separately for each trial to eliminate any potential delay that may occur between Bluetooth modules transmitted data from StretchSense^{TM}, and mobile devices (i.e., smartphones, laptops) received the Bluetooth data transmission. Further, only the DF and PF datasets from StretchSense^{TM} SRS were used to determine the timing delay, as the INV and EVR data values did not present linear results with the 3D motion capture due to the potential for coupling of foot movements while some participants were walking (coupling is detailed further during the Limitations Subsection). As was done for previous studies, line plots were created for each of the preprocessed trials that were then validated by the researchers as having data aligned adequately over time. Some datasets were hand-trimmed due to errors in the recording systems where the 3D motion capture system would lose tracking of the participant, which was sometimes experienced when a participant would walk too closely to the outside of the capture space. Figure 5.4 provides an example of the formatted data for a participant's left foot when walking across a flat surface. Note that for cross-correlation, the PF and

DF sensor outputs were compared individually to the motion capture flexion data output, and the sensor that produced the highest autocorrelation coefficient of the two was used for adjusting the delay between the SRS data output and the data from 3D motion capture.

After the data was resampled and time-aligned, individual gait cycles were extracted from each of the trials. Due to the nature of gait cycles being unique for each participant, there was not a typical pattern to easily detect for automating separation of each gait cycle. To resolve this, each trial was reviewed in the MotionMonitor™ data playback software. This playback option provided a visual illustration of what movement was occurring in the motion capture system. The beginning of each gait cycle was marked as the beginning of the right foot heel strike. When reviewing the MotionMonitor™ playback, frame numbers were recorded for each point in the 3D motion capture data to mark the beginning and end of each gait cycle. An example of this is illustrated in Figure 5.5. Based on the variable stride length of the participants and the recommended walking path length for gait studies, a minimum of two gait cycles were collected for each trial. When participant stride lengths were shorter, a third gait cycle was collected as well. Three gait cycles were recorded for 80% of all the trials (190/238 trials). For the 20% of the trials where only two gait cycles were collected, participants had longer stride lengths and were not able to complete a third gait cycle within the 6.10 m walk space.

After the frame numbers were collected, they were then converted to seconds and used to trim the preprocessed data into separate files, each representing individual gait cycles. Finally, a third-order Savitzky–Golay filter was applied to the StretchSense™ data for smoothing. This filter was chosen as it is particularly effective at preserving minimum and

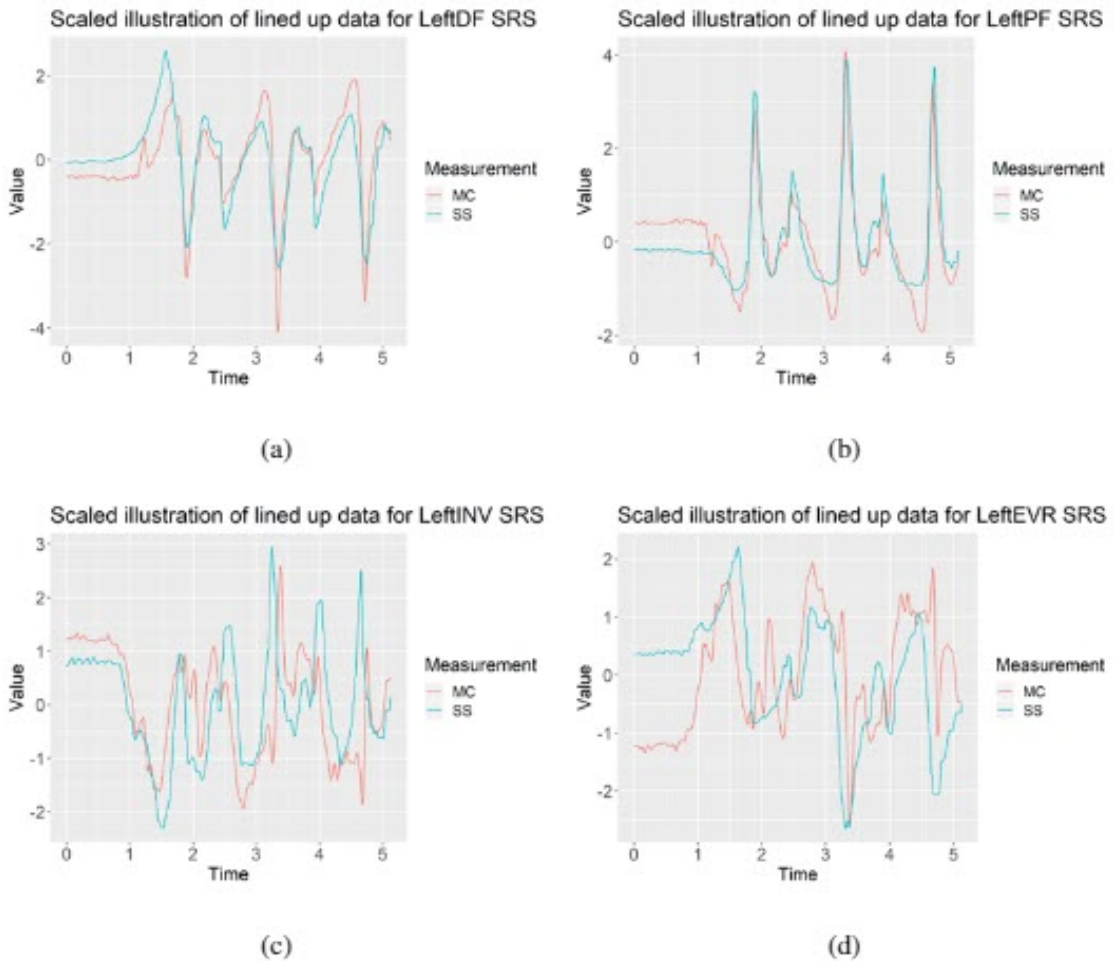

Figure 5.4: **(a)** Scaled output of StretchSense^{TM} DF sensor output (capacitance) compared to motion capture flexion output (degrees); **(b)** scaled output of StretchSense^{TM} PF sensor output compared to the inverted motion capture flexion output; **(c)** scaled output of StretchSense^{TM} INV sensor output compared to motion capture inversion output; **(d)** scaled output of StretchSense^{TM} EVR sensor output compared to motion capture inversion output.

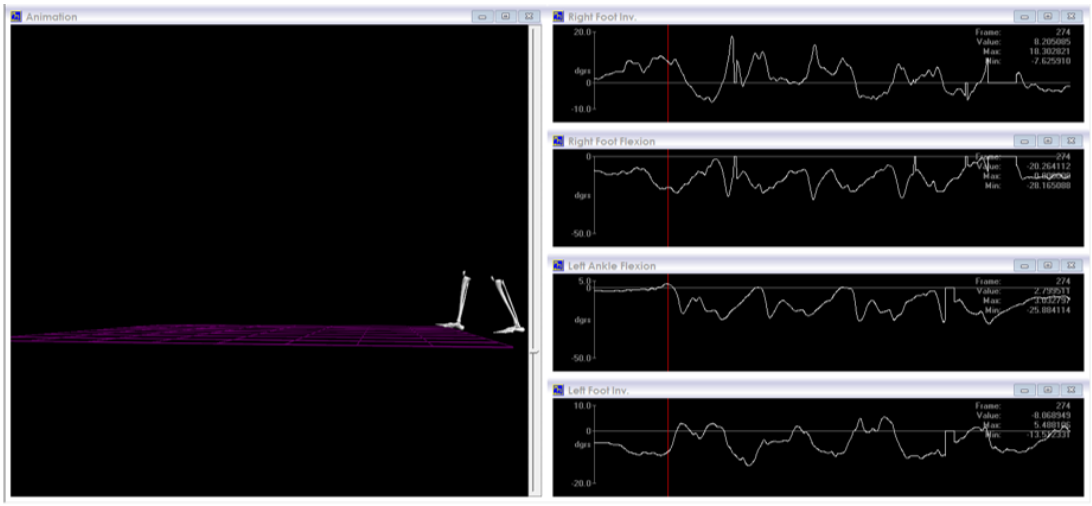

Figure 5.5: Example of MotionMonitor™ playback used to record right heel strike frame numbers. Pictured on the left is the frame where the first right foot heel strike occurs. On the right are examples of the graphs depicting the output of the motion capture measurements.

maximum values after filtering [90]. Further, this filter application has been used in other applications for human motion analysis [19, 78, 4]. This filter was used to mitigate the effects of the aliasing that occurred when upsampling the StretchSense™ data to the same sampling rate as the 3D motion capture data. A filter length of 39 was used as this produced the best results when correlating the StretchSense™ data to the 3D motion capture data. An example of the improvements to the data made through this filtering is observed in Figure 5.6.

5.2.6 Statistical Analysis

Initially, the analysis was performed one-at-a-time on a single sensor basis in a similar manner as previous studies [89, 13]. In this approach, linear models were generated for

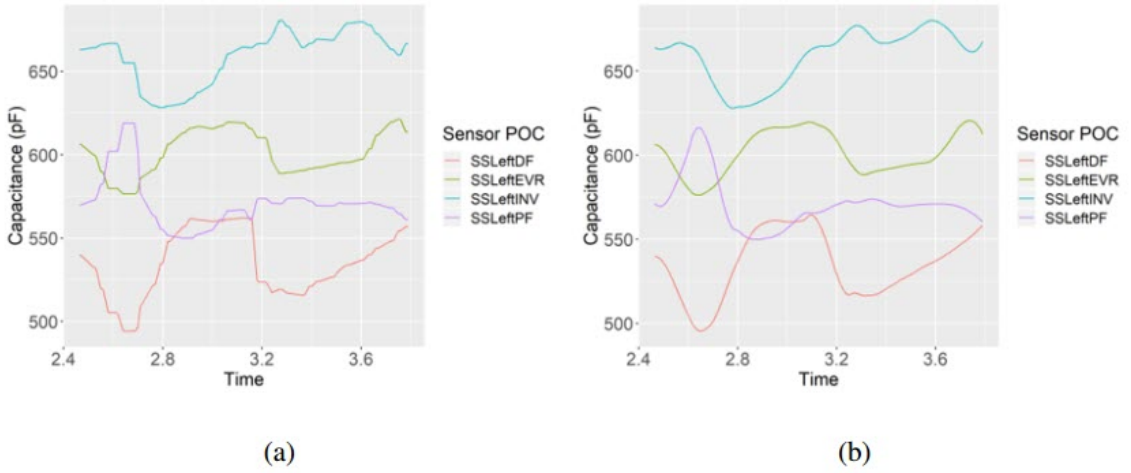

Figure 5.6: **(a)** Upsampled StretchSense^{TM} gait cycle data for the left foot collected before filtering. **(b)** Upsampled StretchSense^{TM} gait cycle data for the left foot after filtering (third-order, window length of 39).

each individual sensor and compared to its corresponding movement (i.e., PF and DF sensors modeled to motion capture flexion; INV and EVR sensors modeled to motion capture inversion). DF and INV sensors were only compared to the positive angle values of the corresponding 3D motion capture data, while PF and EVR sensors were only compared to the negative values of the corresponding data. However, researchers discovered that this approach led to poor results for gait assessment, due to the occurrence of multiple foot-ankle movements at the same time. Due to the POC of the sensors, a coupling of movements occurred where sensor output would be affected by foot-ankle movements that they were not positioned to measure (e.g., a sensor positioned for flexion could also measure inversion movements).

Therefore, a multivariate linear model was developed to better predict the angle output of the motion capture data. For predicting both flexion and inversion data, all four sensors on each foot were used to predict the output of these two, primary foot-ankle movements. Figures 5.7 and 5.8 illustrate the difference in prediction performance versus motion, surface, and foot. Various combinations of multivariate linear models were investigated as well to determine how much prediction accuracy was lost with the removal of different sensors. A model was developed where only PF and DF were used to predict flexion motion, and INV and EVR were used to predict inversion motion. Further, models were generated with each sensor removed individually. Results from all combinations of multivariate linear models are depicted in Table 5.1.

5.3 Results

Table 5.1 provides a summary of the key performance statistics of the experiment. In addition to using the root mean square error (RMSE) and adjusted R^2 to determine measurement performance as was done for previous experiments [89, 13], the mean absolute error (MAE) was added as a performance metric. MAE was found to be a desirable metric as it still provides a measure of the prediction performance of the stretchable SRS but—unlike RMSE—it does not add significant weight to large errors. Therefore, individual outliers do not drastically penalize prediction performance. Similar to RMSE, MAE is negatively oriented, so a lower value is better [43]. Including both metrics, in addition to adjusted R^2, provides an idea of how much prediction performance was affected by significant outliers in the output of the SRS. The first column provides the mean and standard deviation MAE,

RMSE, and adjusted R^2 values when using all four SRS to predict inversion and flexion of the foot. Additional columns were added to show the loss in performance when certain sensors were removed from the model. The second column provides the performance results for using only the PF and DF SRS to predict flexion and using the INV and EVR SRS to predict inversion. The last four columns give the performance results when one sensor is removed when modeling both motions with the remaining three sensors.

Table 5.1: Results for various combinations of multivariate linear models to predict motion output. Best results highlighted.

Statistic (°)	All Sensors **for each Motion**	Two Sensors **for each Motion**	No PF **Sensor**	No DF **Sensor**	No INV **Sensor**	No EVR **Sensor**
Mean MAE	1.54	1.96	1.85	1.88	1.81	1.89
Mean RMSE	1.96	2.45	2.36	2.34	2.29	2.36
Mean Adjusted R^2	0.854	0.779	0.806	0.802	0.781	0.791
Standard Deviation MAE	0.612	0.761	0.790	0.848	0.683	0.753
Standard Deviation RMSE	0.779	0.935	1.030	1.030	0.849	0.920

Figure 5.7 presents violin plots showing a breakdown of the RMSE and MAE performance against the motion being predicted, the foot that SRS was mounted to, and the surface being walked on. These violin plots represent a kernel density distribution portrayed vertically. A greater horizontal width of a curve in the plot indicates a greater portion of participants that produced results near the value on the y-axis. More information on these types of plots and their benefits when performing these kinds of assessments can be found in Part II [89]. Violin plots of the adjusted R^2 performance compared against these

same factors can be seen in Figure 5.8. Adjusted R^2 was used as an additional metric to determine goodness-of-fit of the model, while also incorporating the model's degrees of freedom, accounting for the four sensors that are included in the model. It represents the proportion of total variance explained by the model [33].

5.4 Discussion

Part II of the "closing the wearable gap" paper series explored basic, static movements of the foot-ankle complex to assess optimal placement of stretchable SRS for mirroring 3D motion capture data as closely as possible. The results indicated two critical pieces of information: (a) Where stretchable SRS should be positioned around bony landmarks for optimal movement data capture and that (b) R^2 and RMSE were excellent assessment methodologies for indicating robustness of SRS output compared to 3D motion capture output [89]. High R^2 values indicate a successful relative measure of fit between sensor placement and data versus the gold standard of 3D motion capture data. Whereas low RMSE values indicated an absolute measure of fit between the two sets of data collected about foot-ankle complex movement. Part III of the paper series explored a similar stretchable SRS data collection method versus 3D motion capture study via fast, dynamic movements such as expected and unexpected slips and trips. Goodness-of-fit was validated again through high R^2 and low RMSE for many of the study's participants [13]. However, some of the participants did not share the same robustness as others due to a myriad of reasons mainly relating to technology (lower SRS refresh rates versus quicker movements) and methodology (the jerky and abrupt stoppage of the dynamic movements challenging

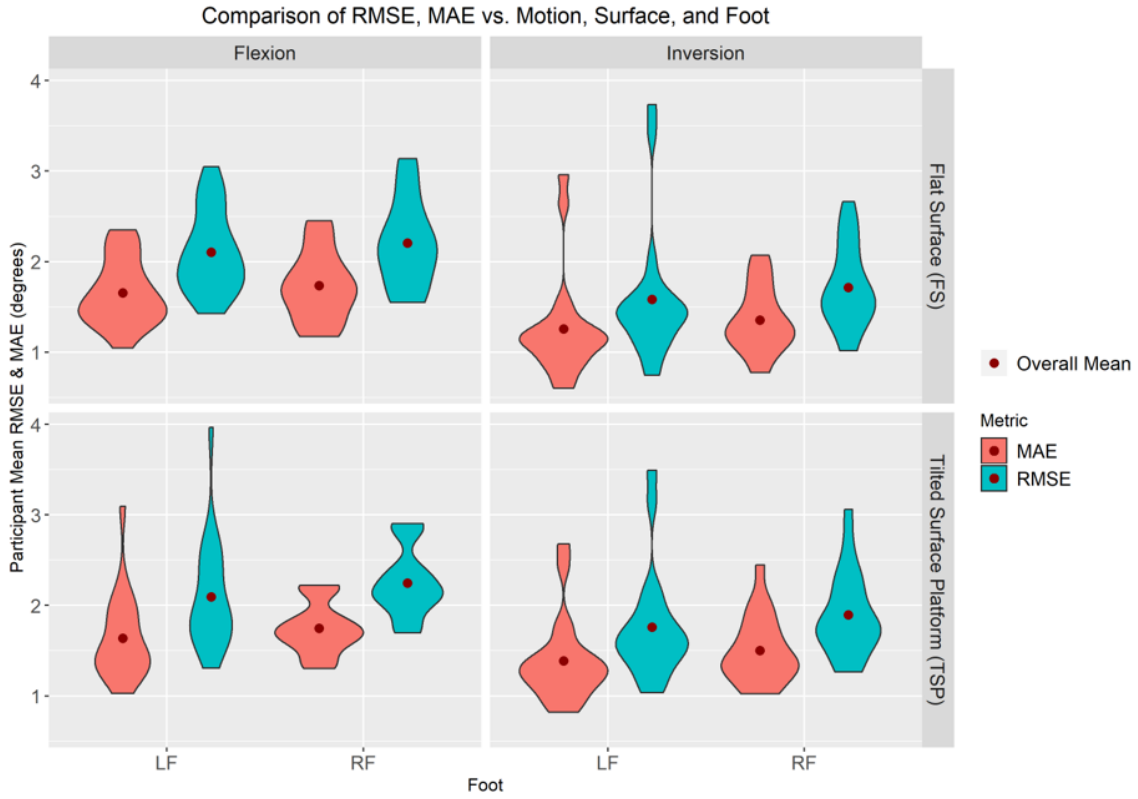

Figure 5.7: Violin plot of root mean square error (RMSE) and mean absolute error (MAE) metric showing the mean and spread of results with respect to various factors. Flexion and inversion columns represent the motion that was being predicted. Rows represent the two types of surfaces the participant walked on. Left foot and right foot sensors are represented in the graph as LF and RF, respectively.

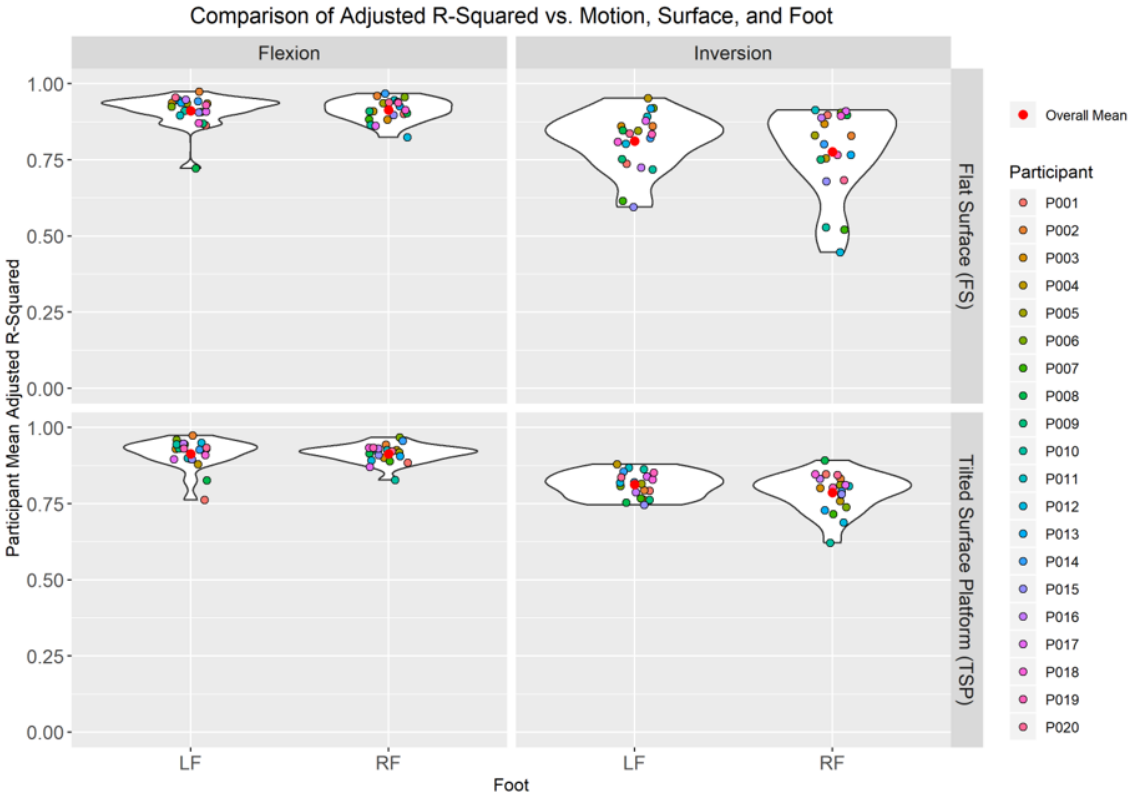

Figure 5.8: Violin plot of adjusted R^2 metric showing mean and spread of results with respect to various factors. Colored points represent individual participant means. Flexion and inversion columns represent the motion that was being predicted. Rows represent the two types of surfaces the participant walked on. Left foot and right foot sensors are represented in the graph as LF and RF, respectively.

the placement security of the motion tracking markers) limitations [13]. For this reason, average R^2 and RMSE values suffered across the population of all participants. RMSE values suffer further due to the nature of this assessment methodology given that scores are penalized more for more significant prediction errors—errors in this instance representing the differences in movement capture data between the golden standard (3D motion capture) and the stretchable SRS. The desire to achieve goodness-of-fit while exploring all the ways to evaluate the said fit were carefully considered for this study, Part IV, where lessons learned were applied to the SRS capture of gait cycles.

The purpose of this study was to use 3D motion capture and stretchable SRS to collect foot-ankle movement on participants as they performed walking gait cycles on both a flat surface and a sloped platform with the primary goal being to assess the data output delta between the gold standard and a new wearable sensor solution. SRS POC for the primary foot-ankle movements (PF, DF, INV, and EVR) identified in Part II [89] were used, and the data assessment methodologies detailed in Parts II and III where utilized and added upon for this study [89, 13]. Given the complex nature of using a linear solution to accurately quantify movement of a triaxial joint during a dynamic movement such as walking, 20 participants performing multiple walking trials were used. The participant gait trial data was then upscaled (for the SRS), time-aligned (based on the right heel strike), and smoothed using filtering methods. Due to the coupling of movements discovered in output of the SRS data, the basic linear models utilized in the previous studies [89, 13] were determined to not be successful for gait assessment. A multivariate linear model combined with multiple linear models was developed to predict specific flexion better (from PF and

DF) and inversion (INV and EVR) movements. With both data sets (3D motion capture and SRS) properly aligned, researchers could return to standard assessment methods of adjusted R^2 and RMSE. A new assessment measure to compare the difference between two continuous variables, MAE, was added to provide additional information that contributes a complementary perspective to RMSE. Where RMSE penalizes the average more when larger errors occur, errors found in MAE are penalized less. Since there is variability within the gait cycle between all people [113]—there is value in using both methods. This is further explained in the following subsections.

5.4.1 Mean MAE

For mean MAE, the lower the value, the closer the fit between the 3D motion capture and stretchable SRS. A mean MAE score of 1.54 across flexion (PF and DF) and inversion (INV and EVR) of both left and right feet for all 20 participants while walking on a flat surface and a tilted platform is a positive result indicating a successful experiment. A low mean MAE was achieved despite having outliers as a result of noisy data from the left foot of two participants. Given that the right foot of these outlier participants didn't generate the same noisy output, this would seem to indicate that the issue was not with the individuals performing the gait cycles but with the setup of either the 3D motion capture or the attachment of the SRS (this will be discussed in more detail in the Limitations Subsection). Despite the noisy data occurring on the left foot, the mean MAE was consistently higher in all situations for the right foot, indicating slightly less goodness-of-fit for the right. The right foot heel strike was the indicator for the beginning of the gait cycle and the alignment

of the data, so an inference could be made that the right foot for all participants for all gait cycles was more accurately aligned than the left foot. However, until more data is captured on more participants, the reasoning behind a slightly worse fit for the right foot will require further investigation. Regardless, there is room to improve upon this low mean MAE score with continuous refinement of this study through the discovery and elimination of reasons leading to outlier participant trials.

5.4.2 Mean RMSE

Mean RMSE will always be higher than the mean MAE due to the nature of squaring the prediction error, as was indicated in the 1.96 score. Less accuracy between the joint angle measurements calculated by the stretchable SRS versus the golden standard will increase the overall mean RMSE score. For example, a 10-degree joint angle prediction error will impact the appropriateness-of-fit score much more than a five-degree prediction error. Whereas the mean MAE will be more forgiving of larger prediction errors treating them, not equally, but less harshly in the fit score. Since every person has a unique gait [113], the process of creating a wearable tool that accurately assesses movement at a complex, triaxle joint such as the foot-ankle may indefinitely encounter prediction difficulties simply because of wide varieties in the anthropometry and gait cycles of people. Therefore, utilizing the mean MAE for fit considers that not all errors may be preventable and should not overly penalize the fit score.

However, given that the goal of this entire project and "closing the wearable gap" paper series is to design a device that meets the needs of the practitioners by accurately capturing

foot-ankle data "from the ground up" [60], then perhaps the more penalized score provided by mean RMSE is a more realistic appropriation of fit. Variance by five degrees in the calculation of a joint angle may not be viewed by a practitioner as problematic for flexion-based movements given that the foot-ankle joint can move in much wider arcs in the sagittal plane. However, perhaps a 10-degree joint angle prediction error in flexion is too high. Likewise, the inversion angle movement within the frontal plane is far more limited in range, and any degree of error may be too high given that a common ankle sprain, the plantarflexion inversion, can occur at minimal joint angles. The point is to emphasize that perhaps a more substantial penalty for larger errors warrants a worse fit score indicating that further improvement is needed for practitioners to get the technology and data they're requesting to aid in the appropriate decision-making process for human health and safety.

5.4.3 Mean Adjusted R-Squared

Whereas mean MAE and RMSE indicate fit by lower scores, goodness-of-fit is shown via the mean adjusted R^2 by values closer to one. For this experiment, a score of 0.854 was found indicating a good fit between SRS and 3D motion capture, and this was despite the left and right foot outliers of participants' gait cycles. Compared to the static movements of the individual joint angles collected in Part II [89], however, the fit for dynamic gait movements shows an increase in errors between 3D motion capture and when all four sensors are donned.

5.4.4 Stretch SRS Reduction Combinations

While using the capacitance values captured from all four SRS in the multivariate linear model created promising fit scores, two and three SRS combinations created higher mean MAE and RMSE values and lower mean adjusted R^2 values indicating worse fit. The purpose behind this part of the study was to understand if any sensor was largely redundant considering that PF and DF are both movements that occur in the sagittal plane, and both INV and EVR movements occur in the frontal plane. Again, stressing that the purpose of this research is to create a wearable product using a unique type of sensor and noting that the stretchable SRS are the costliest components in the said product, reducing the number of sensors while retaining movement data accuracy would result in a positive economic design decision. Reviewing the two and three SRS combinations in Table 5.1, however, indicates that this research team is not yet ready to move away from the one-to-one ratio of sensors to primary foot-ankle movements. All two and three sensor combinations result in higher mean MAE and RSME scores and lower mean adjusted R^2 scores. Surprisingly, dropping the INV sensor provides the second-best mean MAE and RMSE. Given that PF and INV provide the widest range of flexion and inversion movement types in the sagittal and frontal planes respectively, researchers had initially hypothesized that DF and ENV sensors seem to be the more likely candidates for sensor reduction options. Perhaps the better score achieved when removing INV has more to do with the noisy participant outliers than anything to do with the type of data collected at this foot-ankle movement. Likewise, based on mean adjusted R^2 scores, PF is the recommended sensor to remove. PF also experienced a left foot participant outlier. While the researchers of this study will continue

to assess solutions that remain accurate yet utilize fewer sensors, more work is needed first to improve fit scores further before any sensors are removed from this wearable prototype solution.

5.4.5 Limitations

While the extreme outliers visualized in the violin plots (Figures 5.7 and 5.8) were just from the left feet of two participants and were primarily contained to the INV movement, this noisiness in the SRS data resulted in a mean lower fit across all participants and all feet walking across all surfaces. Upon careful inspection of the data from the participants, the researchers suspect that the left foot of these participants was at or approaching the edge of the motion tracking space, and therefore the resulting errors may have had more to do with noise from the 3D motion capture data rather than issues from the SRS. Given that all participants began all gait trials with their right heel strike, participants with longer gait lengths were reaching the end of the 6.1 m walkway prior to the final footfall of their left foot. Limitations of the lab space aside, this explanation may account for some of the outliers; it does not account for all noise and coupling seen within the participant gait trial data.

Considering all noise and coupling seen within the data results of the experiment, two primary issues have been recognized by the researchers as areas for improvement needed prior to the next SRS-based gait study: (a) Sensors were not pre-strained enough meaning that some minimal movements were not captured because there was potential slack in the SRS and (b) 3D motion capture errors occurred because the marker clusters were not

mounted appropriately. As visualized in Figure 5.2b (for error demonstration) the participant's right foot has a marker cluster that is more closely mounted over the toes instead of being mounted behind the toes as on the left foot. Mounting the cluster over the toes may increase recorded movement between the shank and the foot because, as the participant flexes his or her toes, additional movements are recorded that would not have otherwise occurred had the marker been secured to the top of the foot. This toe flexion or "toe-curling" noise artificially creates movement where it should not be and therefore increase the error between the SRS and what is supposed to be the gold standard.

Another limitation ties back to variance in participant gait patterns and stride length (there is variability within different gait cycles of the same person and between the gait cycles of different people [113]), and INV is more challenging to capture than PF. Depending on the participant, INV interpretation may also be more challenging due to coupling of the different movements due to the sensor position. As Figure 5.9 visualizes, coupling can occur—typically between the PF and INV SRS—but does not consistently occur on the same foot or the same participant or across all gait cycles in a trial. When coupling does occur, however, this, too, can lead to noisy data and outliers that reduce goodness-of-fit scores.

5.4.6 Future Work

Moving forward, there are still other approaches available to investigate to potentially improve goodness-of-fit results even more. A decoupling coefficient matrix could be implemented to potentially mitigate the influence of the coupled movements that are affecting the SRS outputs. Further, there is a need to develop a more generic model that can pre-

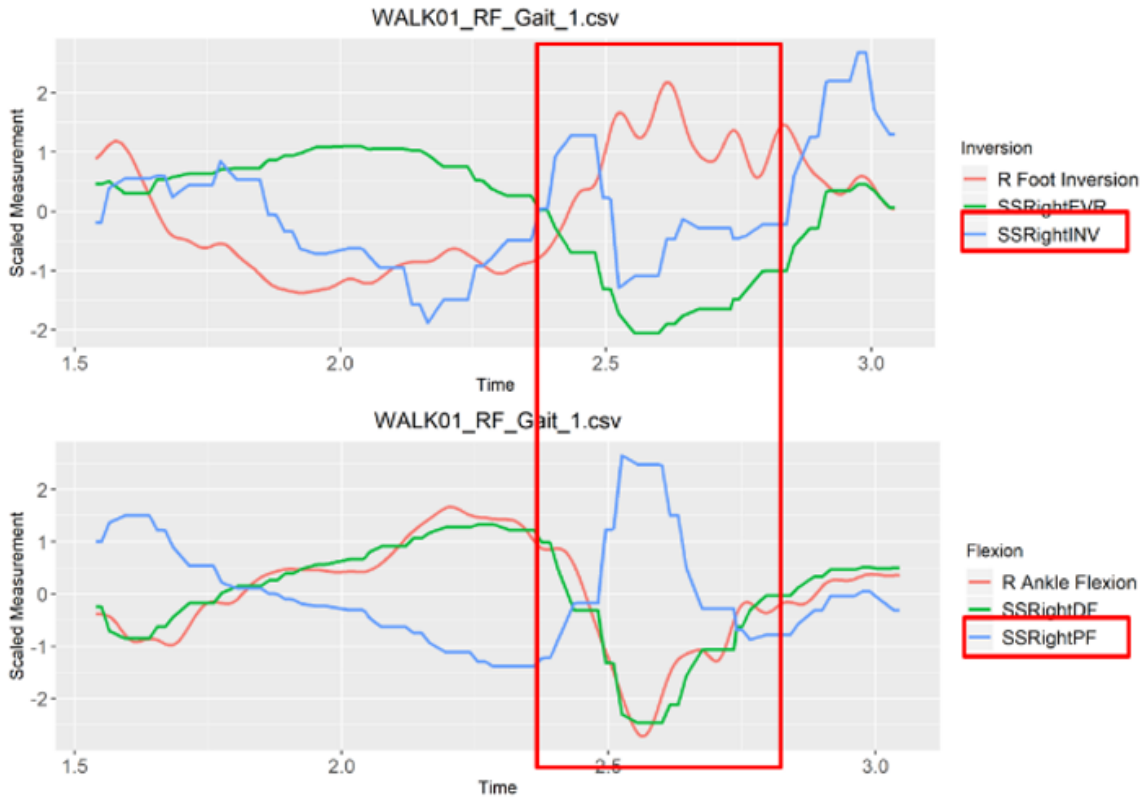

Figure 5.9: Sample participant data demonstrating a coupling effect between INV and PF sensors of the right foot. PF is causing a decrease in the inversion value because tension is being taken off the INV SRS during the gait movement. Therefore, as PF increases, INV incorrectly decreases due to this coupling effect.

dict values accurately across several sessions of using the SRS rather than a per-trial basis. Deep learning techniques could also be applied to improve prediction accuracy. However, a much larger quantity of data will need to be collected for the in-depth learning approach to be feasible. Additionally, a more consistent SRS mounting method will need to be developed to ensure consistency between different data collection sessions when SRS measurements are collected so that a deep learning model would be trained effectively. The researchers are investigating a new hook and eye design to aid in consistency across SRS mounting and to eliminate all future sensor pre-strain issues, thereby ensuring SRS can only be mounted in one way to the sock fabric.

5.4.7 Conclusions

Upon completion of the participant trials, mean MAE, RMSE, and adjusted R^2 were used to determine relative, absolute, and general goodness of fit for the SRS output as compared to the 3D motion capture. Robustness was determined by lower MAE and RMSE scores and higher adjusted R^2 scores. Violin plots were used to visualize the impact of outlier participants while still showing a successful fit between a new wearable solution and the gold standard of movement assessment.

Additional analyses were performed to determine if a two or three SRS combination would provide similar fit scores but a reduced sensor count. Results indicate and expected worse fit for any sensor combination outside of using all four SRS. However, the second-best fit scores were a result of running assessments without INV for mean MAE and RMSE and without PF for mean Adjusted R^2, which is surprising given that these are the primary

movements in their respective frontal and sagittal planes. Researchers perceive this to have been largely impacted by data outliers caused by SRS sensors that were not properly pre-strained or marker clusters placed too close to the participant's toes. Regardless of the challenges, this research team remains confident that an accurate gait assessment that rivals the accuracy of 3D motion capture systems can still be achieved using only four off-the-shelf SRS sensors. As is consistent with the Conclusions Section in Part II of the "closing the wearable gap" paper series: "the solution verified on human participants within this study essentially creates a real-time, continuous, and consistent electric goniometer that a user can wear to assess their movements accurately" [89].

CHAPTER 6

CONCLUSIONS AND FUTURE WORK

During initial testing, I was able to validate a very strong linear trend between extension of a resistive SRS and electrical output (R^2 ¿ 0.99). Going further, I found that temperature had an effect on the base resistance of TPU-based SRS, but not silicone-based SRS. From the range of $75 - 98^{\circ}$ F a strong linear relationship still remained (R^2=0.9239 for the worst case). A micro-controller based measurement unit was developed to collect data from the resistive SRS and was validated against a Micro-Ohm meter and confirmed to have good accuracy (Average percent error: 1.55%). I then validated resistive SRS output against planar movement of the joint ankle complex. The linear models measuring planar flexion indicated good results with a p-value ¡ 0.001. However, when measuring movement in the frontal plane, results could not be trusted as it could not inferred from the SRS output whether INV or EVR was occuring. Additionally, when forcing both planar movements on the mockup at the same time, it was not possible for a single SRS to differentiate the two motions. It was also discovered that DF and PF could not both be measured in this experiment due to limitations of the wooden model. The SRS could be mounted in a manner that kept pre-strain throughout the entire range of motion without exceeding the stretch limitations of the SRS. The next step moving forward was to investigate using SRS

on a real foot, while using multiple SRS to account for the multiple planes of movement and measure full ROM.

I then conducted a study involving ten participants to determine the optimal POC for the SRS. Capacitive SRS were instead used for this study, and were validated against a state-of-the-art motion capture system to determine their viability in measuring foot and ankle kinematics. Four POCs were selected out of the ten POCs investigated in this study, each one selected to measure a specific foot movement (PF, DF, INV, and EVR). While only one POC was investigating for DF due to the small surface to work with, the POC was validated as being strongly linear (mean R^2=0.9567) and accurate (mean RMSE=$1.0568°$). For PF, POC 1 was selected for its optimal linearity (mean R^2=0.9898) and accuracy (mean RMSE=$2.2996°$) as well as its robustness across participants (highest R^2 for six participants and lowest RMSE for five participants). For EVR, POC 2 was selected for its optimal linearity (mean R^2=0.9525) and accuracy (mean RMSE=1.5269), optimal consistency in linearity and accuracy based on standard deviation, and robustness across participants (highest R^2 for seven participants and lowest RMSE for six participants). For INV, both POC 1 and POC 2 were considered nearly equally optimal depending on which factor was being considered, but ultimately POC 2 was chosen due to the consequential symmetry with POC 2 of the EVR SRS. The INV POC 2 SRS had optimal linearity (mean R^2=0.9755) and optimal consistency in linearity and accuracy based on standard deviation. An important observation from this study was that in some cases, particularly when performing EVR, the participants could not always perfectly isolate the planar motion when asked to perform it. This revealed the limitations of using a single sensor model to predict

each movement, when due to the POC of the SRS and the nature of the foot, more than one planar movement could affect the output of a single SRS.

After identifying optimal POCs, the SRS were validated against motion capture during a gait study. Twenty participants were involved and each completed twelve trials, six trials across a flat surface and six trials across a cross-sloped surface. Initial results using a single sensor model indicated a decrease in accuracy and linearity of the sensor, likely due to the coupling of movements that occurred during the triplanar motion when walking. Therefore, a multivariable linear model was investigated to mitigate this issue. This involved developing linear models for both planes of movement using coefficients for all four SRS. It was also discovered that the low sampling rate of the data collection module was contributing to poor results due to aliasing of the data when upsampling to the recording rate of the motion capture system. A Savitzky-Golay filter was applied to the SRS to help smooth the output while preserving minimum and maximum values. Overall results indicate that the SRS had a slight decline in linearity with planar movements (Mean Adjusted R^2=0.854) but retained accuracy (mean RMSE=1.96) when using a multivariable linear model. Models using two-SRS and three-SRS combinations were also investigated to observe the decrease in accuracy. With the worst case being a modest linearity (mean Adjusted R^2=0.781) and high accuracy (mean RMSE=1.81°) when the INV SRS is removed from the model, there exists potential for future optimization through removing an SRS that could be collecting redundant data.

6.1 Contributions to the Field

Through my experience in this research I developed methods for mounting SRS to socks, and I have documented the challenges that come with using SRS to measure foot and ankle kinematics, such as data synchronization, coupling of SRS to multiple planes of movement, and pre-strain of the SRS prior to the beginning of a trial. I developed an experiment for measuring linearity of an SRS in a controlled setting for linear stretch as well as stretch from a simulated PF and INV movement using a wooden mockup ankle. Further, I identified optimal placement and orientation configuration (POC) for SRS on the joint-ankle complex, which was then validated against the human gait cycle on a flat and cross-sloped surface.

Through the experiments I conducted using SRS to predict joint angle data through motion capture, I have developed a suite of scripts in R to automate the preprocessing and analysis of the two collection methods. I will be publishing an open source project consisting of this set of scripts along with the datasets collected from these studies so that other researchers can reproduce these results and implement their own analysis to continue improving the SRS model predictions. I will also be developing a guide providing tips specific to curating a ”clean” dataset, giving examples of ways to ensure preprocessing of the data is done correctly and how to deal with challenges regarding nuances in motion capture data.

6.2 Future Work

There remains plenty of work to continue this research effort. As new SRS are developed, they can be validated using the same experiments described in this project. For the gait study dataset, researchers can investigate more advanced modeling techniques to further improve the linearity and accuracy of the SRS model. A calibration method will need to be developed so that the SRS can be used to predict joint angles without using motion capture as a reference. A circuit will need to be developed that doesn't use COTS products from StretchSense™, to overcome the limited Bluetooth transmission rate that impacted the results of the experiments in this project.

Ideally, another gait experiment would be performed on a treadmill, allowing the researchers to collect a large amount of data that could be used to training a deep learning model. Other deep learning applications would include classification of phases within the gait cycle, determining positional and rotational data of body limb segments from SRS similar to [48], and capturing performance metrics for exercises such as squatting, jumping, and running. Since SRS has now been validated as a reliable method for measuring kinematics at the ankle joint complex, this approach can be extended to measure kinematics of other parts of the body, such as the knee joint, hip, upper body, arms, and wrists.

REFERENCES

[1] Z. O. Abu-Faraj, G. F. Harris, P. A. Smith, and S. Hassani, "Human gait and clinical movement analysis," *Wiley Encyclopedia of Electrical and Electronics Engineering*, 1999, pp. 1–34.

[2] P. I. Akçetin, S. Ç. Ergen, and T. M. Sezgin, "HMM based inertial sensor system for coaching of rowing activity," *Signal Processing and Communications Applications Conference (SIU), 2012 20th*. IEEE, 2012, pp. 1–4.

[3] A. Atalay, V. Sanchez, O. Atalay, D. M. Vogt, F. Haufe, R. J. Wood, and C. J. Walsh, "Batch Fabrication of Customizable Silicone-Textile Composite Capacitive Strain Sensors for Human Motion Tracking," *Advanced Materials Technologies*, vol. 2, no. 9, 2017.

[4] M. A. Awal, S. S. Mostafa, and M. Ahmad, "Performance analysis of Savitzky-Golay smoothing filter using ECG signal," *International Journal of Computer and Information Technology*, vol. 1, no. 02, 2011.

[5] O. Aziz and S. N. Robinovitch, "An analysis of the accuracy of wearable sensors for classifying the causes of falls in humans," *IEEE transactions on neural systems and rehabilitation engineering*, vol. 19, no. 6, 2011, pp. 670–676.

[6] C. L. Bennett, C. Odom, and M. Ben-Asher, "Knee angle estimation based on imu data and artificial neural networks," *Biomedical Engineering Conference (SBEC), 2013 29th Southern*. IEEE, 2013, pp. 111–112.

[7] L. Bianchi, D. Angelini, G. Orani, and F. Lacquaniti, "Kinematic coordination in human gait: relation to mechanical energy cost," *Journal of neurophysiology*, vol. 79, no. 4, 1998, pp. 2155–2170.

[8] S. Blair, M. J. Lake, R. Ding, and T. Sterzing, "Magnitude and variability of gait characteristics when walking on an irregular surface at different speeds," *Human movement science*, vol. 59, 2018, pp. 112–120.

[9] P. Bonato, "Wearable sensors and systems," *IEEE Engineering in Medicine and Biology Magazine*, vol. 29, no. 3, 2010, pp. 25–36.

[10] A. Bonnefoy-Mazure, S. Armand, F. Cavanese, and J. Deslandes, "Normal gait," *Orthopedic management of children with cerebral palsy*, Nova Science, 2015, pp. 199–214.

[11] C. L. Brockett and G. J. Chapman, "Biomechanics of the ankle," *Orthopaedics and trauma*, vol. 30, no. 3, 2016, pp. 232–238.

[12] M. Chan, D. Estève, J.-Y. Fourniols, C. Escriba, and E. Campo, "Smart wearable systems: Current status and future challenges," *Artificial intelligence in medicine*, vol. 56, no. 3, 2012, pp. 137–156.

[13] H. Chander, E. Stewart, D. Saucier, P. Nguyen, T. Luczak, J. E. Ball, A. C. Knight, B. K. Smith, R. Prabhu, et al., "Closing the Wearable Gap—Part III: Use of Stretch Sensors in Detecting Ankle Joint Kinematics During Unexpected and Expected Slip and Trip Perturbations," *Electronics*, vol. 8, no. 10, 2019, p. 1083.

[14] E. Charry, M. Umer, and S. Taylor, "Design and validation of an ambulatory inertial system for 3-D measurements of low back movements," *Intelligent Sensors, Sensor Networks and Information Processing (ISSNIP), 2011 Seventh International Conference on*. IEEE, 2011, pp. 58–63.

[15] K. J. Chesnin, L. Selby-Silverstein, and M. P. Besser, "Comparison of an in-shoe pressure measurement device to a force plate: concurrent validity of center of pressure measurements," *Gait & posture*, vol. 12, no. 2, 2000, pp. 128–133.

[16] B. Cole, "Zebra Technologies Partners with NFL to Track Player Movements,", http://www.fangraphs.com/techgraphs/zebra-technologies-partners-with-nfl-to-track-player-movements/, 2015, Date accessed: Oct. 28, 2016.

[17] G. Cooper, I. Sheret, L. McMillian, K. Siliverdis, N. Sha, D. Hodgins, L. Kenney, and D. Howard, "Inertial sensor-based knee flexion/extension angle estimation," *Journal of biomechanics*, vol. 42, no. 16, 2009, pp. 2678–2685.

[18] A. d'Avella, A. Portone, L. Fernandez, and F. Lacquaniti, "Control of fast-reaching movements by muscle synergy combinations," *Journal of Neuroscience*, vol. 26, no. 30, 2006, pp. 7791–7810.

[19] N. Davey, A. Wixted, Y. Ohgi, and D. James, "A low cost self contained platform for human motion analysis," *The impact of technology on sport II*, 2008, pp. 101–111.

[20] S. M. M. De Rossi, N. Vitiello, T. Lenzi, R. Ronsse, B. Koopman, A. Persichetti, F. Giovacchini, F. Vecchi, A. J. Ijspeert, H. van der Kooij, and M. C. Carrozza, "Soft artificial tactile sensors for the measurement of human-robot interaction in the rehabilitation of the lower limb," *2010 Annual International Conference of the IEEE Engineering in Medicine and Biology*. 2010, pp. 1279–1282, IEEE.

[21] M. Elbawab, J. Olesik, F. Aghazadeh, F. Amankrah, D. Horqque, and L. Zane, "Motion capture garment,", jun 2017, WO Patent App. PCT/CA2016/051,398.

[22] H. G. Espinosa, J. Lee, and D. A. James, "The inertial sensor: A base platform for wider adoption in sports science applications," *Journal of Fitness Research*, vol. 4, 2015.

[23] M. Esposito, M. Macagno, and D. G. Vigano, "Sensors, interfaces and sensor systems for data collection and integrated remote monitoring of conditions at or near body surfaces,", jan 2015, US Patent 8,925,392.

[24] A. Filippeschi, N. Schmitz, M. Miezal, G. Bleser, E. Ruffaldi, and D. Stricker, "Survey of Motion Tracking Methods Based on Inertial Sensors: A Focus on Upper Limb Human Motion," *Sensors*, vol. 17, no. 6, 2017, p. 1257.

[25] R. Floyd and C. W. Thompson, *Manual of Structural Kinesiology*, 20th edition, McGraw-Hill, New York, NY, 2018.

[26] F. Foerster, M. Smeja, and J. Fahrenberg, "Detection of posture and motion by accelerometry: a validation study in ambulatory monitoring," *Computers in Human Behavior*, vol. 15, no. 5, 1999, pp. 571–583.

[27] D. T.-P. Fong and Y.-Y. Chan, "The use of wearable inertial motion sensors in human lower limb biomechanics studies: a systematic review," *Sensors*, vol. 10, no. 12, 2010, pp. 11556–11565.

[28] E. A. Fuller, "Center of pressure and its theoretical relationship to foot pathology," *Journal of the American Podiatric Medical Association*, vol. 89, no. 6, 1999, pp. 278–291.

[29] T. J. Gabbett, "Quantifying the physical demands of collision sports: does microsensor technology measure what it claims to measure?," *The Journal of Strength & Conditioning Research*, vol. 27, no. 8, 2013, pp. 2319–2322.

[30] T. A. Gisby, *Smart artificial muscles*, doctoral dissertation, University of Auckland, 2011.

[31] C. Glaros, D. I. Fotiadis, A. Likas, and A. Stafylopatis, "A wearable intelligent system for monitoring health condition and rehabilitation of running athletes," *4th International IEEE EMBS Special Topic Conference on Information Technology Applications in Biomedicine, 2003.*, 2003, pp. 276–279.

[32] N. A. Gomeñuka, R. L. Bona, R. G. da Rosa, and L. A. Peyré-Tartaruga, "The pendular mechanism does not determine the optimal speed of loaded walking on gradients," *Human movement science*, vol. 47, 2016, pp. 175–185.

[33] K. Grace-Martin, "Assessing the fit of regression models," *The Analysis Factor*, vol. 2015, 2018, Accessed: 29 May 2019.

[34] P. A. Gribble and J. Hertel, "Effect of lower-extremity muscle fatigue on postural control," *Archives of physical medicine and rehabilitation*, vol. 85, no. 4, 2004, pp. 589–592.

[35] S. K. Grimston, B. M. Nigg, D. A. Hanley, and J. R. Engsberg, "Differences in ankle joint complex range of motion as a function of age," *Foot & ankle*, vol. 14, no. 4, 1993, pp. 215–222.

[36] J. Hailstone and A. E. Kilding, "Reliability and validity of the Zephyr™ BioHarness™ to measure respiratory responses to exercise," *Measurement in Physical Education and Exercise Science*, vol. 15, no. 4, 2011, pp. 293–300.

[37] F. L. Hammond, Y. Mengüç, and R. J. Wood, "Toward a modular soft sensor-embedded glove for human hand motion and tactile pressure measurement," *2014 IEEE/RSJ International Conference on Intelligent Robots and Systems*. IEEE, 2014, pp. 4000–4007.

[38] J. Hertel, "Functional anatomy, pathomechanics, and pathophysiology of lateral ankle instability," *Journal of athletic training*, vol. 37, no. 4, 2002, p. 364.

[39] J. Hertel, C. R. Denegar, M. M. Monroe, and W. L. Stokes, "Talocrural and subtalar joint instability after lateral ankle sprain.," *Medicine and science in sports and exercise*, vol. 31, no. 11, 1999, pp. 1501–1508.

[40] B. Huang, M. Li, T. Mei, D. McCoul, S. Qin, Z. Zhao, and J. Zhao, "Wearable stretch sensors for motion measurement of the wrist joint based on dielectric elastomers," *Sensors*, vol. 17, no. 12, 2017, p. 2708.

[41] H. Hurkmans, J. Bussmann, E. Benda, J. Verhaar, and H. Stam, "Accuracy and repeatability of the Pedar Mobile system in long-term vertical force measurements," *Gait & Posture*, vol. 23, no. 1, 2006, pp. 118–125.

[42] P. K. Jamwal, S. Hussain, Y. H. Tsoi, M. H. Ghayesh, and S. Q. Xie, "Musculoskeletal modelling of human ankle complex: Estimation of ankle joint moments," *Clinical Biomechanics*, vol. 44, 2017, pp. 75–82.

[43] JJ, "MAE and RMSE–Which Metric Is Better? - Medium,".

[44] Johnson Sports Trainining, "What Does Zephyr GPS Measure?,", http://zephyrathlete.weebly.com/what-does-zephyr-measure.html, 2016, Date accessed: Nov. 4, 2016.

[45] A. Karatsidis, G. Bellusci, H. Schepers, M. de Zee, M. Andersen, and P. Veltink, "Estimation of Ground Reaction Forces and Moments During Gait Using Only Inertial Motion Capture," *Sensors*, vol. 17, no. 1, 2016, p. 75.

[46] J. J. Kavanagh, S. Morrison, D. A. James, and R. Barrett, "Reliability of segmental accelerations measured using a new wireless gait analysis system," *Journal of biomechanics*, vol. 39, no. 15, 2006, pp. 2863–2872.

[47] C. Keplinger, M. Kaltenbrunner, N. Arnold, and S. Bauer, "Capacitive extensometry for transient strain analysis of dielectric elastomer actuators," *Applied Physics Letters*, vol. 92, no. 19, 2008, p. 192903.

[48] D. Kim, J. Kwon, S. Han, Y.-L. Park, and S. Jo, "Deep full-body motion network for a soft wearable motion sensing suit," *IEEE/ASME Transactions on Mechatronics*, vol. 24, no. 1, 2018, pp. 56–66.

[49] J.-H. Kim, R. Roberge, J. Powell, A. Shafer, and W. J. Williams, "Measurement accuracy of heart rate and respiratory rate during graded exercise and sustained exercise in the heat using the Zephyr BioHarness^{TM}," *International journal of sports medicine*, vol. 34, no. 6, 2013, p. 497.

[50] J. Kwon, J.-H. Park, S. Ku, Y. Jeong, N.-J. Paik, and Y.-L. Park, "A Soft Wearable Robotic Ankle-Foot-Orthosis for Post-Stroke Patients," *IEEE Robotics and Automation Letters*, vol. 4, no. 3, 2019, pp. 2547–2552.

[51] Y.-H. Kwon, L. Hutcheson, J. B. Casebolt, J.-H. Ryu, and K. Singhal, "The effects of railroad ballast surface and slope on rearfoot motion in walking," *Journal of applied biomechanics*, vol. 28, no. 4, 2012, pp. 457–465.

[52] O. D. Lara and M. A. Labrador, "A survey on human activity recognition using wearable sensors.," *IEEE Communications Surveys and Tutorials*, vol. 15, no. 3, 2013, pp. 1192–1209.

[53] K. Lebel, P. Boissy, M. Hamel, and C. Duval, "Inertial measures of motion for clinical biomechanics: Comparative assessment of accuracy under controlled conditions–changes in accuracy over time," *PloS one*, vol. 10, no. 3, 2015, p. e0118361.

[54] Liquid Wire, "Introducing Metal Gel,", https://liquidwire.io/, 2018, Date accessed: Jan. 28, 2018.

[55] D. Litteken, "Evaluation of Strain Measurement Devices for Inflatable Structures," *58th AIAA/ASCE/AHS/ASC Structures, Structural Dynamics, and Materials Conference*, 2017, p. 0426.

[56] H. Liu, R. Dai, and P. Gauthier, "Multi-node motion measurement and analysis system,", apr 2017, US Patent App. 15/208,028.

[57] K. Liu, T. Liu, K. Shibata, Y. Inoue, and R. Zheng, "Novel approach to ambulatory assessment of human segmental orientation on a wearable sensor system," *Journal of biomechanics*, vol. 42, no. 16, 2009, pp. 2747–2752.

[58] N. Lu, C. Lu, S. Yang, and J. Rogers, "Highly sensitive skin-mountable strain gauges based entirely on elastomers," *Advanced Functional Materials*, vol. 22, no. 19, 2012, pp. 4044–4050.

[59] T. Luczak, R. Burch, E. Lewis, H. Chander, and J. Ball, "State-of-the-art review of athletic wearable technology: What 113 strength and conditioning coaches and athletic trainers from the USA said about technology in sports," *International Journal of Sports Science & Coaching*, 2019, p. 1747954119885244.

[60] T. Luczak, D. Saucier, V. Burch, F. Reuben, J. E. Ball, H. Chander, A. Knight, P. Wei, T. Iftekhar, et al., "Closing the wearable gap: mobile systems for kinematic signal monitoring of the foot and ankle," *Electronics*, vol. 7, no. 7, 2018, p. 117.

[61] H. J. Luinge and P. H. Veltink, "Measuring orientation of human body segments using miniature gyroscopes and accelerometers," *Medical and Biological Engineering and computing*, vol. 43, no. 2, 2005, pp. 273–282.

[62] K. MacDonald, R. Bahr, J. Baltich, J. L. Whittaker, and W. H. Meeuwisse, "Validation of an inertial measurement unit for the measurement of jump count and height," *Physical Therapy in Sport*, vol. 25, 2017, pp. 15–19.

[63] F. Marsland, K. Lyons, J. Anson, G. Waddington, C. Macintosh, and D. Chapman, "Identification of cross-country skiing movement patterns using micro-sensors," *Sensors*, vol. 12, no. 4, 2012, pp. 5047–5066.

[64] C. McGarry, ""Review: Sensoria's smart socks are a futuristic novelty that no runner really needs,", https://www.macworld.com/article/2936611/review-sensorias-smart-socks-are-a-futuristic-novelty-that-no-runner-really-needs.html, 2015, Date accessed: Oct. 28, 2016.

[65] R. S. McGinnis, S. DiCristofaro, N. Mahadevan, E. Sen-Gupta, I. Silva, E. Jortberg, J. A. Wright Jr, R. Ghaffari, A. J. Aranyosi, and S. Patel, "Longitudinal Data from Wearable Sensor System Suggests Movement Improves Standing Posture," *Proc. of the 41st Annual Meeting of the American Society of Biomechanics*, Boulder, CO, 2017.

[66] Y. Mengüç, Y.-L. Park, E. Martinez-Villalpando, P. Aubin, M. Zisook, L. Stirling, R. J. Wood, and C. J. Walsh, "Soft wearable motion sensing suit for lower limb biomechanics measurements," *Robotics and Automation (ICRA), 2013 IEEE International Conference on*. IEEE, 2013, pp. 5309–5316.

[67] Y. Mengüç, Y.-L. Park, H. Pei, D. Vogt, P. M. Aubin, E. Winchell, L. Fluke, L. Stirling, R. J. Wood, and C. J. Walsh, "Wearable soft sensing suit for human gait measurement," *The International Journal of Robotics Research*, vol. 33, no. 14, 2014, pp. 1748–1764.

[68] M. A. Mestrovic, P. M. Petersen, R. W. Cranston, W. B. Stannard, and P. B. D'arcy, "System, garment and method,", aug 2016, US Patent 9,427,179.

[69] M. Miodownik, B. Oldfrey, R. Jackson, and P. Smitham, "A deep learning approach to non-linearity in wearable stretch sensors," *Frontiers in Robotics and AI*, vol. 6, 2019, p. 27.

[70] E. Mishra, S. Jena, C. Bhoi, T. Arunachalam, and S. K. Panda, "Effect of high heel gait on hip and knee-ankle-foot rollover characteristics while walking over inclined surfaces—A pilot study," *The Foot*, vol. 40, 2019, pp. 8–13.

[71] M. Müller, R. Vilzmann, and F. Zierer, "Pressure measuring base for measurement of mechanical pressure distribution on human foot sole of e.g. shoe for medical application for patients with diabetic foot, has electronic unit, and pressure sensors arranged at feed lines,".

[72] B. Najafi, J. Wrobel, and A. Boloori, "Providing motion feedback based on user center of mass,", mar 2015, US Patent 8,979,665.

[73] M. Nordin and V. H. Frankel, *Basic biomechanics of the musculoskeletal system*, Lippincott Williams & Wilkins, 2001.

[74] Notch, "Notch,", https://wearnotch.com/, 2018, Date accessed: Jan 15, 2018.

[75] B. O'Brien, J. Thode, I. Anderson, E. Calius, E. Haemmerle, and S. Xie, "Integrated extension sensor based on resistance and voltage measurement for a dielectric elastomer," *Electroactive Polymer Actuators and Devices (EAPAD) 2007*. International Society for Optics and Photonics, 2007, vol. 6524, p. 652415.

[76] K. J. O'Donovan, R. Kamnik, D. T. O'Keeffe, and G. M. Lyons, "An inertial and magnetic sensor based technique for joint angle measurement," *Journal of biomechanics*, vol. 40, no. 12, 2007, pp. 2604–2611.

[77] E. Papi, Y. N. Bo, and A. H. McGregor, "A flexible wearable sensor for knee flexion assessment during gait," *Gait & posture*, vol. 62, 2018, pp. 480–483.

[78] A. Paraschiv-Ionescu, E. Buchser, B. Rutschmann, B. Najafi, and K. Aminian, "Ambulatory system for the quantitative and qualitative analysis of gait and posture in chronic pain patients treated with spinal cord stimulation," *Gait & posture*, vol. 20, no. 2, 2004, pp. 113–125.

[79] W. Park, K. Ro, S. Kim, and J. Bae, "A soft sensor-based three-dimensional (3-D) finger motion measurement system," *Sensors*, vol. 17, no. 2, 2017, p. 420.

[80] Y.-L. Park, B.-r. Chen, N. O. Pérez-Arancibia, D. Young, L. Stirling, R. J. Wood, E. C. Goldfield, and R. Nagpal, "Design and control of a bio-inspired soft wearable robotic device for ankle–foot rehabilitation," *Bioinspiration & Biomimetics*, vol. 9, no. 1, 2014, p. 016007.

[81] Y.-L. Park, B.-R. Chen, and R. J. Wood, "Design and fabrication of soft artificial skin using embedded microchannels and liquid conductors," *IEEE Sensors journal*, vol. 12, no. 8, 2012, pp. 2711–2718.

[82] L. Parrington, E. Phillips, A. Wong, M. Finch, E. Wain, and C. MacMahon, "Validation of inertial measurement units for tracking 100m sprint data," *ISBS-Conference Proceedings Archive*, 2016, vol. 34, no 1.

[83] J. Perry and J. Burnfield, "Gait analysis: normal and pathological function. 2nd," *Thorofare, NJ: Slack Incorporated*, 2010.

[84] J. Perry, J. R. Davids, et al., "Gait analysis: normal and pathological function," *Journal of Pediatric Orthopaedics*, vol. 12, no. 6, 1992, p. 815.

[85] R. M. Podoloff, M. H. Benjamin, J. Winters, and R. F. Golden, "Flexible tactile sensor for measuring foot pressure distributions and for gaskets,", jul " 23" 1991, US Patent 5,033,291.

[86] RFIDJournal, "Zebra Acquires Active RFID Provider WhereNet,", http://www.rfidjournal.com/articles/view?6652, 2016, Date accessed: Oct. 28, 2016.

[87] M. Rhudy, "Time alignment techniques for experimental sensor data," *Int. J. Comput. Sci. Eng. Surv*, vol. 5, 2014, pp. 1–14.

[88] D. Saucier, S. Davarzani, A. Turner, T. Luczak, P. Nguyen, W. Carroll, V. Burch, F. Reuben, J. E. Ball, B. K. Smith, et al., "Closing the Wearable Gap—Part IV: 3D Motion Capture Cameras Versus Soft Robotic Sensors Comparison of Gait Movement Assessment," *Electronics*, vol. 8, no. 12, 2019, p. 1382.

[89] D. Saucier, T. Luczak, P. Nguyen, S. Davarzani, P. Peranich, J. E. Ball, R. F. Burch, B. K. Smith, H. Chander, A. Knight, et al., "Closing the Wearable Gap—Part II: Sensor Orientation and Placement for Foot and Ankle Joint Kinematic Measurements," *Sensors*, vol. 19, no. 16, 2019, p. 3509.

[90] A. Savitzky and M. J. Golay, "Smoothing and differentiation of data by simplified least squares procedures.," *Analytical chemistry*, vol. 36, no. 8, 1964, pp. 1627–1639.

[91] H. Schwameder, M. Andress, E. Graf, and G. Strutzenberger, "Validation of an IMU-System (Gait-Up) to Identify Gait Parameters in Normal and Induced Limping Walking Conditions," *ISBS-Conference Proceedings Archive*, 2016, vol. 33, no. 1.

[92] T. Seel, J. Raisch, and T. Schauer, "IMU-based joint angle measurement for gait analysis," *Sensors*, vol. 14, no. 4, 2014, pp. 6891–6909.

[93] S. Seneviratne, Y. Hu, T. Nguyen, G. Lan, S. Khalifa, K. Thilakarathna, M. Hassan, and A. Seneviratne, "A Survey of Wearable Devices and Challenges," *IEEE Communications Surveys and Tutorials*, vol. 19, no. 4, 2017, pp. 2573–2620.

[94] SensoriaFitness.com, "Sensoria Fitness Socks and Anklet,", http://store.sensoriafitness.com/sensoria-fitness-smart-socks, 2016, Date accessed: Oct. 28, 2016.

[95] Springer, "Linear interpolation - Encyclopedia of Mathematics,".

[96] STATSports.com, "STATSport,", http://statsports.com/, 2018, Date accessed: Jan. 15, 2018.

[97] R. N. Stauffer, E. Chao, and R. C. Brewster, "Force and motion analysis of the normal, diseased, and prosthetic ankle joint.," *Clinical orthopaedics and related research*, , no. 127, 1977, pp. 189–196.

[98] Stretchsense, "The Evolution Of Circuits For Stretch Sensors,".

[99] W. Tao, T. Liu, R. Zheng, and H. Feng, "Gait analysis using wearable sensors," *Sensors*, vol. 12, no. 2, 2012, pp. 2255–2283.

[100] W. Tao, T. Liu, R. Zheng, and H. Feng, "Gait analysis using wearable sensors," *Sensors*, vol. 12, no. 2, 2012, pp. 2255–2283.

[101] T. Taylor, "NFL Using Zebra RFID Chips to Track Player Movements, Gather Data,", http://www.si.com/edge/2015/03/05/nfl-player-tracking-technology-new-orleans-saints, 2015, Date accessed: Nov. 4, 2016.

[102] P. A. G. Teixeira, A.-S. Formery, B. Gwenaël, G. Lux, L. Isabelle, G. Hossu, and A. Blum, "Comparison between Subtalar Joint Quantitative Kinematic 4-D CT Parameters in Healthy Volunteers and Patients with joint Stiffness or Chronic ankle instability: a preliminary study," *European Journal of Radiology*, 2019.

[103] TheStreet, "Zebra Technologies Makes Fast Company's List Of Most Innovative Companies,", https://www.thestreet.com/story/13459311/1/zebra-technologies-makes-fast-companys-list-of-most-innovative-companies.html, 2016, Date accessed: Oct. 27, 2016.

[104] M. Totaro, T. Poliero, A. Mondini, C. Lucarotti, G. Cairoli, J. Ortiz, and L. Beccai, "Soft smart garments for lower limb joint position analysis," *Sensors*, vol. 17, no. 10, 2017, p. 2314.

[105] E. J. Walker, A. J. McAinch, A. Sweeting, and R. J. Aughey, "Inertial sensors to estimate the energy expenditure of team-sport athletes," *Journal of science and medicine in sport*, vol. 19, no. 2, 2016, pp. 177–181.

[106] E. Waltz, "A wearable turns baseball pitching into a science [News]," *IEEE Spectrum*, vol. 52, no. 9, 2015, pp. 16–17.

[107] S. Weindel, R. Schmidt, S. Rammelt, L. Claes, A. v. Campe, and S. Rein, "Subtalar instability: a biomechanical cadaver study," *Archives of orthopaedic and trauma surgery*, vol. 130, no. 3, 2010, pp. 313–319.

[108] Wikipedia, "Butterworth filter - Wikipedia,".

[109] Wikipedia, "Cross-correlation - Wikipedia,".

[110] Wikipedia, "Linear interpolation - Wikipedia,".

[111] Wikipedia, "Stretch sensor,", June 2019, Page Version ID: 902673259.

[112] D. Winter, "A review of kinematic parameters in human walking," *Gait analysis: theory and application*, 1995.

[113] D. A. Winter, "Biomechanical motor patterns in normal walking," *Journal of motor behavior*, vol. 15, no. 4, 1983, pp. 302–330.

[114] D. A. Winter, "Kinematic and kinetic patterns in human gait: variability and compensating effects," *Human movement science*, vol. 3, no. 1-2, 1984, pp. 51–76.

[115] J. G. Wrightson, L. Schäfer, and N. J. Smeeton, "Dual-task prioritization during overground and treadmill walking in healthy adults," *Gait & posture*, vol. 75, 2020, pp. 109–114.

[116] G. Wu, S. Siegler, P. Allard, C. Kirtley, A. Leardini, D. Rosenbaum, M. Whittle, D. D D'Lima, L. Cristofolini, H. Witte, et al., "ISB recommendation on definitions of joint coordinate system of various joints for the reporting of human joint motion—part I: ankle, hip, and spine," *Journal of Biomechanics*, vol. 35, no. 4, 2002, pp. 543–548.

[117] D. Xu, T. G. McKay, S. Michel, and I. A. Anderson, "Enabling large scale capacitive sensing for dielectric elastomers," *Electroactive Polymer Actuators and Devices (EAPAD) 2014*. International Society for Optics and Photonics, 2014, vol. 9056, p. 90561A.

[118] T. Yamada, Y. Hayamizu, Y. Yamamoto, Y. Yomogida, A. Izadi-Najafabadi, D. N. Futaba, and K. Hata, "A stretchable carbon nanotube strain sensor for human-motion detection," *Nature nanotechnology*, vol. 6, no. 5, 2011, pp. 296–301.

[119] Zebra, "Zebra Buys Navis, Proveo,", http://www.rfidjournal.com/articles/view?3682, 2007, Date accessed: Oct. 28, 2016.

[120] Zebra, "Zebra Sports Solutions,", https://www.zebra.com/us/en/solutions/location-solutions/zebra-sport-
solution.html, 2018, Date accessed: Jan 15, 2018.

[121] Zebra Technologies, "REVEALED: The Hi-tech GPS Gizmo Liverpool Use to Ensure Gerrard, Suarez and Co are Fit Enough for New Season,", http://www.dailymail.co.uk/sport/football/article-2377757/Liverpool-use-STATSports-Viper-united-ensure-players-fit-enough.html, 2013, Date accessed: Nov. 4, 2016.

[122] Zebra Technologies, "Partners in Innovation,", https://www.zebra.com/us/en/nfl.html, 2016, Date accessed: Nov. 4, 2016
.

[123] Zephyr, "Zephyr Performance Systems,", https://www.zephyranywhere.com/, 2018, Date accessed: Jan 15, 2018.

[124] J. Zhang, Y. Cao, M. Qiao, L. Ai, K. Sun, Q. Mi, S. Zang, Y. Zuo, X. Yuan, and Q. Wang, "Human motion monitoring in sports using wearable graphene-coated fiber sensors," *Sensors and Actuators A: Physical*, vol. 274, 2018.

[125] J.-T. Zhang, A. C. Novak, B. Brouwer, and Q. Li, "Concurrent validation of Xsens MVN measurement of lower limb joint angular kinematics," *Physiological measurement*, vol. 34, no. 8, 2013, p. N63.

[126] H. Zhou and H. Hu, "Human motion tracking for rehabilitation—A survey," *Biomedical Signal Processing and Control*, vol. 3, no. 1, 2008, pp. 1–18.

MSU library requires title page for each appendix

APPENDIX A

DERIVATION FOR MEASURING RESISTIVE SRS

A.1 Derivation for Measuring Resistive SRS

The following equations provide a more detailed explanation of the mathematical calculations used to determine the resistance of the Liquid Wire sensor in the Wheatstone bridge circuit. Please refer to Figure 3.2 for circuit components.

$$V_{12} = \frac{R_2}{R_1 + R_2} \times V_{supply} \tag{A.1}$$

$$V_{34} = \frac{R_{LiquidWire}}{R_3 + R_{LiquidWire}} \times V_{supply} \tag{A.2}$$

$$V_{12} + V_{measured} - V_{34} = 0 \tag{A.3}$$

$$V_{measured} = V_{34} - V_{12} \tag{A.4}$$

$$V_{measured} = \frac{R_{LiquidWire}}{R_3 + R_{LiquidWire}} \times V_{supply} - \frac{R_2}{R_1 + R_2} \times V_{supply} \tag{A.5}$$

$$\frac{V_{measured}}{V_{supply}} = \frac{R_{LiquidWire}}{R_3 + R_{LiquidWire}} - \frac{R_2}{R_1 + R_2} \tag{A.6}$$

$$\frac{V_{measured}}{V_{supply}} + \frac{R_2}{R_1 + R_2} = \frac{R_{LiquidWire}}{R_3 + R_{LiquidWire}} \tag{A.7}$$

$$\alpha = \frac{V_{measured}}{V_{supply}} + \frac{R_2}{R_1 + R_2} \tag{A.8}$$

$$\alpha = \frac{R_{LiquidWire}}{R_3 + R_{LiquidWire}} \tag{A.9}$$

$$R_3 * \alpha + R_{LiquidWire} \times \alpha = R_{LiquidWire} \tag{A.10}$$

$$R_3 * \alpha = R_{LiquidWire} \times (1 - \alpha) \tag{A.11}$$

$$R_{LiquidWire} = \frac{R_3 \times \alpha}{1 - \alpha} \tag{A.12}$$